Host Galaxies of Type Ia Supernovae From the Nearby Supernova Factory

by

Michael Joseph Childress

A dissertation submitted in partial satisfaction of the

requirements for the degree of

Doctor of Philosophy

in

Physics

in the

Graduate Division

of the

University of California, Berkeley

Committee in charge:

Dr. Greg Aldering, Co-Chair

Professor Saul Perlmutter, Co-Chair

Professor Marc Davis

Professor Chung-Pei Ma

Fall 2011

Host Galaxies of Type Ia Supernovae
From the Nearby Supernova Factory

Abstract

Host Galaxies of Type Ia Supernovae
From the Nearby Supernova Factory

by

Michael Joseph Childress

Doctor of Philosophy in Physics

University of California, Berkeley

Dr. Greg Aldering, Co-Chair

Professor Saul Perlmutter, Co-Chair

Type Ia Supernovae (SNe Ia) are excellent distance indicators, yet the full details of the underlying physical mechanism giving rise to these dramatic stellar deaths remain unclear. As large samples of cosmological SNe Ia continue to be collected, the scatter in brightnesses of these events is equally affected by systematic errors as statistical. Thus we need to understand the physics of SNe Ia better, and in particular we must know more about the progenitors of these SNe so that we can derive better estimates for their true intrinsic brightnesses. The host galaxies of SNe Ia provide important indirect clues as to the nature of SN Ia progenitors. In this Thesis we utilize the host galaxies of SNe Ia discovered by the Nearby Supernova Factory (SNfactory) to pursue several key investigations into the nature of SN Ia progenitors and their effects on SN Ia brightnesses. We first examine the host galaxy of SN 2007if, an important member of the subclass of SNe Ia whose extreme brightnesses indicate a progenitor that exceeded the canonical Chandrasekhar-mass value presumed for normal SNe Ia, and show that the host galaxy of this SN is composed of very young stars and has extremely low metallicity, providing important constraints on progenitor scenarios for this SN. We then utilize the full sample of SNfactory host galaxy masses (measured from photometry) and metallicities (derived from optical spectroscopy) to examine several global properties of SN Ia progenitors: (i) we show that SN Ia hosts show tight agreement with the normal galaxy mass-metallicity relation; (ii) comparing the observed distribution of SN Ia host galaxy masses to a theoretical model that couples galaxy physics to the SN Ia delay time distribution (DTD), we show the power of the SN Ia host mass distribution in constraining the SN Ia DTD; and (iii) we show that the lack of ultra-low metallicities in the SNfactory SN Ia host sample gives provisional support for the theorized low-metallicity inhibition of SNe Ia. Finally we revisit recent studies which found that the *corrected* brightness of SNe Ia (after application of the standard light curve width and color corrections) correlate with the masses of their host galaxies. We confirm this trend with host mass using SNfactory data, and for the first time confirm that an analogous trend exists with host metallicity. We then apply a spectroscopic standardization technique developed by SNfactory and show that this method significantly reduces the observed bias. In this Thesis we show that SN Ia host galaxies continue to provide key insight into SN Ia progenitors, and also illuminate possible biases in SN Ia brightness standardization techniques.

To my wife,
Elonwy Elvenstar Hickey,
who is the awesomest wife ever,
and our fantastic son,
Fionntán Malcolm Hickey,
born June 2nd, 2011.

Contents

List of Figures

List of Tables

Acknowledgments

First I'd like to thank my wife Elonwy, whose love and support have made it possible for me to achieve all that I have in recent years. Also I want to thank our cats, Tulip and Lunch, for providing vital comic relief throughout the writing process. I also want to thank my young son, Fionntán Malcolm Hickey, born on June 2nd, 2011. He has been my inspiration for completing my graduate work and advancing in my scientific career.

This work would not have been possible without the guidance and tutelage of my advisor, Greg Aldering, who has worked diligently with me over the years of my thesis research and helped build me into the scientist I am today. I would also like to thank my associate advisor, Saul Perlmutter, who has been very supportive of my work and has contributed to many engaging scientific discussions. I also thank the additional members of my thesis committee, Prof. Marc Davis and Prof. Chung-Pei Ma, for their time and interest in my work.

I'd also like to thank my many SNfactory collaborators and their parent institutions: Rollin Thomas, Peter Nugent, Stephen Bailey, Hannah Fakhouri, Eric Hsiao, Stu Loken, Richard Scalzo, Ben Weaver, Cecilia Aragon, Karl Runge, and Sarah Poon from Lawrence Berkeley National Lab; Pierre Antilogus, Seb Bongard, Arnaud Canto, Reynald Pain, and Charling Tao from the Laboratoire de Physique Nucléaire et des Hautes Énergies in Paris; Clément Buton, Nico Chotard, Yannick Copin, Emmanuel Gangler, Rui Periera, and Gerard Smadja from the Institut de Physique Nucléaire de Lyon in Lyon, France; Emmanuel Pecontal from the Centre de Recherche Astronomique de Lyon in Lyon, France; Charlie Baltay and Dave Rabinowitz from Yale University; Matthias Kerschhaggl, Marek Kowalski, and Kerstin Paech from the Universität Bonn in Bonn, Germany.

My research for this thesis was funded in part by the University of California Berkeley Department of Physics. Research funding at LBNL was supported by the Director, Office of Science, Office of High Energy Physics, of the U.S. Department of Energy under Contract No. DE-AC02-05CH11231 and by a grant from the Gordon & Betty Moore Foundation. This research used resources of the National Energy Research Scientific Computing Center, which is supported by the Director, Office of Science, Office of Advanced Scientific Computing Research, of the U.S. Department of Energy under Contract No. DE-AC02-05CH11231. We thank them for a generous allocation of storage and computing time. HPWREN is funded by National Science Foundation Grant Number ANI-0087344, and the University of California, San Diego. This research was also funded in part by a grant from the NASA GALEX Archival Research program (Cycle 5).

Chapter 1

Introduction

The expansion of the Universe was first observed just under a century ago when Edwin Hubble noted that distant galaxies appeared to be moving away from us more rapidly than nearby galaxies, with recession velocities proportional to their distance. Since then the study of the Universe's expansion rate and its evolution over cosmic time has been of great interest to cosmologists as it provides constraints on the mass-energy content of the Universe. The best astrophysical tools for measuring large cosmological distances to facilitate this goal are Type Ia Supernovae (SNe Ia), which are both extremely luminous ($L \approx 10^{41} L_{\odot}$) and relatively uniform in brightness ($\Delta L/L \lesssim 50\%$), making them excellent *standard candles*. Further empirical brightness correction techniques have made SNe Ia even better *standardizable candles* ($\Delta L/L \lesssim 15\%$). Observations of SNe Ia yielded the surprising result that the expansion of the Universe is accelerating (Perlmutter et al. 1999; Riess et al. 1998). When coupled with observations of the cosmic microwave background (CMB), this observation implied that the mass-energy content of the Universe is dominated not by normal matter, but by a mysterious dark energy which exerts a negative pressure in a manner similar to Einstein's cosmological constant.

SN Ia cosmology has progressed rapidly since the discovery of dark energy just over a decade ago, with major SN Ia surveys completed at low (Hicken et al. 2009), intermediate (Kessler et al. 2009), and high redshifts (Riess et al. 2007; Wood-Vasey et al. 2007; Guy et al. 2010; Amanullah et al. 2010). Combinations of these data yield precise estimates on the matter and dark energy densities $(\Omega_M, \Omega_\Lambda)$, as well as the dark energy equation of state parameter w and its first order derivative in redshift w_a. In this era of precision SN Ia cosmology, the high number of SNe Ia has decreased the statistical uncertainties in cosmological analyses to such a degree that systematic uncertainties are becoming a significant source of error in the estimation of the cosmological parameters. Major progress in SN Ia cosmology now requires a closer inspection of our methods for standardizing SNe Ia and a deeper physical understanding of these exceptional astrophysical events.

As plans are developed for future SN Ia cosmology experiments designed to find SNe Ia at even higher redshifts (up to $z \sim 1.7$), the necessity to have a deeper understanding of the physics of SNe Ia becomes even more acute. The SN Ia cosmology method hinges upon comparison of brightnesses of distant events to those in the nearby universe to measure accurate distances. Inherent in this technique is the assumption that the physical mechanism behind SNe Ia behaves similarly at all redshifts, but concerns remain that the younger stellar ages and lower metallicities of high redshift environments could bias cosmological measurements if the corrected brightnesses of SNe Ia

vary with these parameters. A promising source for clues to the origin of this residual brightness diversity is the study of SN Ia environments.

The goal of this thesis is to study the host galaxies of SNe Ia to gain deeper insight into the nature of SN Ia progenitors, in order to ultimately improve our ability to standardize SNe Ia for measuring cosmological distances. Using the SN Ia and host galaxy data set from the Nearby Supernova Factory (SNfactory – Aldering et al. 2002), I examine the physical properties of SN Ia host galaxies and their relationships to the properties of the SNe Ia they produced.

1.1 Type Ia Supernova Cosmology

Type Ia Supernovae are used to measure cosmological distances by comparing the brightnesses of very distant SNe Ia to those of nearby SNe Ia whose brightnesses have been calibrated with independent distance measurements such as Cepheid Variables (e.g. Riess et al. 2011). Observationally, the brightness of an SN Ia rises quickly over the course of 15-20 days and fades slowly over the course of several hundred days (Filippenko 1997), and the observation of this *light curve* is used to estimate the peak brightness of the SN Ia in some broadband photometric filter (typically B-band). The raw observed peak brightnesses of SNe Ia in B-band typically have a dispersion of about 0.4 magnitudes, making them excellent standard candles.

Several empirical relationships have been developed to further standardize SN Ia brightnesses. Early studies of SN Ia light curves observed a correlation between the observed peak brightnesses of SNe Ia and the width of their light curves (Phillips 1993). The light curve width, or "stretch" (Perlmutter et al. 1997), can then be used to derive an empirically corrected SN Ia brightness. Similarly, the observed colors of SNe Ia were found to be correlated with peak brightness (Riess et al. 1996; Tripp 1998), allowing for a second empirical SN Ia brightness correction. These stretch and color corrections have become a common set of tools in deriving cosmological distances using SNe Ia.

The typical application of SNe Ia for cosmology involves plotting the difference between the observed SN Ia magnitude and its expected magnitude (after the empirical brightness corrections), called the distance modulus (μ), against its recession velocity as tracked by the redshift (z) of its spectrum. The location of SNe Ia on this diagram, known as the *Hubble Diagram*, can be compared to predictions for cosmologies with specific values of the matter density (Ω_M), dark energy density (Ω_Λ), and the dark energy equation of state parameter (w). Marginalization over parameter space allows SN Ia Hubble Diagrams to provide quantitative constraints on these cosmological parameters.

Modern compilations of multiple SN Ia data sets provide Hubble Diagrams with hundreds of SNe Ia. When combined with other cosmological probes such as the cosmic microwave background (CMB) and baryon acoustic oscillations (BAO), a recent compilation of over 500 SNe Ia (Amanullah et al. 2010) has helped constrain the deviation of the Universe from flat geometry to be $\Omega_k = -0.005^{+0.007}_{-0.007}$, and the dark energy equation of state parameter to be $w = -1.026^{+0.055}_{-0.059}$ (for a cosmological fit where Ω_M, Ω_Λ, and w are free parameters). Thus SNe Ia have shown that the Universe is consistent with a flat spatial geometry with expansion currently dominated by a dark energy whose equation of state is consistent with Einstein's cosmological constant. Future SN Ia surveys will facilitate a measurement of the evolution of w and provide constraints on theoretical dark energy models.

1.2 Progenitors of SNe Ia

Observationally, SNe Ia are classified spectroscopically by broad absorption features from intermediate mass elements (IMEs: O, Mg, Si, S, Ca) and no observable hydrogen features (Filippenko 1997). Their spectral energy distributions peak in the optical, and their optical light curves rise quickly over the course of 15-20 days and fade slowly over the course of several hundred days. The consistent decay of optical luminosity at intermediate and late times has led to the generally accepted belief that SN Ia light curves are powered by the radioactive decay of ^{56}Ni to ^{56}Co (which later decays to ^{56}Fe) formed in fusion reactions during the violent SN explosion.

The generally accepted scenario for the production of a SN Ia is the total disruption of a carbon-oxygen (CO) white dwarf (WD) by thermonuclear runaway as accretion from a binary companion drives it toward the Chandrasekhar mass (M_{Ch}). In the single-degenerate scenario (SD; Whelan & Iben 1973), the WD accretes material from a less-evolved companion, either a main-sequence or red giant star (e.g. Hachisu et al. 2008). In the double-degenerate scenario (DD; Iben & Tutukov 1984), two WDs coalesce following orbital decay from gravitational radiation. To date there exists no overwhelming observational evidence to favor one of these scenarios over the other. We currently have no clear identification of any SN Ia progenitor system in archival imaging data of recent SNe Ia, nor has there been an unambiguous identification of the companion star for the Galactic SN Ia remnants.

The fact that the progenitor system of the most important cosmological distance indicator remains uncertain has been a source of great consternation for observers and theorists alike, even leading Livio (2001) to declare:

> "The fact that we do not know yet what are the progenitor systems of some of the most dramatic explosions in the universe has become a major embarrassment and one of the key unsolved problems in stellar and binary star evolution."

Thus knowledge of the SN Ia progenitor mechanism is a research goal of key interest not only to SN Ia cosmologists, but also to those studying stellar evolution and binary stellar systems.

1.3 Why Study SN Ia Host Galaxies?

Given the challenge of directly observing SN Ia progenitor systems, the study of their host galaxies serves as an instructive indirect probe of their progenitor environments. Host galaxies provide information about mean stellar ages in the vicinity of the SN, as well as chemical composition of the gas or stars near the SN location. These environmental conditions may affect the properties of the resultant SN Ia, and are particularly important to study because ages and metallicities of higher redshift SN Ia progenitors will differ from those in the nearby universe.

Early studies of SN Ia host galaxies found correlations between the host galaxy properties and the properties of the SNe Ia they hosted (Filippenko 1989; Branch & van den Bergh 1993; Hamuy et al. 1996). Earlier (later) and more (less) massive type galaxies were found to host fainter (brighter), faster-declining (slower-declining) SNe Ia with higher (lower) ejecta velocities. This evident progenitor-driven brightness effect was assumed to be compensated for by the application of stretch-based luminosity corrections, thereby removing any potential cosmological bias at high

redshifts. However, recent studies (Kelly et al. 2010; Sullivan et al. 2010; Lampeitl et al. 2010) discovered that the *corrected* brightnesses of SNe Ia still showed a very subtle correlation with the stellar mass of their host galaxies. Though not sufficient to negate the detection of dark energy, this effect biases cosmological parameter estimates, especially the dark energy equation of state parameter w. The source of this bias is currently a source of vigorous study and will be investigated in this thesis (see Chapter 6) using SNfactory data.

In addition to providing a means of searching for possible cosmological biases in SN Ia standardization techniques, the study of SN Ia hosts also offers insight into the physics of SNe Ia and yields some constraints on SN Ia progenitor scenarios. For example, recent studies of SN Ia rates in galaxies of varying types showed strong evidence for SNe Ia associated with young stellar populations (Mannucci et al. 2005; Sullivan et al. 2006; Aubourg et al. 2008), as well as association of other SNe Ia with older stellar populations which were popularly believed to be the exclusive source of SNe Ia. Such studies provide observational constraints on the age distribution of SN Ia progenitors which must be met by any acceptable SN Ia progenitor theory.

1.4 Organization of this Thesis

This chapter and the following chapter introduce both the motivation for studying SN Ia host galaxies and the pertinent research to-date in this field. In Chapter 2 we present a more detailed description of the proposed SN Ia progenitor scenarios with a particular emphasis on how the variations of these scenarios may affect SN Ia brightnesses. This Chapter continues to describe relevant studies of SN Ia host galaxies and how these studies have provided constraints on SN Ia progenitors.

The data from SNfactory used in this thesis are described in Chapter 3, beginning with a brief description of the SNfactory experiment and SN Ia data set. The main effort of this thesis is the analysis of the host galaxy data for SNfactory hosts, particularly host galaxy photometric data from various public sources and SNfactory observations, as well as spectroscopic data from over 50 nights of classical observing where I obtained long-slit spectroscopy of the SNfactory hosts. This data and extraction of galaxy physical parameters (mass, metallicity, star-formation activity, etc.) are described in that Chapter.

In Chapter 4 we analyze the host galaxy of SN 2007if, a key member of the subclass of SNe Ia that are likely to have originated from a progenitor system that significantly exceeds the Chandrasekhar mass. Using emission lines measured from the host spectrum and deep photometry from Keck LRIS observations, we show this host to be extremely low mass and lower gas-phase metallicity than any previously reported SN Ia host. Balmer absorption features in the stellar continuum constrain the age of the stellar populations in this galaxy, providing key constraints on possible progenitor scenarios. Finally we inspect the hosts of other likely super-Chandrasekhar-mass SNe Ia and show that they are lower in stellar mass than the normal SN Ia host sample, perhaps indicating a preference for low metallicity formation of super-Chandrasekhar SNe Ia.

Chapter 5 presents our investigations of the statistical properties of the full sample of SN Ia host galaxies. Here we inspect the agreement of SN Ia hosts with the normal galaxy mass-metallicity relation, a key assumption of many previous authors' work that has yet to be confirmed observationally. We also inspect the SN Ia host galaxy stellar mass distribution and how this can constrain the SN Ia delay time distribution. Finally this chapter focuses in on SNe Ia in low luminosity hosts to assess the observational support for theorized low-metallicity inhibition of SNe Ia.

In Chapter 6 we use SNfactory data to investigate the relationship between SN Ia brightnesses and the properties of their host galaxies. We confirm the previous discovery of the correlation between stretch- and color-corrected SN Ia brightnesses and the stellar masses of their host galaxies. We then apply an alternative SN Ia standardization technique developed by SNfactory using a spectroscopic SN Ia luminosity indicator, and investigate whether this residual host bias remains with our new methods.

Finally in Chapter 7 we revisit the conclusions of this thesis and its contributions to the field of SN Ia science and cosmology, then present prospects for future analyses to extend the work of this thesis.

Chapter 2

Host Galaxies of SNe Ia

The study of SN Ia host galaxies provides an indirect means of investigating the progenitors of SNe Ia, as the properties of the stellar populations from which SNe are born serve as context for the nature of the SN progenitors themselves. Statistical analyses of the stellar populations of all SN Ia host galaxies can provide key information about the nature of SN Ia progenitor ages and metallicities. SN Ia host studies also provide a critical cross check for ensuring SN Ia brightness standardization techniques are unbiased with regard to stellar age and metallicity, as these quantities evolve with redshift and could bias cosmological parameters if their effect on SN Ia brightnesses is not properly corrected. Below we describe the currently favored SN Ia progenitor models and the ways in which the study of SN Ia host galaxies facilitates both SN Ia progenitor studies and cosmological analyses.

2.1 SN Ia Progenitors

SNe Ia are widely believed to be the result of the total disruption of a carbon-oxygen white dwarf (CO-WD) by thermonuclear runaway following the accretion of material from a binary companion until the WD approaches the Chandrasekhar mass (M_{Ch}). The precise details of the SN Ia progenitor scenario remain unknown, but a wealth of theoretical models exist which explain many of the observed characteristics of SNe Ia.

Of critical concern for the continued use of SNe Ia as cosmological probes is how variations in the progenitor properties affect the brightnesses of SNe Ia, and whether these variations are properly accounted for by our accepted standardization techniques. In this section we review the important basic details of SN Ia explosion physics, the proposed binary evolution scenarios which may lead to SNe Ia, and some proposed effects of progenitor metallicity on the properties of the resultant SN Ia.

2.1.1 SN Ia Explosion Physics

We stated above that SNe Ia are generally agreed to be the thermonuclear explosion of an accreting carbon-oxygen white dwarf (CO-WD) in a binary system at or near the Chandrasekhar mass. Here we outline the reasons for this interpretation and discuss the outstanding questions regarding the nature of the SN explosion.

Progenitor Composition. A SN Ia shows no spectroscopic hydrogen features, meaning it must have resulted from a progenitor star that has shed its hydrogen envelope. An obvious single-star scenario that satisfies this criterion is that of an intermediate mass ($M \sim 12 - 20 M_{\odot}$) star that has reached the end of its fusion cycle and undergoes core collapse, which is precisely the accepted scenario for SNe Ib/Ic (Filippenko 1997). This scenario does not fit for SNe Ia for several reasons: (i) this scenario allows for a range of progenitor masses and thus explosion energies that exceed the observed diversity of SNe Ia, (ii) the timescale for this single-star evolutionary scenario is very short ($t \sim 10$ Myr) which is incongruous with the presence of SNe Ia in elliptical galaxies where the stellar ages are several Gyr old. An accreting CO-WD near M_{Ch} satisfies the lack of hydrogen, the uniformity of explosion energies, and the potentially long timescale for progenitor evolution. Although other compositions of WDs are possible (e.g. He-WD or O-Ne WDs), these are unlikely to be the progenitors of SNe Ia (Livio 2001). He-WDs produce too few IMEs in the SN explosion, and O-Ne WDs are likely not numerous enough to produce a sufficient number of SNe Ia to match the observed rate, and the explosion of an O-Ne WD may be more likely to result in accretion-induced collapse than thermonuclear runaway (Nomoto & Kondo 1991).

Progenitor Mass. Several models have been proposed in which SNe Ia arise from the explosion of WDs below M_{Ch} that ignite by an external trigger, typically a detonation in the surface He layer of the accreting WD (e.g. Weaver & Woosley 1980; Nomoto 1980). The He ignition drives a strong shock into the C+O layer, causing a secondary carbon detonation. The main advantages of these "sub-Chandra" models are the favorable binary population statistics (Yungelson & Livio 1998; Livio 2000) and the natural tunability of the initial WD mass to explain the observed SN Ia diversity (Ruiz-Lapuente et al. 1995). However, these models suffer severe disadvantages in that they predict spectra that are too blue and predict high-velocity Ni and He (rather than Si and Ca) in early spectra, contrary to observed SN Ia spectral features (Nugent et al. 1997; Höflich & et al. 1997). Though recent efforts by the MPA group (Fink et al. 2010; Kromer et al. 2010) have developed improved sub-Chandra models that effectively eliminate the He shell products in the SN Ia explosion, these models produce colors that are too red and spectra whose features do not fully match observations. Thus Chandrasekhar-mass SN Ia models are still preferred over sub-Chandra models for explaining the observed properties of SNe Ia.

Explosion Mechanism. There are several proposed explosion models to the describe the propagation of the flame in the exploding WD. In a detonation the nuclear burning front propagates faster than the local sound speed, while a deflagration is characterized by subsonic flame propagation. Full detonation models are generally disfavored as being inconsistent with SN Ia spectra (Hillebrandt & Niemeyer 2000) because they fail to produce sufficient amounts of IMEs (Arnett 1969, 1971). Pure deflagration models (Ivanova et al. 1974; Woosley et al. 1984) are still viable mechanisms, as are delayed detonation models (Khokhlov 1991; Woosley & Weaver 1994) in which the flame front begins as subsonic and then becomes supersonic during the SN expansion.

The SN Ia progenitor composition, mass, and explosion mechanism are all key inputs to hydrodynamical simulations of SN Ia explosions, which provide key predictions to be compared with observations. Though the precise values (and distributions) of these progenitor properties are still under investigation, an abundance of observational and theoretical work has significantly narrowed the viable SN Ia progenitor properties.

2.1.2 Binary Evolution and SNe Ia

There are currently two proposed binary evolution scenarios which may lead to a SN Ia. In the single-degenerate scenario (SD; Whelan & Iben 1973), the exploding WD reaches M_{Ch} by accreting material from a less evolved companion (either a main sequence or red giant star), while in the double-degenerate scenario (DD; Iben & Tutukov 1984) M_{Ch} is reached (and possibly exceeded) by the merger of two WDs which coalesce following orbital decay from gravitational radiation. The dynamical evolution of these two scenarios is very different, and thus will be described separately here.

Single Degenerate Evolution

In the SD scenario, the CO-WD (primary) star accretes material from its less evolved companion (secondary) star until it reaches M_{Ch} and undergoes thermonuclear runaway. One of the main advantages of this scenario is that it has a natural mechanism for producing the uniformity of SN Ia explosions by having a consistent means of reaching M_{Ch}. A major concern for this scenario is the large amount of unburned H and He material left in the system (from the secondary) at the time of the SN Ia explosion.

In the SD scenario, the secondary can either be a main sequence (MS) companion on a red giant (RG). This accretion period occurs when the secondary expands to fill its *Roche lobe*, the path on which the gravitational potential energy from the two stars is balanced and which crosses between the two stars. When material from the secondary overflows into this path, it can freely flow to orbit around the primary and eventually accrete onto the primary after losing some angular momentum to radiative cooling.

The material accreted onto the surface of the CO-WD primary is typically composed of unburned H and He from the secondary. In order to accumulate more CO material from this accretion process, the accreted H/He material undergoes nuclear burning on the surface of the WD. If the accretion rate is too high, the WD builds up a H- and He-rich envelope and develops structure more similar to a red giant star, and thus will lead to other evolutionary paths that do not produce SNe Ia (Nomoto 1982). If the accretion rate is too low, the hydrogen shell burning on the WD surface becomes unstable and results in He "flashes" which eject some material and make the net accretion efficiency lower. While this low accretion could still ultimately produce an SN Ia, its efficiency is much lower and likely to produce a much smaller fraction of SNe Ia observed today. Thus most SD SNe Ia are likely to originate from WDs whose companion accretion falls within a narrow range which is also a function of the initial WD mass (Nomoto 1982).

Thus an SD progenitor system must meet several key requirements to produce an SN Ia that we observe today. First, the system must be sufficiently massive to reach M_{Ch} even after mass loss episodes leading up to the final accretion stage. Secondly, the orbital separation must be sufficiently small to allow Roche lobe overflow to proceed when the secondary undergoes expansion (either as part of late MS or the transition to the RG phase). Thirdly, the combination of the Roche lobe overflow rate and the orbital separation (and also stellar metallicity) must produce an accretion rate that falls within the stable accretion range, as well as an accretion rate sufficient to drive the WD to M_{Ch} within a Hubble time.

Double Degenerate Evolution

In the double degenerate scenario, two CO-WDs in a binary system merge after orbital decay due to gravitational radiation. A major advantage for this scenario in explaining SNe Ia is the natural lack of unburned H and He material in the system. However, the large range of allowable progenitor system masses presents a challenge in explaining the uniformity of SN Ia brightnesses.

Though DD systems end up as two CO-WDs, several potential routes to this end state are possible. Initially the more massive of the two stars in the system (the primary) evolves off the main sequence to become a WD. When the less massive star (the secondary) evolves off the main sequence and begins to fills its Roche lobe, the outer H and He layers of the star are stripped in an episode known as a "common envelope" (CE) phase. This stripping of the outer layers of the secondary carries away a significant amount of angular momentum and the total system orbital separation decreases significantly.

All DD systems should undergo at least one CE phase, but the next stage of binary evolution is dependent on the masses and orbital separation of the binary after this first CE episode. Mennekens et al. (2010) describe two possible channels to SNe Ia from this stage. In the first, some steady mass transfer occurs between the WDs via Roche lobe overflow, and the WDs merge after a relatively long ($\sim$1 Gyr) time. In the second, an additional CE phase brings the WDs to extremely close orbital separations so that they merge on a very short ($\sim$100 Myr) time scale.

Alternatively, Blais & Nelson (2011) proposed a "single-CE" channel of the DD scenario in which the two stars in the DD system begin with very similar masses ($M_1/M_2 > 0.95$). The two stars evolve off the main sequence almost simultaneously and undergo a single very large CE episode. The remnant WDs then merge after the usual orbital energy dissipation via gravitational radiation.

SN Ia progenitor systems in the DD scenario then must originate from binaries where the initial masses and separation of the two stars produce a binary evolution which results in two WDs. These WDs must have sufficient mass to exceed M_{Ch} and must be separated by a distance sufficiently close so that they merge within a Hubble time. The requirements for DD progenitor systems are much more dependent on binary dynamical evolution (and stellar evolution of the individual stars) than potential SD progenitor systems.

Observational Predictions of SD vs. DD

The requirements for the SD and DD scenarios can be combined with binary population synthesis techniques to predict rates of SNe Ia in each scenario at a function of stellar age for a (theoretically) instantaneous burst of star formation. This rate versus age relationship is known as the SN Ia *delay time distribution* (DTD), and is one of the key predictions of any SN Ia model. The theoretical DTD can be compared to observations of the ages of SN Ia host stellar populations, which we will describe in detail in the next Section.

Signatures of the progenitor system in SN Ia observations are somewhat tenuously predicted by theories at this time, but several interesting possibilities have been proposed. A large amount of circum-stellar material (CSM) left in the vicinity of the SN Ia progenitor system would produce spectroscopic evidence of the SN ejecta interacting with the CSM, as well as possible light echoes at late times. However, this involves detailed mass loss estimates for the system prior to the SN itself, a very complicated and variable process.

An interesting observable signature expect for a SD system is partial occlusion of the SN due to the companion star being aligned along the observer's line of sight to the exploding WD. Kasen (2010) showed that MS companions in the SD scenario would produce only very modest changes to the SN Ia light curve and spectra which could be realistically detected only at very early times. However, they showed that an RG companion would produce fairly significant alteration of the early SN Ia light curves. Tucker (2011) and Hayden et al. (2010) examined light curves from the ESSENCE and SDSS-SN surveys, respectively, and found no clear detections of such signatures, indicating the WD+RG channel must produce at most a very small fraction (< 0.25) of the total SN Ia population.

2.1.3 Metallicity Effects in SNe Ia

The study of progenitor metallicity effects on the spectra and light curves of SNe Ia is an active field of research, with many theoretical predictions resulting from hydrodynamical explosion modeling. Hoeflich et al. (1998) produced a suite of SN Ia delayed detonation models in which they varied the pre-explosion heavy element abundances and inspected the resulting SN Ia spectra and light curves. They found only modest changes in the SN Ia spectrum in the optical but some increased variation in the near-UV, with the magnitude of these changes varying with the amount of mixing assumed for the ejecta. They also found that increasing the progenitor metallicity produced more ^{54}Fe in the SN explosion and thus less ^{56}Ni, resulting in a fainter SN Ia. The parametrized deflagration models analyzed by Lentz et al. (2000) at various metallicities produced stronger variations in the optical spectrum of SNe Ia than those found by Hoeflich et al. (1998), and resulted in UV variation opposite to that of the other study. As stated in Lentz et al. (2000), the uncertainty in hydrodynamical modeling and the strong blending of lines in SN Ia spectra make it very difficult to predict spectroscopic features that could be used for reliably measuring SN Ia progenitor metallicity. Thus while these models are greatly insightful for investigating the physics of SNe Ia, they are not yet predictive enough to provide observable measures of SN Ia progenitor metallicity.

Timmes et al. (2003, hereafter TBT) investigated the effect of progenitor metallicity in terms of the nuclear burning products, and found that a high abundance of neutron-rich ^{14}N from the CNO cycle in high metallicity WDs resulted in an overproduction of ^{58}Ni at the expense of ^{56}Ni, thereby decreasing the resultant SN brightness (note this is similar to the effect predicted by Hoeflich et al. 1998). Observational tests of this theory using host galaxy data have been conducted by several groups, and will be discussed in the next Section.

A popular interpretation of the observed correlation between (uncorrected) SN Ia brightnesses and the morphology (or mass) of their host galaxy is that this is the product of a progenitor age effect. More massive galaxies and earlier type galaxies tend to have much older stellar populations than less massive or later type galaxies. Thus it appears that younger stellar populations give rise to brighter, slower declining SNe Ia. The work of Umeda et al. (1999a) was partly motivated to explain this trend, and indeed reproduces the age-luminosity trend. In their models, older WDs have a lower C/O ratio (more C→O fusion has taken place) which results in a fainter SN Ia (due to less nucleosynthetic energy being available). This effect also has some modest dependence on the progenitor metallicity, which affects both the evolution timescale for the WD as well as its final C/O ratio.

A particularly interesting prediction for the effect of progenitor metallicity on the properties of SNe Ia is that of Kobayashi et al. (1998); Kobayashi & Nomoto (2009), who predict that

SNe Ia cannot occur below a metallicity of $[Fe/H] \lesssim -1.1$. In their model, SNe Ia form in the SD scenario where the WD undergoes stable accretion from its less evolved companion, and this accretion is stabilized by a steady outflow wind from the surface of the WD. Fe is the primary source of opacity in this wind, and if the metallicity is too low then the accretion rate is too high and becomes unstable, preventing the WD from successfully accreting enough material to reach M_{Ch}. Thus they predict a low metallicity threshold below which the SN Ia rate is decreased by several orders of magnitude (to effectively zero). Their model has important consequences for Galactic chemical evolution, as it provides a means for SNe Ia to start contributing Fe to the ISM much later than core collapse SNe contribute α-elements and thus explain the high $[\alpha/Fe]$ ratios found at low-metallicity ($[Fe/H] \lesssim -1$) in the Milky Way. More importantly for SN Ia cosmology, their model naturally predicts a decreased rate of SNe Ia at higher redshifts, an important consideration for planning of future high-redshift ground- and space-based SN Ia searches. Few SNe Ia have previously been found in galaxies whose metallicities could approach this threshold, but the sample of SNfactory found numerous SNe Ia whose hosts could potentially test this prediction, and we revisit this with our data in Section 5.3.

2.2 SN Ia Host Galaxies

The study of SN Ia host galaxies provides both indirect clues into the nature of SN Ia progenitors as well as a critical cross-check on potential biases in SN Ia brightness correction techniques. Correlations of observed SN Ia brightnesses with the properties of their host galaxies has yielded clues to the possible effect of progenitor age on SN Ia brightness, while correlation of the *corrected* SN Ia brightnesses with the properties of their hosts has illuminated a potential shortcoming in current SN Ia standardization techniques. The study of SN Ia rates as a function of host properties, as well as the distribution of SNe Ia within their hosts, have shown differing rates of SNe Ia at different progenitor ages, leading to measurements of the distribution of SN Ia progenitor ages.

2.2.1 SN Ia Brightnesses and Host Galaxy Properties

Early studies of SN Ia host galaxies found qualitative evidence for a correlation between the observed peak magnitude, light curve decline rate, and expansion velocity of an SN Ia with the morphological type of its host galaxy (Filippenko 1989; Branch & van den Bergh 1993; Hamuy et al. 1996). It was observed that brighter slower declining SNe Ia preferentially occur in later type (spiral and irregular) galaxies, while fainter slower declining SNe Ia preferentially occur in earlier type (elliptical and S0) galaxies. Similarly, the observed brightnesses of SNe Ia correlate with the stellar mass of their host galaxy (e.g. Howell et al. 2009), such that more massive hosts produce preferentially fainter SNe Ia. As the mean properties of stellar populations in galaxies vary along the morphological sequence as well as with stellar mass, these correlations provided indications that the properties of SN Ia progenitors affect the brightness of the SNe themselves. Though stretch-based luminosity corrections appear to account for this progenitor-driven luminosity dependence, concerns remain that the remaining scatter in SN Ia brightnesses could be caused by intrinsic SN Ia progenitor diversity that evolves with redshift.

As stated above, Timmes et al. (2003, TBT) predicted a decreased SN Ia brightness for

high metallicity progenitors, which could potentially introduce cosmological biases if it is present and not corrected for in SNe Ia. The TBT theory has been tested in observational SN Ia data sets at high redshift (Howell et al. 2009) and in the local universe (Neill et al. 2009). In both studies, the photometrically-estimated stellar mass of the SN Ia host galaxies was used as a proxy for metallicity by invoking the well-known mass-metallicity (MZ) relation (Tremonti et al. 2004; Lee et al. 2006). The ^{56}Ni masses were calculated by combining the peak bolometric SN Ia luminosity and its optical rise time using Arnett's Law (Arnett 1982). Though these authors found tentative evidence for a decrease in the average ^{56}Ni production (binned in host mass) in SNe Ia at high host metallicities, the scatter in ^{56}Ni was sufficiently large to be consistent with no trend.

Recent studies examining the correlation of SN Ia Hubble residuals with host galaxy mass (Kelly et al. 2010; Sullivan et al. 2010; Lampeitl et al. 2010) have detected evidence of correlations that could introduce subtle biases to the estimation of cosmological parameters. All of these studies found that the *corrected* brightnesses of SNe Ia (after stretch and color corrections) correlate with the stellar masses of their host galaxies. The popular interpretation of this result has been a possible residual correlation of SN Ia brightness with progenitor metallicity, perhaps caused by the TBT effect. Indeed, Kasen et al. (2009) examined the effect of including TBT in hydrodynamical explosion modeling of SNe Ia, and found that the stretch-luminosity relationship for high- and low-metallicity SNe Ia was different in a way which Sullivan et al. (2010) showed to be qualitatively consistent with their observations. The true origin of this correlation remains unknown, and is a key point of interest for study in this thesis (see Chapter 6).

2.2.2 SN Ia Rates and Host Galaxy Properties

The measurement of SN Ia rates as a function of the properties of their host galaxies is a powerful tool for constraining SN Ia progenitor models. In particular, the rate of SNe Ia in environments of different stellar ages provides information about the efficiency of SN Ia production as a function of stellar age, a key quantity predicted by many SN Ia models from stellar and binary evolution modeling. Below we briefly outline the method of measuring SN Ia rates, then discuss recent studies of SN Ia rates and the insight they have provided with regard to SN Ia progenitor models.

The general method for measuring SN Ia rates as a function of stellar mass or luminosity involves careful study of not only the host galaxies of those SNe Ia discovered, but also all field galaxies observed in the survey in which an SN could have been detected. For each observed galaxy, the SN Ia rate is derived from a quantity known as the control time (Zwicky 1942; van den Bergh 1991; Cappellaro et al. 1997; Leaman et al. 2011), which essentially captures the total time during which the SN could have been observed in that galaxy. This value is a function of the assumed SN luminosity function, the distance of the observed galaxy, and the limiting magnitude of the SN survey. For repeated observations where the observation interval is shorter than the maximum possible SN control time for that galaxy, the control time for that observation is then the interval between subsequent observations. Coupling this control time to the mass or luminosity of the galaxy and summing over the whole survey yields SN rates as a function of galaxy stellar mass or luminosity (see Leaman et al. 2011, for a thorough description). SN rates are typically reported in units of SNuX, the number of SNe per century per $10^{10} L_{\odot}$ in band X, or SNuM, the number of SNe per century per $10^{10} M_{\odot}$, while rates for an individual galaxy are typically reported in simple SNu (SNe per century). For a galaxy with the size and star-formation intensity of the Milky Way, the typical

SN Ia rate would be approximately 0.5 SNu (Li et al. 2011).

SN Ia rates studies from a few years ago discovered that the SN Ia rate is dependent on the properties of the SN Ia host galaxies. Mannucci et al. (2005) found that SN Ia rates in redder and earlier type galaxies were significantly lower than the rate in bluer later type galaxies. Similarly, Sullivan et al. (2006) showed that galaxies with a higher specific star formation rate (sSFR, the SFR per unit stellar mass) had higher SN Ia rates. These and other authors (Scannapieco & Bildsten 2005; Mannucci et al. 2006; Aubourg et al. 2008) interpreted these observations as an indication that SNe Ia arose from both old and young stellar populations. The rate of SNe Ia from old stellar populations (dubbed "tardy" or "delayed" SNe Ia) is proportional to the total stellar mass of the galaxy, while the rate of SNe Ia associated with young stellar populations (dubbed "prompt" SNe Ia) is proportional to the galaxy star formation rate. This was dubbed the two-component or "A+B" model by Scannapieco & Bildsten (2005) with a total SN Ia rate described by the equation:

$$\mathrm{SNR} = A \cdot M_* + B \cdot \mathrm{SFR} \tag{2.1}$$

where M_* is the total galaxy stellar mass, SFR is the galaxy star formation rate, and A and B are the rate constants for the two components. This relation is in fact a simplification of the more complicated effect of the SN Ia delay time distribution, which we discuss in the observational context below and revisit as part of the analysis in Chapter 5.

2.2.3 Observational Measurements of the SN Ia Delay Time Distribution

Perhaps the most effective constraints on SN Ia progenitors models have come from observational measurement of the SN Ia delay time distribution (DTD). The DTD represents the rate of SNe Ia as a function of time following an instantaneous burst of star formation. In theory the DTD is set by the physics of SNe Ia, specifically the stellar and binary evolution of the SN Ia progenitor system. In practice it is measured from the ages of SN Ia host galaxy stellar populations and the relative rates of SNe Ia at various progenitor ages. This is a complex procedure which we will briefly outline below, and present some of the recent measurements of the DTD and its constraining power on SN Ia progenitor models.

There are several practical methods for measuring the SN Ia DTD (see Maoz 2010, for a thorough review), all of which rely on the same underlying principles. The rate of SNe Ia in a galaxy as a function of time $R_{Ia}(t)$ is the convolution of the galaxy's star formation history $\psi(t)$ and the SN Ia DTD $\eta(t)$:

$$R_{Ia}(t) = \int_0^t \psi(t-\tau)\eta(\tau)d\tau \tag{2.2}$$

This illustrates the basic principle of measuring the DTD: one must measure the SN Ia rate and the star formation histories of the observed galaxies and from this information perform an effective deconvolution to recover the SN Ia DTD.

Early attempts to constrain the SN Ia DTD simplified the above problem by considering the SN Ia rate in broader age bins. Indeed the "A+B" formalism effectively splits the SN Ia DTD into two age bins such that the observed SN Ia rate today is proportional to the sum of the rate in old stellar populations ("A") multiplied by the total star formation in the old age bin (i.e. the total stellar mass M_*) and the rate in young stellar populations ("B") multiplied by the star formation rate in the young age bin (i.e. the current SFR). Implicit in this simplification is the assumption that the DTD

is only weakly varying over the whole age bin (which is not true, see below) and the coefficients "A" and "B" trace the average DTD value in their respective bins.

A slightly more sophisticated analysis in this spirit was conducted by Totani et al. (2008) who measured the rate of SNe Ia in elliptical galaxies as discovered by the the Subaru/XMM-Newton Deep Survey (SXDS). Here they used the mean stellar age of each galaxy in the survey to assign each galaxy to an age bin, and measured the SN Ia rate per unit mass for each bin. They found that a simple power law functional form for the SN Ia DTD with $\eta(t) \propto t^{-1}$ fit their data well.

Perhaps the first comprehensive SN Ia DTD analysis was conducted by Maoz et al. (2011), who measured the SN Ia DTD using SNe Ia discovered by the Lick Observatory Supernova Search (LOSS). Using spectra of the $\sim$15,000 galaxies in the LOSS survey, they used the code VESPA (Tojeiro et al. 2007) to derive the star formation histories of all galaxies in the LOSS survey. This measurement coupled with the SN Ia rates form the survey enabled a measurement of the SN Ia DTD. Their values, when coupled with other measurements (Maoz 2010), are consistent with a power law SN Ia DTD of $\eta(t) \propto t^{-1.1}$.

One very broad application of the general DTD method is to compare the global SN Ia rate as a function of redshift compared to the cosmic star formation history in order to derive the SN Ia DTD. Such an analysis was undertaken in Barbary et al. (2010), who derived the SN Ia rate at $0.9 < z < 1.45$ and used other SN Ia rates to constrain the form of the SN Ia DTD. Their results are consistent with a power law SN Ia DTD $\eta(t) \propto t^s$ with exponent $s = -1.3 \pm 0.5$, consistent with previous measurements.

Thus the measurement of the SN Ia DTD is a rapidly advancing field which shows promise for constraining SN Ia progenitor scenarios. Unfortunately, as often happens, many SN Ia progenitor models are now fine tuning the variable parameters of their models to match the observed SN Ia DTD. However, as observational constraints improve the DTD estimate, the DTD will continue to be a powerful tool for constraining SN Ia progenitors, especially when coupled with other observable SN Ia properties.

2.2.4 Spatial Distributions of SNe Ia in their Host Galaxies

While the study of global SN Ia host galaxy properties provides information about the statistical sample of stellar populations from which SNe Ia are drawn, the study of local stellar populations in the SN Ia vicinity (as compared to those across the whole galaxy) provides a more detailed picture of preferred SN Ia birth environments. Such studies are challenging, however, as they are limited by the spatial resolution of the SN Ia host galaxies, which typically limits such studies to very nearby SN Ia hosts. Below we will describe some results from such studies and how they have shed light on SN Ia progenitors.

Fruchter et al. (2006) and Kelly et al. (2008) conducted very similar analyses of the location of gamma ray bursts (GRBs) and SNe of all types within their host galaxies in order to compare the environment preferences of these various transients. In both studies, they used optical photometry of the transient hosts and rank-ordered the pixels within the galaxy by intensity. They then assigned a score to the transient based on the intensity of the pixel at the transient's location with respect to the total optical flux in the galaxy such that a score of 0 corresponded to the faintest galaxy pixel and a score of 1 the brightest, and a score of 0.5 meant that half the galaxy flux was contained in pixels of lower intensity than the pixel where the transient was located. They then

compared the cumulative distribution function of these scores for all transients of a given type and examined which transients had the most similar or dissimilar distributions. They found that SNe Ib/Ic and long-duration GRBs had similar distributions, while SNe Ia and SNe II exhibited clearly different distributions. While these analyses did not necessarily predict the progenitor mechanism for these transients, they did provide a meaningful comparison from which to asses progenitor similarities across transient types. Raskin et al. (2008) sought to make the connection between these SN location intensity distributions and the underlying progenitor mechanism (or more specifically the DTD). They generated several galaxy evolution models from which they computed the final galaxy optical density, and used various SN Ia progenitor delay times to predict the distribution functions of Fruchter et al. (2006) and Kelly et al. (2008). While they found that a single progenitor age was insufficient to reproduce the observed distribution, they demonstrated a means to connect such SN spatial distributions with progenitor models which could potentially be employed in future studies.

In a somewhat analogous work, James & Anderson (2006) examined similar rank-order pixel distributions for SNe of various types using Hα imaging to specifically trace galaxy star formation. For SNe Ia, they found a large fraction of SNe Ia were associated with regions of no star formation (score=0) while others were found in regions of star formation, even some in regions of very vigorous star formation (score$\approx$1). This observation gives qualitative support to the "A+B" model where some SNe Ia are born from very old stellar populations while others are born from very young stellar populations. Similarly, Förster & Schawinski (2008) examined the radial distribution of SN Ia locations in (morphologically) elliptical galaxies. They found that the distribution of SN Ia radii (as compared to the galaxy half light radius) was very consistent with a standard de Vaucouleurs (1948) profile, implying that SNe Ia in old stellar populations indeed trace the location of stellar mass in their host galaxies.

Chapter 3

SN and Host Galaxy Data

In this Chapter we describe the data used for the analyses in this thesis. First we describe the SNfactory experiment and the SN Ia data used in comparisons of SN Ia properties with the properties of their host galaxies. We then describe the host galaxy photometric data set, including our prescriptions for estimating galaxy stellar mass and star formation rate from photometry. Finally we present the host galaxy spectroscopy from which host redshifts and gas-phase metallicities are derived.

3.1 Supernova Sample: The Nearby Supernova Factory

The SNe Ia whose hosts are analyzed here were observed as part of the ongoing science operations for the Nearby Supernova Factory (SNfactory – Aldering et al. 2002). The SNfactory was designed to observe several hundred SNe Ia in the nearby smooth Hubble flow ($0.03 < z < 0.08$) with the goals of achieving a deeper physical understanding of SNe Ia, building better SN Ia templates for cosmological applications, and anchoring the low-redshift Hubble Diagram. The SNfactory conducted its own SN Ia search from 2004-2008 and discovered several hundred SNe Ia. Many of these SNfactory discoveries, as well as some publicly announced SNe Ia, were followed extensively using our custom instrument SNIFS to obtain flux-calibrated spectral time series. The details of these operations are described below.

3.1.1 SNfactory Search

From 2004 to 2008, the SNfactory conducted a wide-field search of the northern and equatorial sky using the QUEST-II CCD camera (Baltay et al. 2007) on the Samuel Oschin 1.2m Schmidt telescope on Mount Palomar, California, partly in collaboration with the JPL Near-Earth Asteroid Tracking (NEAT) component of the Palomar-QUEST consortium. Typical search images consisted of 60 s exposure with an RG610 filter, with each field revisited multiple times in order to detect asteroids (which we reject). The SNfactory search covered an average unique area of (on average) 600 deg^2 per night and covered over half the sky (≈20,000 deg^2) each year.

Search data was transferred from Palomar to the High Performance Storage System (HPSS) at the National Energy Research Scientific Computing Center (NERSC) in Oakland, California, via the wireless HPWREN network and the ESnet network. The images were then processed using the

Parallel Distributed System Facility (PDSF) at NERSC. Images were bias subtracted, flat fielded, and given astrometric solutions derived from matching field stars to the USNO-A1.0 POSS-E catalog (Monet 1996).

New search images and reference images were convolved to a common point spread function (PSF) and scaled in flux in order to perform direct image subtraction. Potential new source objects in subtraction images were identified automatically using our custom pipeline and ranked by a series of scores which were then passed to a boosted decision tree algorithm (Bailey et al. 2007). Those new objects which passed a cut based on their final boosted decision tree score were passed on to human scanners for visual confirmation of viable SN candidates. Typing of SN candidates and followup of known SNe Ia was conducted with our instrument SNIFS, which will be described below.

In 28 months of searching, the SNfactory discovered over 1000 supernovae of all types, and spectroscopically confirmed over 600 of those. A total of 396 SN Ia discoveries were spectroscopically confirmed, and SNe Ia discovered before B-band maximum light (as estimated by spectroscopic typing) were followed up extensively with SNIFS. In addition to those SNe Ia discovered by SNfactory, some SNe Ia discovered by other searches were followed with SNIFS. This work analyzes all SNe Ia discovered or followed by SNfactory, a total of 469 SNe Ia observed from 2004-2010.

3.1.2 SNfactory Followup: SNIFS

Spectroscopic typing of search candidates and followup observations of SNe Ia were obtained with the SuperNova Integral Field Spectrograph (SNIFS – Aldering et al. 2002; Lantz et al. 2004), mounted continuously on the University of Hawaii 2.2-m telescope on Mauna Kea. SNIFS is a custom built integral field spectrograph optimized for observing point sources on a diffuse background. Its $6'' \times 6''$ field of view (FOV) is broken into a 15×15 spatial grid by means of a micro-lens array (MLA) which focuses the light from each spatial element (spaxel) before passing it through a dispersing element. SNIFS has two spectroscopic channels which cover simultaneously 3200-5200 Å (blue) and 5100-10000 Å (red) with moderate resolution ($\sim$3 Å). Simultaneous to spectroscopic observations, the field surrounding the SN is monitored with the SNIFS photometric channel equipped with the SNIFS "multi-filter". The multi-filter is composed of filters of various pass bands spanning the full SNIFS spectroscopic range and is used to monitor field stars in order to simultaneously monitor atmospheric extinction, thereby enabling observations under non-ideal photometric conditions. SNIFS is also equipped with an internal calibration unit with arc lamps and continuum lamps, and observation of spectrophotometric standard stars are routinely used to derive accurate flux calibration for all observations.

The novel aspect of SNIFS is that it enables us to observe supernovae spectrophotometrically, meaning we obtain spectra derived from the full object source flux without suffering the usual slit loss of longslit spectroscopy. Our flux-calibrated spectral time series (an example of which is presented in Figure 3.1) then provide direct measurement of the SN Ia spectral energy distribution (SED) at multiple epochs. Classical photometry magnitudes for various filters (e.g. B, V, R) can be synthesized directly by convolving the filter throughputs with the observed SN SED. This is directly analogous to many stellar population synthesis analyses which use model stellar population SEDs convolved with filter throughputs to predict broadband magnitudes for comparison to observations. For our SN work, we measure the SED directly and synthesize magnitudes in order to apply the

standard SN Ia light curve analysis techniques. One major advantage of our approach is that we are able to circumvent the standard S- and K-corrections (see below). Additionally, the wealth of information contained in the spectral time series is unique in the field of SN Ia physics and provides insight into new ways to standardize SNe Ia. The unique science possible with the SNfactory data set will be described below.

3.1.3 SNfactory Light Curve Fits

The typical method for measuring cosmological distances with SNe Ia is to observe their light curves and compare their (stretch- and color-corrected) fitted peak brightnesses to their expected peak brightnesses. Here we will describe the general methods for doing so, and the specific light curve fitting implementation used by SNfactory.

Light Curve Fitting Techniques

To use an SN Ia for measuring cosmological distances, we must measure its peak magnitude (typically in B-band), light curve width, and color. These are typically derived by obtaining broadband photometry of the SN at multiple epochs and fitting for these parameters using a SN Ia light curve (LC) template. Probably the two most popular light curve fitting tools are MLCS (Riess et al. 1996; Jha et al. 2007) and SALT (Guy et al. 2005, 2007), which have very different treatments of SN Ia LCs that will now be briefly described.

The Multicolor Light-Curve Shapes (MLCS) method of fitting SN Ia photometry was first developed by Riess et al. (1996) and later refined into its modern form known as MLCS 2k2 (Jha 2002; Jha et al. 2007). This code assumes that the LC shape is a function only of a single width parameter Δ, and that variations in the color or SNe Ia are the result of obscuration by foreground dust which obeys the reddening law ($\mathcal{R}$) of CCM (Cardelli et al. 1989). Their model then is described by the equation:

$$m(t - t_0) = \mu_0 + M_0 + P\Delta + Q\Delta^2 + A_V\mathcal{R} \tag{3.1}$$

The template light curve shape (M_0, P, and Q) is derived from a set of training data (typically from low-redshift SNe Ia), and this template is then applied to observed SN Ia light curves to derive their decline rate Δm_{15} (defined as the decline in the SN Ia brightness in magnitudes from peak to 15 days after peak) and color (as parametrized by the visual extinction in magnitudes A_V).

The Spectral Adaptive Light-curve Template (SALT) method was developed by Guy et al. (2005, 2007) and uses a spectrophotometric SN Ia template. The template models the SN Ia spectral energy distribution (SED) as a function of phase p (date with respect to maximum light) according to the formula:

$$F(p, \lambda) = x_0 \times [M_0(p, \lambda) + x_1 M_1(p, \lambda) + ...] \times \exp[cCL(\lambda)] \tag{3.2}$$

where x_0 is related to the peak luminosity, c is the color parameter (defined by $B - V$ color at max), $CL(\lambda)$ is the color correction law, and the components M_i describe the SN Ia spectral template according to the components which encapsulate the most SN Ia variability. The parameter x_1 is ultimately very closely tied to LC width, and the color law corrects simultaneously for intrinsic color variations and extrinsic reddening due to dust (without distinguishing the two).

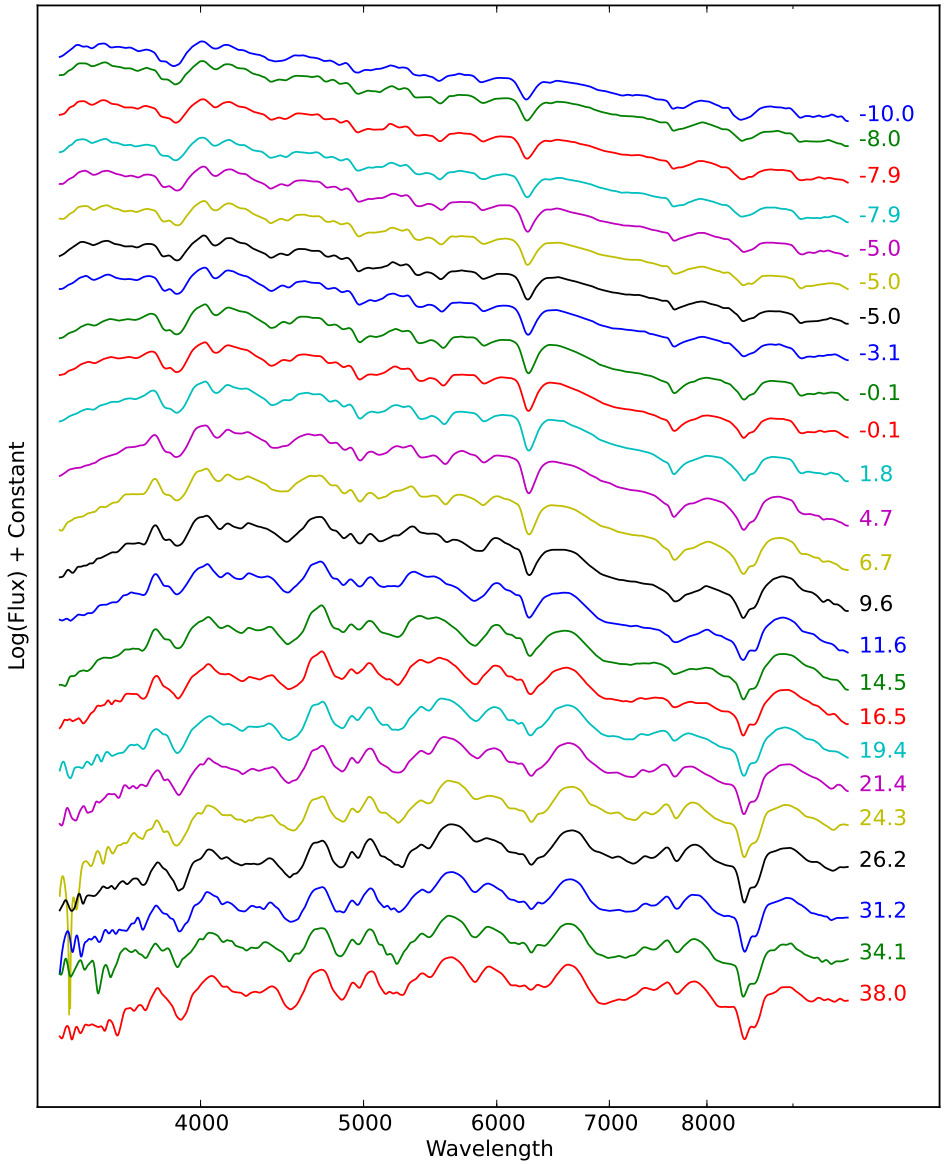

Figure 3.1 An example SNfactory spectral time series, here for the SN Ia SNF20080514-002.

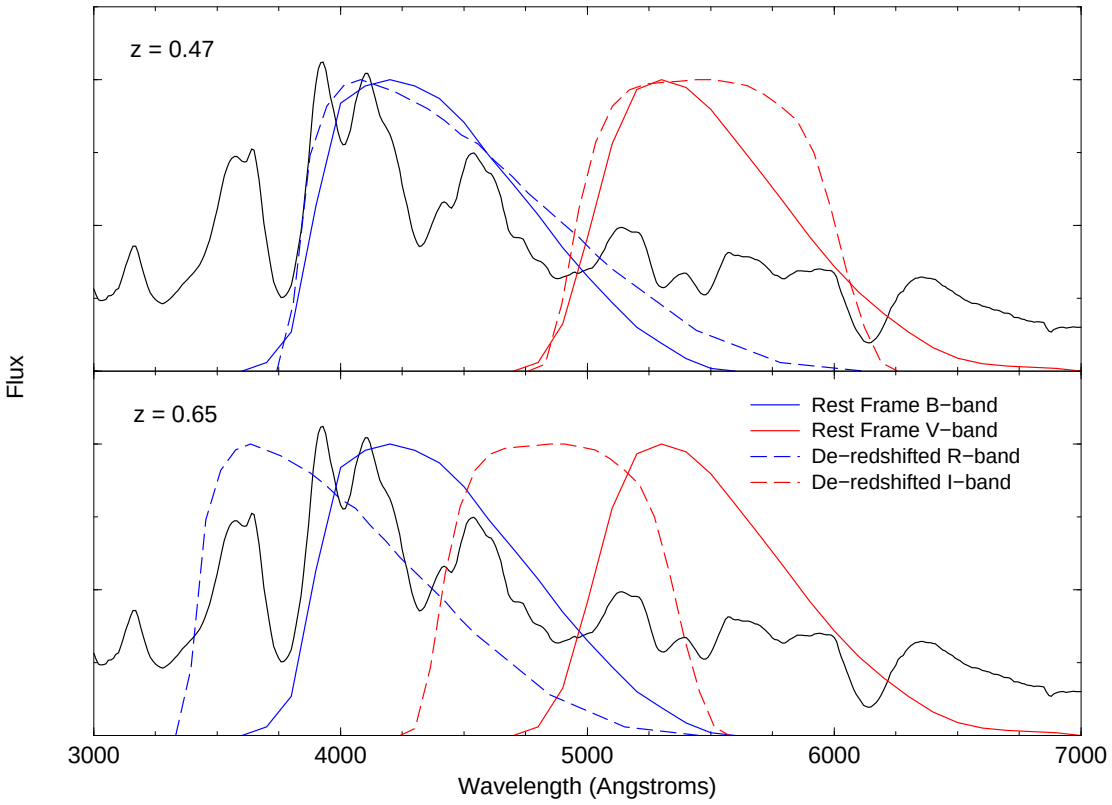

Figure 3.2 Example K-Corrections from Nugent et al. (2002).

K-Corrections and S-Corrections

When using SN Ia data to constrain cosmological parameters, complications arise from the inhomogeneities between and within SN Ia data sets due to different instrument throughputs and different SN redshifts. When SNe are at different redshifts, the same observer-frame filter samples different parts of the SN SED in its rest frame. This is illustrated in Figure 3.2, taken from Nugent et al. (2002), which shows how the sampling of filters at certain redshifts approximate (or don't) those of different filters in rest-frame. In the first example shown (top panel), the R- and I-band filters sample the SED of a supernova at redshift $z = 0.47$ in a very similar way to rest-frame B- and V-band filters. Thus comparing the fluxes in these redder bands for the high-redshift SN to the blue bands of low-redshift SNe is likely to suffer from only minor systematic errors. The situation in the lower panel is precisely the opposite: the redder filters in observer-frame sample regions of the SN SED that fall between the bluer filters in rest-frame.

The standard method used to correct this effect is to employ what are known as cross-filter K-corrections (**?**Kim et al. 1996; Nugent et al. 2002). In this technique, an assumed form of the SN SED is convolved with the filter throughputs in rest frame and observer frames to estimate the amount of flux that would have been measured in the desired rest-frame filter (i.e. B or V from the previous example) given a flux measured in the observer-frame filter (R or I above). Analytically

K-corrections take the form:

$$K_{xy} = -2.5\log\left(\frac{\int \lambda Z(\lambda) S_x(\lambda) d\lambda}{\int \lambda Z(\lambda) S_y(\lambda) d\lambda}\right) + 2.5\log(1+z) - 2.5\log\left(\frac{\int \lambda F(\lambda) S_x(\lambda) d\lambda}{\int \lambda F[\lambda/(1+z)] S_y(\lambda) d\lambda}\right) \tag{3.3}$$

where $F(\lambda)$ is the assumed form of the SN SED, $Z(\lambda)$ is the SED of some zeropoint source whose colors are (by construction) equal to 0, and $S_x(\lambda)$ and $S_y(\lambda)$ represent the throughputs of the rest frame (B/V) and observer frame (R/I) filters respectively.

A subtler variation of this principle takes the form of what is known as an S-correction (Suntzeff 2000). This term is calculated to account for the differing instrument throughputs for the same fiducial filter. For example, the transmission profiles of the optics in different telescopes is almost certain to be different, so even filters with the same coatings will produce different overall throughput when considered with the instrument. The analytical correction works exactly the same way as for cross-filter K-corrections.

SNfactory Light Curves

SNfactory SN Ia light curves are synthesized from flux calibrated spectral time series in three filters approximating the same wavelength ranges as the standard Bessel B, V, and R filters. These filters, labeled B_{SNf}, V_{SNf}, and R_{SNf} are simple boxcar functions in wavelength. The synthesized photometry points (and filter throughputs) are analyzed using SALT2 to derive the B-band peak magnitude (m_B), stretch (x_1), and color (c) for each SN Ia. An example SNfactory SN Ia LC and its best SALT2 fit (and 1σ errors) are shown in Figure 3.3.

Cosmological analyses then use the observed distance modulus ($\mu_B = m_B - M_B$) and redshift values compared to those predicted by a set of cosmological parameters. The difference between the observed brightness of an SN Ia and that predicted by the best fit cosmology is known as the *Hubble residual* and is defined as:

$$d\mu_B = m_B - M_B - \mu(z; H_0, \Omega_M, \Omega_\Lambda) \tag{3.4}$$

After application of empirical corrections for light curve stretch and color, the corrected Hubble residuals are:

$$d\mu_{B,corr} = d\mu_B + \alpha \cdot x_1 - \beta \cdot c \tag{3.5}$$

In this (and most other) cosmological analysis, a combined minimization procedure is conducted to minimize the sum of the corrected Hubble residuals. The best fitting values of H_0, Ω_M, Ω_Λ, M_B, α, and β are found by this minimization procedure, and final Hubble residuals are computed using these values. Since SNfactory cosmology results are still being developed, the cosmological parameter values used here (and in our previously published analyses) are derived from SNfactory data alone and left blinded.

3.1.4 SNfactory Science

The novel spectral time series data of SNfactory has enabled scientific analyses involving both SNe Ia with interesting spectroscopic behavior, as well as investigation of new techniques for standardizing SNe Ia for cosmology.

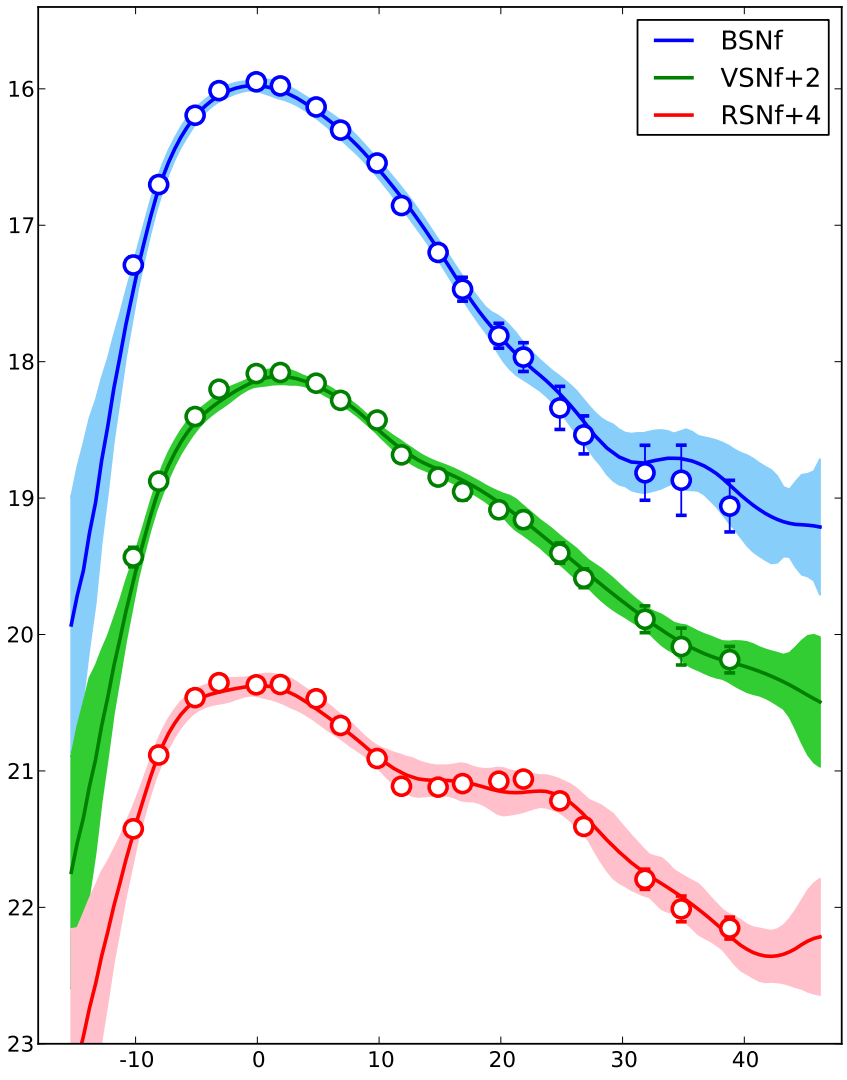

Figure 3.3 An example SNfactory light curve synthesized from an SNfactory time series, again for SNF20080514-002. The three filters shown here are labeled B_{SNf}, V_{SNf}, and R_{SNf}. These filters have similar wavelength coverage to the standard Bessel BVR filters, but are idealized filters with a boxcar throughput function. The solid lines are the best fit SALT2 LC template synthesized for the same three filters. The filled bands correspond to the 1σ errors on the best fit LC template.

SNfactory observations of several unique SNe Ia have provided new insight into the nature of SNe Ia. In Aldering et al. (2006), we analyzed the spectral time series of SN 2005gj, a unique SN Ia with clear IME absorption features but with unusual Hα emission. We showed that this emission is very likely to be a signature of interaction of the SN ejecta with a circum-stellar medium (CSM), which due to its high electron density we argued could potentially be left over from the WD's accretion disk. Our early spectra of SN 2006D (Thomas et al. 2007) showed unambiguous detection of carbon absorption features, indicating the presence of unburned carbon not consumed during the SN Ia explosion. This result has important implications for the amount of mixing in the SN Ia ejecta and possibly also the nature of the explosion mechanism. Our spectroscopy and photometry of SN 2007if (Scalzo et al. 2010) provided strong evidence that this SN Ia originated from a progenitor system whose mass significantly exceeded M_{Ch}, and the study of its young low-metallicity host galaxy (Childress et al. 2011) provided constraints on both the age and metallicity of its likely progenitor system (and was one of the projects comprising this thesis – see Chapter 4).

The unique nature of SNfactory data allows the investigation of alternate SN Ia brightness standardization techniques using the full SN Ia SED. Our first such analysis was presented in Bailey et al. (2009), where we investigated the use of spectral flux ratios as an SN Ia standardization parameter in the same sense as stretch and color in the traditional SN Ia cosmology technique. We showed that the ratio of SN Ia fluxes at two wavelengths as measured from a single SN Ia spectrum could standardize SN Ia brightnesses to better than 0.13 mag (RMS of Hubble residuals, equivalent to 7% in distance), an improvement over the usual stretch- and color-corrected brightnesses which typically achieve about 0.16 mag precision (8% distance). This standardization technique will be revisited below in our investigation of SN Ia Hubble residual correlations with the properties of their host galaxies (Chapter 6).

One of the major frontiers in SN Ia standardization today is the separation of intrinsic SN Ia color from extrinsic reddening due to dust. The SNfactory data set enabled us to conduct a unique investigation of this effect in Chotard et al. (2011). In that analysis, we derived empirical linear correction factors for the brightnesses of SNe Ia at ALL wavelengths (i.e. spectral correction laws) using the equivalent widths of the Si II λ4131 and Ca II H&K SN Ia spectral absorption features. This effectively removed the influence of light curve width (via Si II) and intrinsic color (via Ca II) on the brightnesses of SNe Ia, and also allowed us to determine a spectroscopic color law for extrinsic reddening due to dust (which we found to be close to the Milky Way reddening law).

3.1.5 SNfactory Host Galaxy Sample

The full sample of SNe Ia discovered by the SNfactory provides a unique advantage in the study of SN Ia host galaxies because the nature of the SNfactory search provided an impartial sample of SN Ia environments. Here we will discuss some of the advantages of the SNfactory host galaxy sample in the study of SN Ia progenitors and environments.

The SNfactory was the first large area nearby SN survey employing CCDs that did not specifically target known galaxies. Thus the parent sample of galaxies targeted in the SNfactory search is representative of a normal field galaxy sample found from any random patch of sky. Thus our sample of SNe Ia is likely to be the sample with the least amount of bias against selection by host properties.

The discovery efficiency of SNfactory was determined to be very good. The ability of our search algorithms to detect new objects was rigorously tested by injection of artificial SNe into

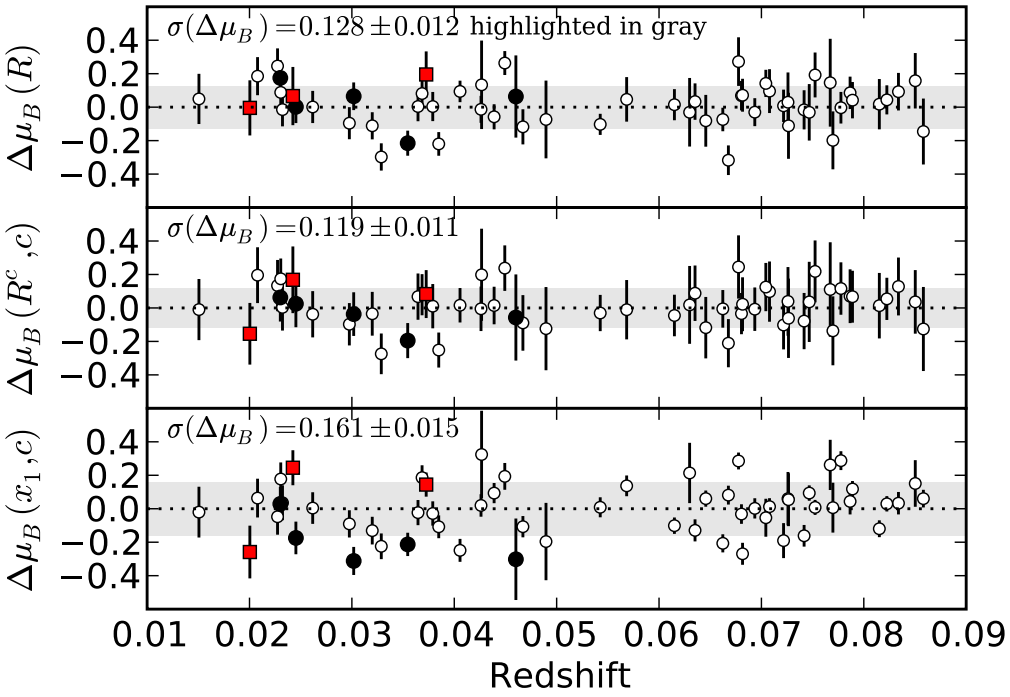

Figure 3.4 From Bailey et al. (2009), Hubble residuals for SNfactory SNe Ia using several standardization techniques: (top) single flux ratio corrections, (middle) flux ratio and color corrections, and (bottom) standard stretch and color corrections. Single flux ratios alone produce better Hubble residuals than standard techniques, and the inclusion of a color correction further improves the SN Ia standardization.

search images which were then run through the same object detection code as the true search data. We found our detection efficiency to be very high across the full range of galaxy sizes and types, with only a marginal decrease in efficiency in the bright cores of some galaxies. This likely results in a minimal reduction in sample completeness since the number of SNe directly on the galaxy core is likely to be small. We also checked the efficiency of our boosted decision tree algorithm to select viable SN candidates by inspecting those candidate objects which slightly missed the boosted decision tree cut. We found that the vast majority of these objects were image artifacts, and the fraction of objects which might have warranted human scanning was very small.

Our prioritization of search candidates for spectroscopic screening was performed by a skilled set of scientists, all of whom were either PhDs or graduate students, with no undergraduate students or citizen scientists performing any of the "scanning" work. Furthermore, an analysis of the rate at which search candidates were sent for spectroscopic followup showed no statistically significant differences between 6 SNfactory scanners. Thus our followup prioritization was of a high, uniform quality.

Of particular interest for some of our host studies (Section 5.3) is the efficiency of finding SNe Ia in low luminosity galaxies. In this regime, one possible source of concern could be the potentially lower followup prioritization for SNe without a clear host compared to those with clear galaxy associations. This is unlikely to be a major problem, as SNfactory found a significant number of SNe Ia and core-collapse SNe in low luminosity hosts. Specifically, we found a fair number of SNe whose low luminosity hosts were not clearly visible in the shallower search images but were identified later with deeper imaging (see Section 3.2). Similarly, we found a number of previously unknown cataclysmic variable stars, whose search images were clearly not associated with a host galaxy and showed no detectable object in reference images at the candidate location. Moreover, we also found a surprising fraction of SNe Ia with no identifiable hosts even with significantly deep imaging (see Section 5.3.2), so the lack of clear hosts in search data did not prevent us from classifying objects found in our search.

However, we must note that one possible source of missed SNe in low luminosity hosts could come from misclassification of faint blue hosts as QSOs by SDSS. It is a known problem for high redshift QSO target selection that low redshift blue dwarf galaxies have similar colors and apparent magnitudes and thereby contaminate these samples. One cause for rejection of SNfactory search candidates was if they occurred on a galaxy classified as a QSO by SDSS, so in principle some SNe Ia in nearby blue dwarfs could have been rejected for this reason. However, we have a log of all these instances and work by other in the SNfactory collaboration is currently underway to assess this potential bias. We do note that this would only have been an issue for SNe in the SDSS (pre-BOSS) field, which covered about half of the SNfactory search area. Thus this cannot have removed all possible SNe in faint hosts, and is likely to have impacted only a small fraction of possible SNf.

We showed above that the overall search efficiency of SNfactory was tested to be very high. This implies that the sample of SN Ia host galaxies from SNe Ia discovered by SNfactory is likely to be very close to an unbiased representation of the true distribution of SN Ia hosts. This provides unique advantages in the study of SN Ia progenitors, which we will particularly exploit in Chapter 5.

3.2 Host Galaxy Photometric Data

Photometric data for SNfactory SN Ia host galaxies was gathered from public sources as well as targeted observations. Optical photometry was collected from the Sloan Digital Sky Survey (SDSS York et al. 2000) Eighth Data Release (DR8 Aihara et al. 2011). NIR images from 2MASS (Skrutskie et al. 2006) were obtained at the NASA/IPAC Infrared Science Archive (IRSA[1]). UV data were obtained from the GALEX online data archive at MAST[2].

The public photometric coverage of our hosts was very good. Roughly 75% of our hosts fell within the SDSS photometric footprint (with a significant number added with the BOSS imaging footprint added in DR8), 95% have 2MASS data, and 85% have GALEX AIS (All-Sky Imaging Survey - a shallow imaging survey) images. Additionally, about 20% of our host have deeper GALEX imaging, mostly from the MIS (Medium Imaging Survey). The typical photometric depth for these surveys (for this work, this limit is effectively where the flux errors reach 5-10%) are 20th magnitude for SDSS, 17th magintude for 2MASS, 19th magnitude for GALEX AIS, and 21st magnitude for GALEX MIS.

For those hosts without optical photometry from SDSS, we used our instrument SNIFS in imaging mode to obtain optical images. SNIFS was also used to obtain deeper photometry for those faint hosts whose SDSS images were not deep enough (typically for $m_g > 19.0$). For some hosts, g-band photometry was obtained with Keck LRIS prior to spectroscopic observations of the hosts, and was later zero-pointed to either SDSS or SNIFS photometry.

Below we describe our reduction of the SNIFS photometry, our method of combining multi-band imaging data to obtain accurate common aperture photometry, and the means of deriving galaxy stellar masses and star formation rates from photometry. A mosaic image of several SNfactory host galaxies is shown in Figure 3.5, utilizing both SDSS and SNIFS optical data and spanning a large range (4 orders of magnitude) of stellar masses.

3.2.1 SNIFS Photometry

For those hosts without publicly available optical photometry from SDSS, or those faint hosts for which the photometric depth of SDSS was insufficient, we obtained optical photometry using the SNIFS instrument in imaging mode. The photometric imager (P-channel) on SNIFS consists of two 2k$\times$4k E2V CCDs, with one "guider" chip undergoing fast continuous readout to perform guiding during observations, and the other "science" chip dedicated to photometry. In normal SNIFS SN Ia observation mode, the P-channel uses our custom "multi-filter" (see description above). The SNIFS P-channel is also equipped with a variety of broadband filters covering the full science chip, including the standard Gunn $ugriz$ filters employed by SDSS. Because the SNIFS P-channel CCDs are different from those on the SDSS imager, the effective SNIFS filter throughputs vary slightly from those of SDSS. We show in Figure 3.6 the fiducial SNIFS filter throughputs derived from the throughput of all the optical components involved and our Mauna Kea extinction curve (Buton et al., in prep.) compared to the SDSS filter throughputs.

SNIFS images were processed in IRAF[3] using standard techniques. Overscan subtraction

[1] http://irsa.ipac.caltech.edu

[2] http://galex.stsci.edu

[3] IRAF is distributed by the National Optical Astronomy Observatory which is operated by the Association of Universities for Research in Astronomy, Inc., under cooperative agreement with the National Science Foundation.

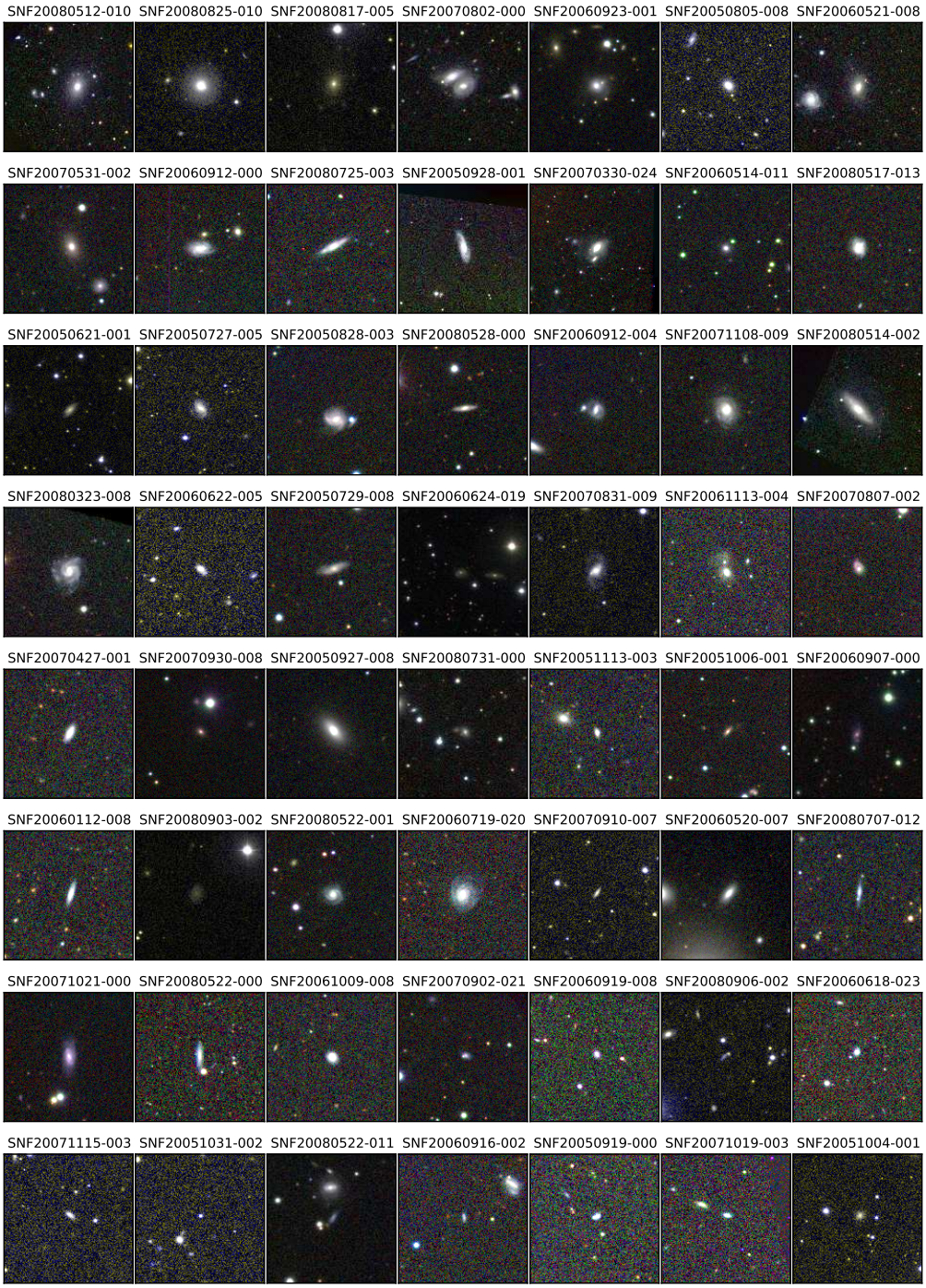

Figure 3.5 A subsample of the SNfactory host galaxies, presented in gri color composites. Galaxies are order by stellar mass from highest (upper left) to lowest (lower right).

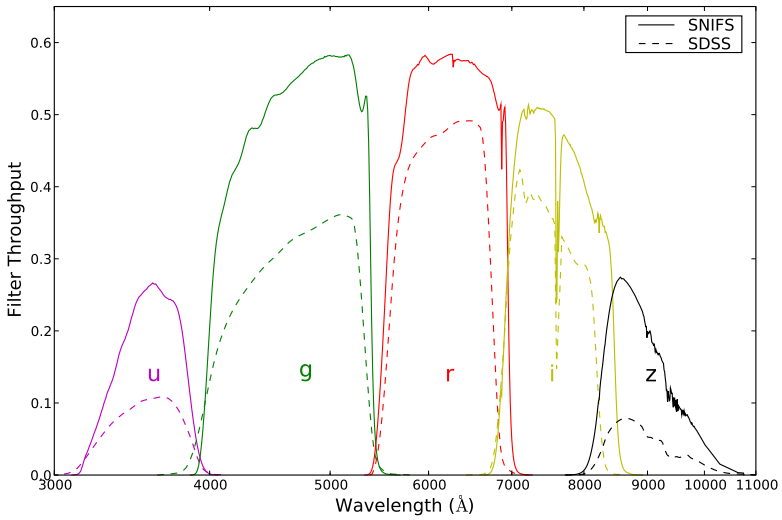

Figure 3.6 SNIFS filter throughputs, compared to those of SDSS.

was performed for both amplifiers on the science chip, and data from each amp scaled by its gain. Images were trimmed to remove occultation by the filter casing, then divided by normalized flatfield dome images to remove pixel variations in detector efficiency. For the reddest filters (i- and z-band), fringe patterns were removed by scaling a master fringe frame to the fringing measured in sky pixels for each science image. Master fringe frames were constructed from numerous long exposures, and identification of sky pixels and fringe scaling were performed using custom software. Cosmic rays were then removed using `LA Cosmic` (van Dokkum 2001). Astrometric solutions for all images were derived using `WCSTools` (Mink 2006), then refined using `SCAMP` (Bertin 2006) matching to 2MASS (Skrutskie et al. 2006). Images from fields with multiple exposures were combined with `SWARP` (Bertin et al. 2002) using median addition.

The observing priorities for the SNIFS host photometry program were to obtain g-band and i-band photometry of all our hosts. The optical $g - i$ color is a very good color for determining mass-to-light ratios (Gallazzi & Bell 2009) and thus serves as a minimal filter set for obtaining accurate galaxy masses. Many observations were taken between the Seventh Data Release (DR7 Abazajian et al. 2009) and Eighth Data Release (DR8 Aihara et al. 2011) of SDSS, which added a significant area to the SDSS imaging footprint. Thus we have a large number of fields observed in the SDSS footprint, especially in g and i, and with many of those observed on photometric nights when photometric calibration solutions were derived. This enables both the study of SNIFS-SDSS color terms as well as an independent measurement of the accuracy of our photometric calibrations, and we describe these two studies below.

Photometric zeropoints for imaging in the SDSS footprint were obtained by matching photometric measurements of field stars from each science image to their values in SDSS DR8. Formal zeropoints and their uncertainties were derived as the weighted mean (weighted by photometric error) of the zeropoints for individual field stars after the exclusion of severe outliers. In

Table 3.1 we summarize the total number of fields visited in each band, the average zeropoint error for a given field, and the total number of stars matched over all fields. Most of our zeropoints are derived from ≈ 30 field stars and have an accuracy of 0.01-0.02 mag.

As stated above, the filter throughputs from SNIFS differ slightly from those of SDSS, so we might expect small but nonzero color terms between the two filter sets. We can measure these from the same field stars used for zeropointing SNIFS photometry in the SDSS footprint. To do so, we compare the residual magnitude offsets (after application of the fitted zeropoint) of these field stars as a function of their color (as measured by SDSS). We derive the weighted mean offsets in bins of color (typically 0.2 mag wide) and perform a minimization to derive the optimal color term and its uncertainty for each filter. These are summarized in Table 3.1. As can be seen, the color terms are consistent with zero for all of the filters except i-band, which has a small but significant detection of a color term. This may be due to the different amount of water vapor at the SNIFS site (Mauna Kea) compared to the SDSS site (Apache Peak), or may be due to the slightly different red wavelength roll-off of the filter throughputs.

Table 3.1 SNIFS color terms

Filter	N_{fields}	N_{stars}	$\langle\sigma_{ZP}\rangle$	Color Term	Color
u	9	192	0.0185	-0.0009 ± 0.0269	$u-g$
g	160	4914	0.0094	0.0004 ± 0.0087	$g-r$
r	12	790	0.0109	0.0014 ± 0.0104	$g-r$
i	157	12452	0.0143	-0.0222 ± 0.0115	$r-i$
z	12	1068	0.0294	0.0081 ± 0.0561	$i-z$
g	–	–	–	-0.0010 ± 0.0044	$g-i$
i	–	–	–	0.0099 ± 0.0056	$g-i$

Photometric zeropoints for fields outside the SDSS footprint were derived for each observing night in each passband using observations of standard stars spanning a large range of airmasses. Our standards were selected from the Smith et al. (2002) sample, placing our measurement on the standard $ugriz$ system employed by SDSS. For each night (in each filter) we fit for a global zeropoint and an atmospheric extinction term, and our extinction terms were consistent with predicted by the fiducial Mauna Kea extinction curve (C. Buton & SNfactory, in prep.). Typical dispersion of standard star magnitudes about the best fit calibration solution were about 0.02 mag in gri and 0.03 mag in u and z. New science images were assigned a zeropoint based on their airmass and exposure time as calculated with the fitted extinction solutions.

As stated above, a number of the fields for which we obtained new zeropoints were included in the subsequent SDSS data release, enabling us to derive external zeropoints to cross-check our calibration solutions. We compared the SNIFS-based zeropoints to those derived by matching to SDSS and found good agreement (mean zeropoint offsets less than about 0.005 mag) with a dispersion consistent with the dispersion seen in our calibration solutions (about 0.02-0.03 mag). Since the SDSS zeropoints are more precise, we use those in favor of SNIFS zeropoints where available.

3.2.2 Host Galaxy Common Aperture Photometry

With the final processed SNIFS imaging and public data from SDSS, 2MASS, and GALEX, we obtain magnitudes for our hosts in each band by performing common aperture photometry. We

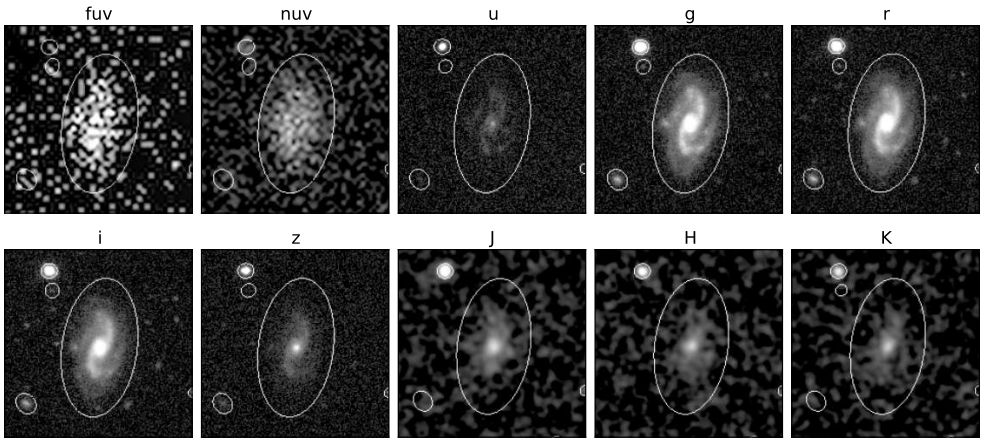

Figure 3.7 Example of common aperture photometry for the host of SNF20060609-002, showing the resampled images in each band and the photometric aperture.

use the g-band image to define the galaxy aperture, then measure the host flux in each band by resampling the image to the resolution of the aperture image using `SWARP` and running `SExtractor` (Bertin & Arnouts 1996) in dual image mode. We use the `SExtractor` `FLUX_AUTO` output parameter, which measures the flux inside an elliptical Kron-like aperture, and derive final magnitudes and their errors using the zeropoints and noise characteristics for each image. Finally we convert all magnitudes to the AB systems by applying Vega-AB offsets for 2MASS magnitudes (SDSS and GALEX zeropoints are already on the AB system). Observed magnitudes were then corrected for foreground Milky Way reddening using the dust maps of Schlegel et al. (1998) and the reddening law of Cardelli et al. (1989). An example of our common aperture photometry method is shown in Figure 3.7.

3.2.3 Host Galaxy Masses and Star-Formation Rates from Photometry

Calculation of galaxy stellar mass and star formation rate from photometry requires the use of stellar population synthesis (SPS) techniques. The basic principle involves using model stellar population spectral energy distributions (SEDs) to predict the flux in various photometric filters, then comparing these model predictions to observations. SPS techniques typically combine model SEDs for stars of a single age with masses distributed according to some initial mass function (IMF), thereby deriving the SED for what is known as a simple stellar population (SSP) of uniform age and metallicity. Full galaxy SEDs are calculated by preparing a model star-formation history (SFH) and convolving the SSP SEDs with the relative weights prescribed by the galaxy SFH.

The field of galaxy stellar population synthesis is a rich and constantly evolving field. The best SPS models require stellar evolutionary tracks as well as observed (and modeled) stellar SEDs spanning the full parameter space of stellar evolution. While most SPS techniques give very similar results, it is important to understand and track the differences between SPS techniques employed by different authors. Perhaps the two most popular sets of models in the past decade have been

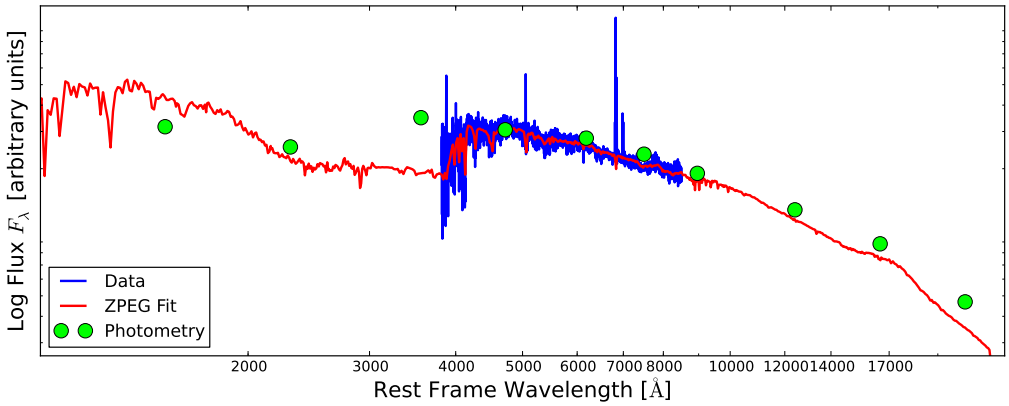

Figure 3.8 Example ZPEG fit for the host of SNF20060609-002. The blue curve is the observed galaxy spectrum from SDSS; the green points represent photometry measurements from GALEX, SDSS, and 2MASS; and the red curve is the SED for the best fit PEGASE model as chosen by ZPEG.

GALAXEV (Bruzual & Charlot 2003, hereafter BC03) and PEGASE (Fioc & Rocca-Volmerange 1997). Most of the major galaxy evolution analyses from SDSS employed the BC03 models (Kauffmann et al. 2003; Brinchmann et al. 2004; Tremonti et al. 2004). Many SN Ia host galaxy studies from recent years (Sullivan et al. 2006; Howell et al. 2009; Neill et al. 2009; Kelly et al. 2010; Sullivan et al. 2010; Lampeitl et al. 2010) have made use of PEGASE, but fortunately these models give consistent results when scaled appropriately (see, e.g., Kelly et al. 2010).

In particular, these SN Ia host studies employ the code ZPEG (Le Borgne & Rocca-Volmerange 2002), which matches observed photometry to the PEGASE models for a user-input set of galaxy evolution scenarios. Though designed primarily as a tool for deriving photometric galaxy redshifts, ZPEG inherently derives galaxy masses and star-formation rates by choosing the appropriate model SED to scale to the observed galaxy photometry. For consistency (and simplicity), we also employ ZPEG to derive galaxy stellar masses and SFRs from photometry. We show in Figure 3.8 an example ZPEG fit to the photometry of an SNfactory host. The SFRs reported here are the average SFR over the last 0.5 Gyr of the galaxy SFH.

The Effect of Uneven Photometric Coverage

Because our host galaxies do not all have the same set of photometric filters, it is vital to ensure that this uneven coverage does not bias our results. To this end, we computed ZPEG masses and SFRs for our hosts using different subsets of filters: (i) ALL available filters, (ii) optical filters only (no UV/NIR), and (iii) g- and i-band only, as this pair of filters comprised our minimum required filter set. We show in Figure 3.9 the comparison of galaxy stellar mass and SFR values for these subsets of filters. It is evident from these plots that even the minimal filter set provides a consistent value of the mass and SFR. This is because the photometric colors are very effective at distinguishing between evolutionary scenarios, which set the mass-to-light ratio and SFH of the best fit model.

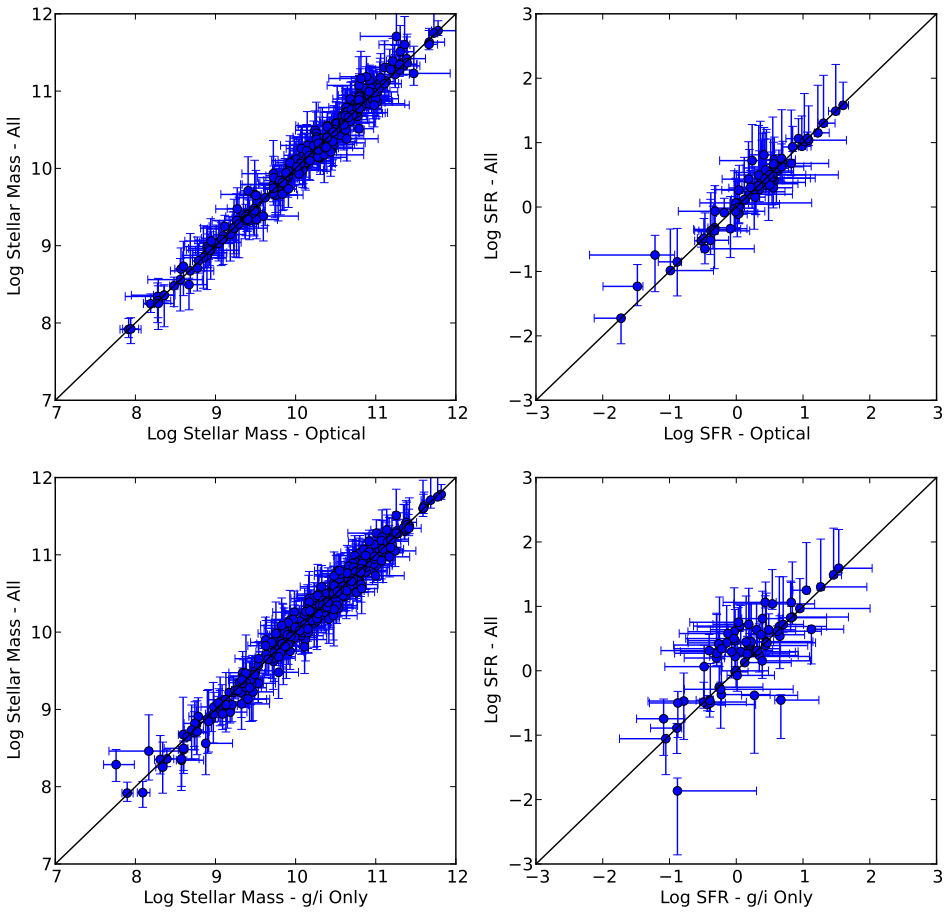

Figure 3.9 Output ZPEG stellar mass and star-formation rate values for various filter sets. The top left shows the comparison of stellar masses derived using all available photometry versus that obtained with only optical filters, while the top right is the analogous comparison of SFRs. The bottom two plots offer the same comparisons, but for the galaxy parameters derived using only g and i band.

Limitations and Future Work

It is important to note the limitations of the code ZPEG in its derivation of galaxy physical parameters. While this code has become popular in the supernova community (probably due to its ease of use), it was originally designed as a means of deriving photometric redshifts. The code chooses between several (user-input) galaxy evolution scenarios and determines which scenario best fits the observed photometry. Doing so requires scaling of the model SED to the observed photometry, which amounts to a measurement of the galaxy mass. The galaxy specific star-formation rate (sSFR – the SFR per unit mass) is essentially set by the chosen evolutionary scenario, and the total SFR is thus the input sSFR scaled by the measured mass. The errorbars reported by ZPEG for the mass and SFR are determined only from how well the photometry matches the best-fit SED, and does NOT include systematic uncertainties due to how well the photometry constrains the galaxy star formation history (SFH). Thus the errorbars from ZPEG for galaxy mass and SFR underestimate the full mass and SFR uncertainty, but at least accurately reflect the photometric measurement uncertainty propagated to those physical parameters.

A more detailed study of the galaxy mass and SFR uncertainty requires fitting the observed galaxy photometry to a large suite of SPS models spanning a large range of galaxy SFHs. Such a study is currently underway and we hope to have results to present soon. However, since these uncertainties do not enter significantly into the analyses in this thesis, we use the values derived by ZPEG for the work presented here.

3.3 Host Galaxy Spectroscopic Data

Galaxy spectroscopy is useful for gaining finer insight into the galaxy SED than can be gleaned from broadband photometry. In particular, absorption features in the stellar continuum of the galaxy SED can be compared to stellar evolution models to estimate stellar age and metallicity, while narrow emission lines from ionized HII regions surrounding young stars can yield both gas-phase metallicity of the galaxy interstellar medium (ISM) as well as the current rate of star formation. Additionally, reddening in the galaxy ISM and near the ionized HII regions can be estimated from galaxy spectra. In this Section we describe both the SNfactory host galaxy spectroscopic data set as well as the extraction of galaxy physical parameters from these data.

3.3.1 SNfactory Host Spectroscopy Observations

Longslit spectra for our SN Ia host galaxies were obtained during numerous observing runs at multiple telescopes from 2007-2011. The instruments used were the Kast Double Spectrograph (Miller & Stone 1993) on the Shane 3-m telescope at Lick Observatory, the Low Resolution Imaging Spectrometer (LRIS – Oke et al. 1995) on the Keck I 10-m telescope on Mauna Kea, the R-C Spectrograph on the Blanco 4-m telescope at Cerro Tololo Inter-American Observatory, the Goodman High Throughput Spectrograph (Clemens et al. 2004) on the Southern Astrophysical Research (SOAR) 4-m telescope on Cerro Pachon, and GMOS-S (Davies et al. 1997) on the Gemini-S 8-m telescope on Cerro Pachon. The instrument configurations, including wavelength coverage and effective resolution, are presented in Table 3.2.

Table 3.2 Instrument Configurations

Instrument	Dichroic/ Filter	Disperser	Slit (arcsec)	Wavelength Coverage (Å)	Effective Resolution (Å)
Kast blue	d55	600/4310	2.0	3900-5550	3.1
Kast red	d55	300/7500	2.0	5450-10500	9.1
LRIS blue	D560	600/4000	1.0	3500-5600	3.9
LRIS red	D560	900/5500	1.0	5500-7650	4.2
Goodman HTS	GG385	300 l/mm	1.0	3850-7700	13.7
R-C Spec	GG385	300/7500	1.0	3850-7700	9.1
GMOS-S	GG455	B600	1.5	5040-7920	6.8

Spectroscopy Reduction

Longslit spectra were reduced in IRAF using standard techniques. After overscan subtraction, we subtracted bias frames from two-dimensional longslit data, removed cosmic rays using `LA Cosmic` (van Dokkum 2001), and flatfielded to remove pixel variations in detector efficiency. Two-dimensional wavelength solutions were derived from arc lamp exposures taken either at the same pointing as the object spectrum (for Shane, Blanco, and SOAR data) or using nightly arc lamp exposures (for Keck and Gemini-S data), with a one-dimensional shift applied by measuring atomic (OI) night sky lines in object spectra. Object spectra were reduced to one dimension using the IRAF function `apall`, and nightly flux calibrations were derived from standard stars observed at appropriate ranges of airmass. Telluric absorption features were then removed using the nightly standard star spectra. Observer motion with respect to the heliocentric frame was then corrected, and finally spectra were dereddened to correct for Milky Way extinction using the dust maps of Schlegel et al. (1998) and the reddening law of Cardelli et al. (1989).

Some hosts had spectra available from SDSS DR8 (Aihara et al. 2011). These spectra were downloaded and then converted to air wavelengths for consistency with reduction of our own observations.

3.3.2 Redshifts and Emission Line Fluxes

SN Ia host galaxy redshifts, metallicities, Hα star-formation rates, and internal reddening were calculated using emission line fluxes from the host galaxy spectra. Accurate measurement of emission line fluxes in star-forming galaxies requires proper accounting for stellar absorption. To this end we fit the emission line fluxes and stellar background in each host spectrum simultaneously using a modified version of the IDL routine `linebackfit` from the `idlspec2d`[4] package developed by the SDSS team. This routine allows the user to provide a list of template spectra fit in linear combination with Gaussian emission line profiles. We have modified this code to force the background coefficients to be non-negative and fit for internal reddening in the host (using a CCM

[4] http://spectro.princeton.edu/idlspec2d_install.html

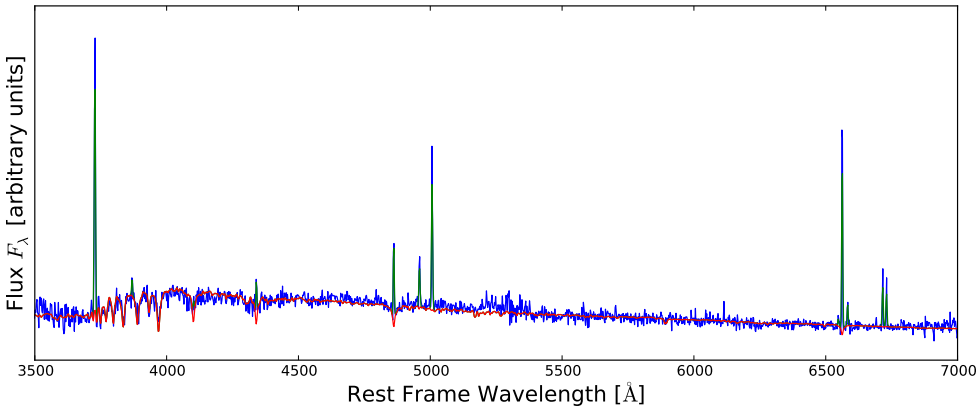

Figure 3.10 An example of our fits to galaxy spectroscopy, here for the host of SNF20080908-000 which was observed with LRIS on Keck. The blue curve is the data, the green is the stellar continuum fit, and the red is the fitted emission line profiles.

law with $R_V = 3.1$ with $E(B-V)$ as a fit parameter). Additionally, we have incorporated the ability to fit for a scaling factor between the blue and red channels of two-arm spectrograph data. For background templates we chose a set of simple stellar populations (SSPs) from the stellar population synthesis code GALAXEV (Bruzual & Charlot 2003, BC03) with a Chabrier (2003) IMF and the same time sampling used for background fitting used by Tremonti et al. (2004, T04), which ultimately consists of ten SSPs for each metallicity track. These templates are convolved to the resolution of the particular spectrograph whose data we fit. We note that the use of Salpeter (1955) IMF templates results in negligible differences to the fitted emission line fluxes, and metallicity difference smaller than our typically quoted precision of 0.01 dex. An example fit to spectroscopic data is shown in Figure 3.10

To ensure that our modifications of the code are not producing anomalous results, we compared our fitted emission line fluxes to those derived by the MPA-JHU team for those hosts whose spectra were obtained from SDSS. In Figure 3.11, we plot these values and show that our results are very consistent with those derived by other authors. Thus we believe our emission line flux estimates (including the resultant corrections for continuum absorption) are accurate.

Redshifts for SNfactory host galaxies with strong emission lines were derived as the weighted (by measurement uncertainties) mean of individual emission line redshifts fitted from host spectra. Redshift errors were similarly calculated from the measurement uncertainties on the individual line redshifts. This method is the same as that used by SDSS. For hosts with very weak or no emission lines, redshifts were calculated with a cross-correlation technique using the methods presented by Tonry & Davis (1979). We correlated the best fit stellar continuum spectrum against the observed host spectrum after subtraction of the fitted emission line fluxes. Typical redshift errors for these two methods are of the order $\sigma_z \sim 0.0001$.

Finally, emission line fluxes were corrected for internal reddening within the host galaxy by employing the Balmer decrement method. In an HII region ionized by young stars, the ratio of emission line flux in the Hα line to that in the Hβ line is fixed by atomic physics (with

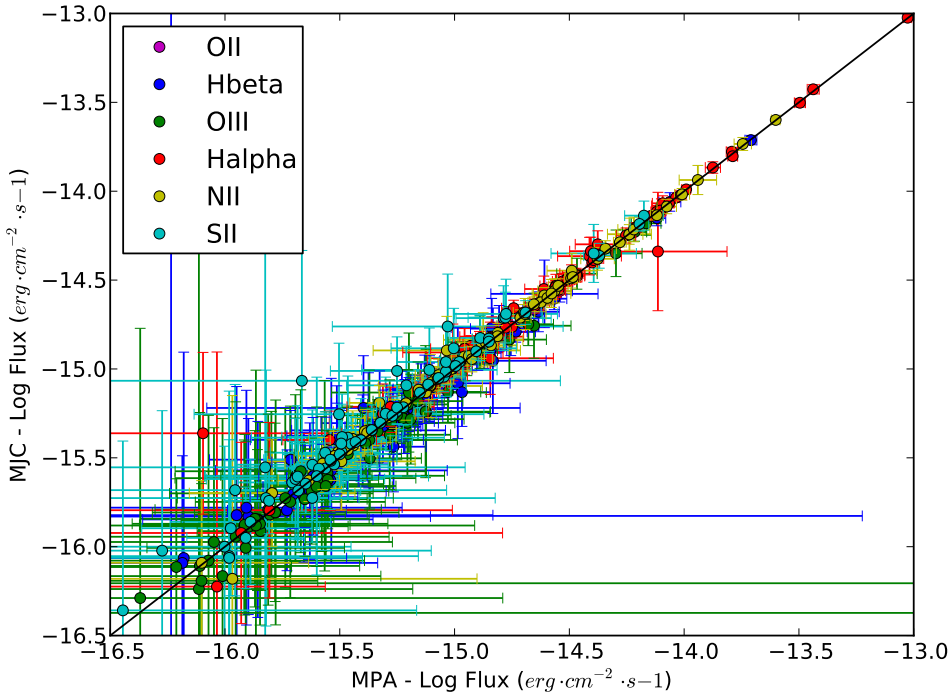

Figure 3.11 A comparison of the fitted emission line fluxes from my modified emission line fitting code (y-axis) vs. the values derived by the MPA-JHU team (x-axis). Points are color coded by emission line, and the line representing unity is the solid black line.

a dependence on the temperature of the gas, which is typically consistent with 10,000 K) to be $F(H\alpha)/F(H\beta) = 2.87$ under Case B recombination (Osterbrock & Ferland 2006), and is known as the Balmer decrement. Reddening by dust causes the observed value of this flux ratio to exceed its canonical value, and one can calculate the amount of reddening by assuming a reddening law such as that of Cardelli et al. (1989). Final emission line fluxes used for calculations of gas-phase metallicity and star-formation rate (from Hα) have been corrected for the internal reddening calculated using this method.

3.3.3 Host Gas Phase Metallicities

Translating emission line fluxes into a gas-phase metallicity depends on the choice of metallicity calibration, as thoroughly describe by Kewley & Ellison (2008). Different calibrations are known to disagree by as much as ~ 0.5 dex, which makes it difficult to place metallicity measurements on a common absolute scale. Additionally, there is no single metallicity metric that is ideal across the entire range of metallicity probed by our sample. For example, metrics that rely on the NII λ6584 line, such as Kewley & Dopita (2002) and Pettini & Pagel (2004) methods, have high signal-to-noise at high metallicity and are monotonic, but at low metallicities this line becomes very weak and produces large errors in metallicity measurements. Additionally, nitrogen at low metallicity saturates at its primary value (Nava et al. 2006) and thus loses sensitivity as a metallicity indicator. The well-known R23 metric (e.g. McGaugh 1991; Zaritsky et al. 1994; Kobulnicky & Kewley 2004) is double-valued with metallicity, and is shallow-sloped at low metallicity (i.e. flux errors propagate into larger metallicity errors). At low metallicities, the preferred metallicity calibration is the T_e(OIII) method (Aller 1984), which relies on the auroral λ4363 oxygen line. This method is considered the most reliable, but relies on a very weak emission line and does not consistently agree with the empirical strong-line methods.

Thus it is challenging to find a consistent metallicity calibration that has high sensitivity over the full observed range of galaxy gas-phase metallicities. Additionally, the lack of consistency of absolute metallicity scales between various calibrations makes it difficult to compare reported metallicity values from numerous authors. In order to utilize the strongest available lines and place our measurements on a well-known common scale, we employ different calibrations at different scales and then place all our metallicities on the common Tremonti et al. (2004) scale using the conversion formulae presented in Kewley & Ellison (2008). For galaxies with $\log(NII/H\alpha) > -1.3$ (i.e. "high" metallicity galaxies), we use the "N2" method of Pettini & Pagel (2004), as NII is a sensitive metallicity indicator in this range and has relatively low sensitivity to both reddening (due to the short wavelength baseline) and the ionization parameter of the HII gas. For very low metallicity galaxies with $\log(NII/H\alpha) < -1.3$, we use the "R23" method of Kobulnicky & Kewley (2004) (as updated by Kewley & Ellison 2008), as this method depends on the relatively strong oxygen lines and also fits iteratively for the ionization parameter. Although the R23 metric is doubly valued with metallicity, the choice of our $\log(NII/H\alpha)$ cut places these galaxies firmly on the low-metallicity "branch." Metallicities calculated from these original methods are finally converted to the T04 scale. It is worth noting that the dispersion in the conversion formulae of Kewley & Ellison (2008) is analogous to the systematic uncertainty in the metallicity calibrations themselves. Thus unless otherwise noted, all metallicities reported here are on the T04 scale after application of the above described conversion.

Finally, we employ a cut in our metallicity calculations that excises those galaxies whose

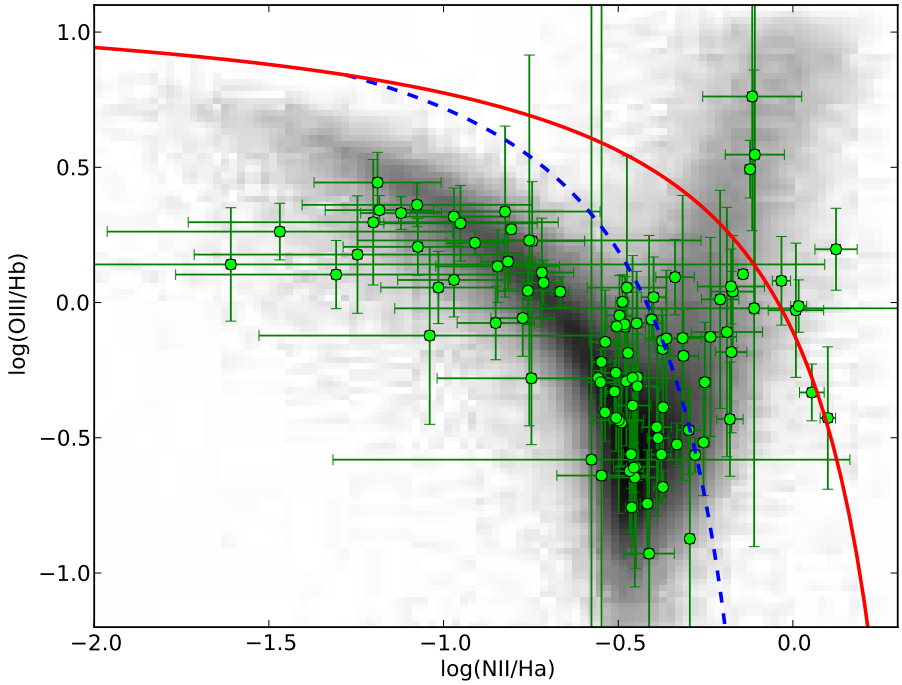

Figure 3.12 SN Ia hosts from SNfactory in the BPT diagram. The diffuse grey background represents SDSS galaxies whose emission line fluxes were measured by the MPA-JHU team. Galaxies above the solid red line are classified as "AGN" galaxies, those below the dashed blue line are "star-forming" galaxies free of AGN contamination, and those galaxies between the two lines are classified as "composite" galaxies.

emission line fluxes are contaminated by AGN activity using the emission line diagnostic diagram of Baldwin et al. (1981, hereafter BPT). In Figure 3.12, we plot the distribution of SNfactory emission line host galaxies on the BPT diagram as compared to the distribution of galaxies from T04, with the boundaries defined by Kewley et al. (2006) to distinguish normal star-forming galaxies from AGNs and composite galaxies.

Chapter 4

The Host Galaxy of SN 2007if

Outliers from the typical SN Ia luminosity distribution present an opportunity to explore the underlying physical mechanism in these systems, and provide a critical cross-check for possible "contamination" of future high-redshift SN Ia surveys focusing on the normal SNe Ia. Recently a potential new subclass of exceptionally overluminous SNe Ia has been discovered, starting with the prototype SN2003fg (SNLS-03D3bb Howell et al. 2006), followed by SN2006gz (Hicken et al. 2007), SN 2007if (Scalzo et al. 2010; Yuan et al. 2010). and SN2009dc (Tanaka et al. 2010; Yamanaka et al. 2009; Silverman et al. 2011; Taubenberger et al. 2011). Howell et al. (2006) were the first to suggest that this new subclass of overluminous SNe Ia are likely the product of super-Chandrasekhar-mass (SC) progenitors systems where substantially more material than M_{Ch} undergoes thermonuclear runaway, producing more ^{56}Ni (see e.g. Raskin et al. 2010) and resulting in a much more luminous explosion. This interpretation is difficult to reconcile with the traditional SN Ia progenitor scenarios in which the SN itself is triggered as the WD approaches M_{Ch}. In the SD scenario where accretion onto the WD is posited to be steady and stable, an accumulation of significantly more mass than M_{Ch} is highly unlikely (Piro 2008). In the DD scenario, the merger of two WDs whose total mass exceeds M_{Ch} (even by a significant amount) is a natural occurrence, and has made this scenario a favored framework for interpreting the origin of super-Chandrasekhar SNe Ia. There are concerns, however, that the merger of two WDs could result in accretion-induced collapse rather than thermonuclear runaway (e.g. Nomoto et al. 1995). Independent constraints on the probable progenitor properties of SC SNe Ia are therefore critical for unraveling the mystery surrounding these exceptional SNe.

In this Chapter we present our analysis of the host galaxy of SN 2007if. SN 2007if is particularly interesting among this new subclass of probable super-Chandrasekhar SNe Ia, as it has been shown to be the most luminous SN Ia ever discovered, with a peak V-band magnitude of $M_{V,07if} = -20.4$ (Scalzo et al. 2010) – nearly a full magnitude brighter than the average SN Ia luminosity of $M_{V,Ia} \sim -19.5$ (Leibundgut 2000). SN 2007if is also interesting for its extremely faint host galaxy ($M_g \sim -14.5$), which we will show below is the lowest-measured metallicity SN Ia host galaxy known. Our data provide important constraints on possible progenitor scenarios for SN 2007if, and indicate this exceptional SN is likely to have been born from a young, low-metallicity progenitor.

4.1 SN 2007if Host Observations

SN 2007if was discovered by the ROTSE-III supernova search (Akerlof et al. 2007) on 2007 August 16.3 UT, and independently by the Nearby Supernova Factory (SNfactory, Aldering et al. 2002) as SNF20070825-001 on 2007 August 25.4 UT (see Scalzo et al. 2010, for details). Located at α_{2000} = 01:10:51.37, δ_{2000} = +15:27:39.9, SN 2007if showed no apparent host in search reference images, or in images from the Sloan Digital Sky Survey (SDSS; York et al. 2000). Our deep co-add of NEAT + Palomar-QUEST search data showed a potential host at $m_i \approx 23.3 \pm 0.4$ (Nugent 2007), which at the estimated redshift of SN 2007if would make its host galaxy (hereafter HOST07if) one of the faintest SN Ia hosts ever discovered, suggesting very low metallicity.

HOST07if was observed with the Low Resolution Imaging Spectrometer (LRIS, Oke et al. 1995) on the Keck I 10-m telescope on Mauna Kea on 2009 August 23 and 24 UT. We employed the Keck-I atmospheric dispersion corrector (ADC; Phillips et al. 2006). On 2009 August 23.6 five exposures of 100 s duration were obtained in imaging mode using the blue camera of LRIS equipped with a g-band filter. The images were dithered to allow rejection of cosmetic defects, cosmic rays, and to provide image coverage across the detector gap. These images were combined to form a deep image of HOST07if and assess the potential for spectroscopic observation. On the following night (2009 August 24.6 UT) five additional imaging exposures of 100 s duration were obtained in g-band to provide additional photometric depth, then the target was aligned on the slit in imaging mode and the instrument configured for spectroscopic observations. The blue side was configured with the 600 l/mm grism blazed at 4000 Å, covering 3500-5600 Å, and on the red side the 900 l/mm grating blazed at 5500 Å was employed, covering 5500-7650 Å. The D560 dichroic beamsplitter was used, and no order-blocking filters were necessary. A $1''$ slit was oriented at a position angle of 128° along the apparent major axis of HOST07if, which fortuitously was only a few degrees away from the parallactic angle. Our final co-added LRIS image for HOST07if is shown in Figure 4.1, along with an overlay of the slit. Analysis of the acquisition and slit images show HOST07if to be aligned on the center of the slit to within 1 pixel ($0\farcs27$). The chosen slit gave resolutions of $\lambda/\Delta\lambda \sim 1000$ (4.4 Å) and ~ 1600 (4.1 Å) for the blue and red sides, respectively. Four spectroscopic exposures of 900 s duration were obtained, starting at airmass 1.00 and ending at airmass 1.02. The Keck-I ADC was employed, so we expect no chromatic slit loss due to atmospheric differential refraction. Processing of the photometry and spectroscopy are described below.

Spectroscopy

The LRIS spectra were reduced in IRAF using standard techniques. Overscan subtraction was performed for each of the four amps, and the data were mosaiced to form individual two-dimensional frames with data from each amp scaled by its gain. We subtracted bias frames from these data, removed cosmic rays using `LA Cosmic` (van Dokkum 2001), and removed pixel variations in detector efficiency by dividing images by wavelength-normalized flat field dome lamp exposures. The two-dimensional wavelength solution for the blue channel was derived from nightly arc lamp exposures with a linear shift in wavelength applied by measuring the [OI] $\lambda5579$ atomic night sky line. This linear shift was verified by cross-correlation of the sky spectrum with a high-resolution night sky spectrum from Hanuschik (2003). For the red channel, two-dimensional wavelength solutions for object exposures were derived from night sky lines in the object exposures, while for standard stars we used nightly arc lamp exposures with a wavelength shift determined

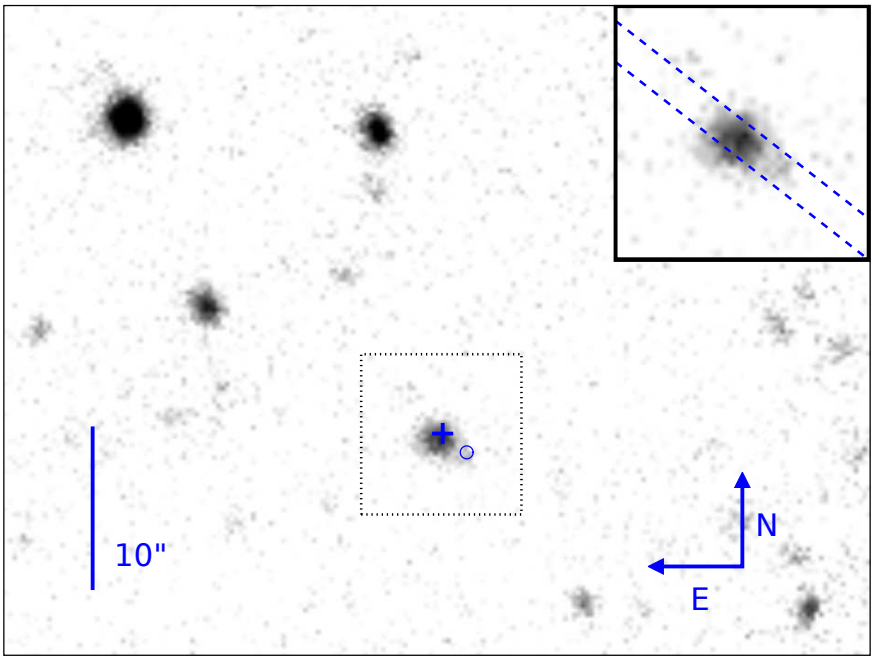

Figure 4.1 Keck LRIS image of HOST07if. The blue cross denotes the location of the supernova. For reference, the "bright" field star in the upper left has magnitude $m_g = 21.1$. The area immediately around HOST07if, denoted by the dotted box, is shown in the upper right inset along with the slit location shown as the dashed lines. The high-redshift background galaxy appears just to the southwest of HOST07if, and its location is marked by the thin blue circle.

from [OI] $\lambda\lambda 6300, 6364$ sky lines. Object spectra were reduced to one dimension using the IRAF function `apall`, and nightly flux calibrations were derived from standard stars observed at appropriate ranges of airmass. Telluric absorption features were then removed using the nightly standard star spectra. Finally, the spectrum was corrected for observer motion with respect to the heliocentric frame, and the Galactic reddening of the spectrum was corrected using the Cardelli et al. (1989) law and the value $E(B-V) = 0.079$ (Schlegel et al. 1998).

The two-dimensional spectrum of HOST07if showed the presence of a background galaxy separated from HOST07if by $1\farcs9$ and displaying a strong [OII] $\lambda\lambda 3727, 3730$ doublet at $\lambda\lambda 7537, 7543$ Å, corresponding to $z = 1.02$. Correction for this object in photometric measurements will be described below. We show portions of the background-subtracted 2D red side spectroscopy image in the top panel of Figure 4.2 to show the offending emission lines from the high-z object. The lower panel of the same figure shows the wavelength-collapsed spatial profile of the 2D blue side spectroscopy image along with the chosen extraction aperture. Based on profile fits to the two objects, we estimate the possible contamination of the extracted HOST07if spectrum by the high-z object to be less than 0.5% at all wavelengths (except at the high-z [OII] doublet position, which does not affect any emission line measurements for HOST07if).

Photometry

LRIS blue channel photometry was processed in IRAF. Overscan subtraction and mosaicing were performed in the same manner as for the spectroscopy, except that blank pixels were inserted between data from the two detectors to account for the physical gap between the two chips. The images were flat-fielded using g-band dome flats taken earlier in the night. Astrometric solutions were derived using `WCSTools` (Mink 2006), then refined using `SCAMP` (Bertin 2006) matching to 2MASS (Skrutskie et al. 2006). Individual exposures were combined with `SWARP` (Bertin et al. 2002) using median addition, and with proper de-weighting of the detector gap regions and weighting of images by exposure time. With the 5×100 s exposures of 2009-08-23 UT, 5×100 s exposures of 2009-08-24 UT, and the 4×60 s exposures used for target alignment, the total imaging time at the target location is 1240 s.

The photometric zeropoint for the target was derived by matching objects in the field to SDSS (York et al. 2000) photometry. We extracted magnitudes for all objects in the field using `SExtractor` (Bertin & Arnouts 1996) using the `MAG_AUTO` output parameter, which measures the flux inside an elliptical Kron-like aperture. We then matched objects in our field to the SDSS DR7 (Abazajian et al. 2009) `PhotoObjAll` g-band model magnitudes, ensuring the photometry was clean and the objects were primary targets (`mode=1`). Given the depth of the LRIS imaging, targets brighter than $m_g \sim 16.5$ saturated the detector, so we chose the bright magnitude limit of our catalog matching to be $m_g \sim 17.0$. The SDSS g-band completeness limit is estimated at $m_g \sim 22.2$ with deviation from Poggson magnitudes beginning at about $m_g \sim 22.6$ (Stoughton et al. 2002), so we conservatively chose a magnitude limit of $m_g \sim 22.0$ for our catalog matching. We therefore calculate the photometric zeropoint using the error-weighted mean of $N = 20$ objects between $17.0 < m_g < 22.0$ and find $m_{ZP} = 32.59 \pm 0.04$.

The raw instrumental g-band magnitude for HOST07if was observed to be $m_{g,inst} = -9.38 \pm 0.03$. Combined with the SDSS zeropoint and error, we determined the raw g-band magnitude of HOST07if as observed with LRIS to be $m_g = 23.21 \pm 0.05$. The Galactic reddening of $E(B-V) = 0.079$ (Schlegel et al. 1998) results in a g-band extinction of $A_g = 0.34$. In our

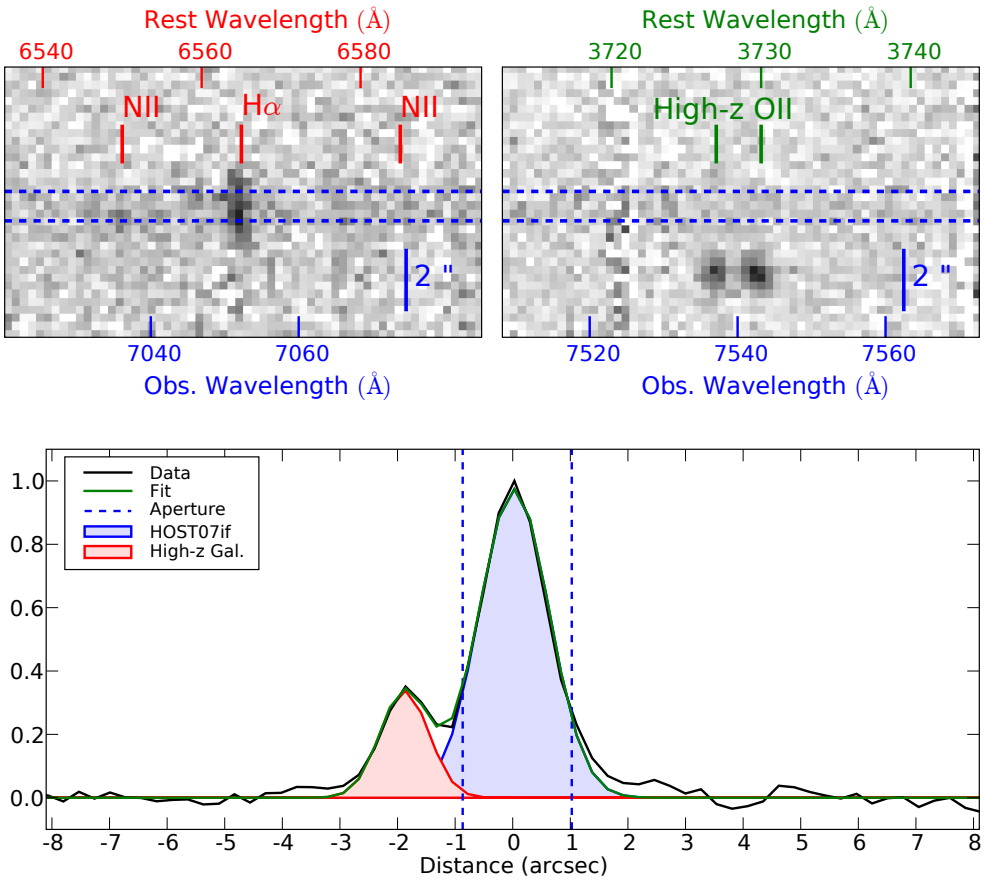

Figure 4.2 *Top:* Portions of the 2D sky-subtracted spectrum image showing (left) the strong Hα feature of HOST07if at $\lambda = 7051$Å corresponding to $z = 0.074$ (note the distinct absence of [NII] $\lambda\lambda 6548, 6584$), and (right) the [OII] $\lambda\lambda 3727, 3730$ feature of the high-z background galaxy at $\lambda\lambda 7537, 7543$Å corresponding to $z = 1.02$. *Bottom:* Wavelength-collapsed object profiles in g-band, showing our two-Gaussian fit to HOST07if and the high-z background galaxy, and the extraction aperture chosen for the HOST07if spectrum. Note the possible contamination from the high-z galaxy is extremely small.

stacked image, HOST07if is blended with the background high-redshift galaxy described above. To account for its contribution to the measured HOST07if flux, we analyze the two-dimensional blue channel spectrum, which was taken during the best seeing conditions of both nights ($\sim 0\farcs6$) and shows a clear separation of the two objects. We subtract the sky background from the 2D spectrum, apply the flux calibration and multiply by the g-band filter throughput in the wavelength direction, then collapse the 2D spectrum in wavelength along the aperture trace. This effectively provides a high signal-to-noise measurement of the object profiles along the slit direction in g-band. We then fit this 1D profile with two Gaussians; the data and fit are shown in Figure 4.2 along with the chosen aperture. The center of both objects fall inside the slit and the seeing was smaller than the slit width, so we predict that the flux within the slit satisfactorily preserves the flux ratio between the two objects. The ratio of the flux of the high-z galaxy to HOST07if in g-band is $F_{\rm high-z}/F_{\rm HOST07if} = 0.27 \pm 0.02$, with a separation of $1\farcs9$. This results in a correction to the observed magnitude of HOST07if of $\Delta m_g = -0.26 \pm 0.02$. Finally we include the known offset between the SDSS and AB magnitude systems (Stoughton et al. 2002) of $m_{g,AB} = m_{g,SDSS} + 0.02$. To derive the rest-frame g-band magnitude, we perform a K-correction (Nugent et al. 2002) using the g-band filter throughput and the HOST07if spectrum, finding $K_g = -0.002$. The reddening, object overlap, SDSS-AB offset, and K-correction effects result in a final rest-frame g-band magnitude of HOST07if of $m_g = 23.15 \pm 0.06$.

To derive the correct distance modulus for HOST07if, we convert the heliocentric redshift derived from nebular emission lines (see §4.2) to the CMB rest frame using the dipole parameters from WMAP5 (Hinshaw et al. 2009) to obtain $z_{\rm CMB} = 0.07336 \pm 0.00015$. Assuming standard ΛCDM cosmology ($H_0 = 70$ km/s Mpc^{-1}, $\Omega_m = 0.3$, $\Omega_\Lambda = 0.7$), we use the code of Wright (2006) to calculate a distance modulus of $\mu = 37.60 \pm 0.004$. (note this corrects a transcription error in the calculation of the host absolute magnitude reported in Scalzo et al. 2010, which did not affect any other values reported in that analysis). With the apparent magnitude derived above, this gives HOST07if an absolute g-band magnitude of $M_g = -14.45 \pm 0.06$.

Since the LRIS g-band observations were the only deep late-time photometry of the host (after the SN had fully faded), we analyze the HOST07if spectrum as a source of galaxy color information. We synthesize rest-frame u- g- and r-band magnitudes from the spectrum using the SDSS filter transmissions[1] and obtain effective observer-frame galaxy colors of $g - r = 0.07 \pm 0.04$ mag and $u - g = 0.67 \pm 0.03$ mag. The relative flux calibration of our spectrum is very good, as we measure the synthetic $g-r$ and $u-g$ colors of the night's standard star observations to match those synthesized from calibration spectra to within $\Delta(g-r) < 0.01$ mag and $\Delta(u-g) < 0.01$ mag, primarily driven by noise in the dichroic region. These colors will be used below to derive the galaxy mass-to-light ratio and to inspect possible reddening due to dust.

4.2 SN 2007if Host Metallicity

Our original objective in observing HOST07if was to secure a host redshift in order to accurately determine the SN 2007if ejecta velocity. This measurement played a key role in establishing the kinetic energy of the explosion and SN 2007if as having a mass greater than the Chandrasekhar limit Scalzo et al. (2010). Fortuitously, the final spectrum showed emission in Hα and [OII] $\lambda\lambda 3727, 3730$ sufficiently strong to measure a gas-phase metallicity.

[1] The SDSS filter transmissions are available at `http://www.sdss.org/dr7/instruments/imager/index.html`.

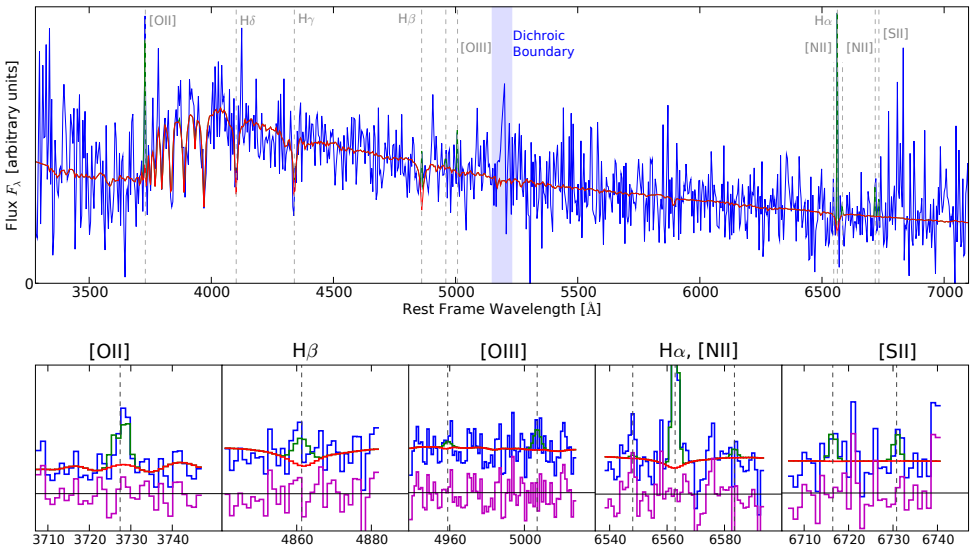

Figure 4.3 *Top:* Spectrum of HOST07if (blue) binned to 4Å for visual clarity, with fitted background (red) and emission lines (green). *Bottom:* Zoomed fit regions for notable emission lines (unbinned), with fit residuals (magenta).

Emission Line Fluxes

Accurate measurement of emission line fluxes in star-forming galaxies requires proper accounting for stellar absorption. To this end we fit the emission line fluxes and stellar background in the HOST07if spectrum simultaneously using a modified version of the IDL routine `linebackfit` from the `idlspec2d`[2] package developed by the SDSS team. This routine allows the user to provide a list of template spectra fit in linear combination with Gaussian emission line profiles. We have modified this code to force the background coefficients to be non-negative and have incorporated the ability to fit for a scaling factor between the blue and red channels of two-arm spectrograph data. For background templates we chose a set of simple stellar populations (SSPs) from the stellar population synthesis code GALAXEV (Bruzual & Charlot 2003, BC03) with a Chabrier (2003) IMF and the same time sampling used for background fitting by Tremonti et al. (2004, T04), which ultimately consists of ten SSPs for each metallicity. We note that the use of Salpeter (1955) IMF templates results in negligible differences to the fitted emission line fluxes, and metallicity difference smaller than the quoted precision of 0.01 dex.

We fit the two LRIS channels simultaneously, with the background templates on each channel convolved to the spectrograph resolution for each channel, namely 4.4 Å and 4.1 Å for the blue and red channels respectively, and fit the cross-channel scaling simultaneously. As with the SDSS spectroscopic pipeline, our emission line fitting is done in an iterative fashion. An initial guess of the redshift is used to set the redshift of the background templates, and the spectrum is fit with the widths and redshifts of all lines allowed to float freely. The best redshift is measured from

[2] http://spectro.princeton.edu/idlspec2d_install.html

the initial emission line fits, and a second iteration is performed with the redshift of the background templates set to this value. The emission line fluxes are then measured with the line redshifts all fixed to this value. We found the best fit χ^2 was obtained when the background templates were drawn from the $Z = 0.004$ track. The uncertainty in the scaling of the blue and red channels is measured to be $\approx 3\%$, and has a value consistent with those measured for our standard stars. The uncertainties from all fit parameters and their covariances are measured by the fitting code, and emission line flux errors accurately reflect the influence of all fit parameters in their estimation (including the cross-channel scaling). The final emission line fluxes from our best fit are presented in Table 4.1, and the fit to the spectrum is shown in Figure 4.3.

Table 4.1 HOST07if Emission Line Fluxes

Line	Obs. Flux[a]	$F(\lambda)/F(H\beta*)$[b]
[OII] $\lambda\lambda 3727, 3730$	48.80 ± 10.56	2.44 ± 0.53
Hβ	22.29 ± 7.17	1.11 ± 0.36
[OIII] $\lambda 4959$	5.22 ± 2.85	0.26 ± 0.14
[OIII] $\lambda 5007$	15.37 ± 8.38	0.77 ± 0.42
Hα	57.46 ± 5.30	2.87 ± 0.26
[NII] $\lambda 6548$	0.93 ± 1.25	0.05 ± 0.06
[NII] $\lambda 6584$	2.77 ± 3.72	0.14 ± 0.19
[SII] $\lambda 6717$	7.46 ± 3.52	0.37 ± 0.18
[SII] $\lambda 6731$	6.68 ± 3.71	0.33 ± 0.19

[a] Fluxes in units of $10^{-19} ergs \cdot cm^{-2} \cdot s^{-1}$

[b] $F(H\beta*) \equiv F(H\alpha)/2.87$; see text for details.

The emission lines from our spectrum of HOST07if provide a formal redshift and uncertainty of $z_{\rm lines} = 0.074500 \pm 0.000010$ in the heliocentric frame. This value is slightly different from the value we quoted in Scalzo et al. (2010), and reflects a more thorough treatment of the spectrum wavelength solution. Additionally, we calculate the contribution of our wavelength solution to the redshift error budget to be $\Delta z_{\rm wsol} \approx 2.5 \times 10^{-5}$. Because our object has extent smaller than the slit, the dominant source of redshift error from our data comes from the centering of the object on the slit. As stated above, we measure this error to be no more than 1 pixel, which corresponds to a redshift error of $\Delta z_{\rm slit} \approx 1.5 \times 10^{-4}$ at Hα, the line which best constrains the redshift. Thus we estimate the final heliocentric redshift and error for HOST07if to be $z_{helio} = 0.07450 \pm 0.00015$.

The Balmer emission line fluxes are typically used to estimate intrinsic reddening in galaxies by comparison to the Case B recombination value of $F(H\alpha)/F(H\beta) = 2.87$ at a temperature of $T = 10,000K$ (Osterbrock & Ferland 2006). This value is well within the 1σ estimate from our measured emission line fluxes (0.62 in the cumulative probability function), but is poorly constrained due to the relatively low S/N of our spectrum. We therefore will report results derived under the assumption of *no intrinsic extinction*. Later, in §4.4, we show that this assumption is supported by multiple facets of the data themselves, and even in the worst case scenario of leaving reddening unconstrained has negligible impact on our final results.

Gas-Phase Metallicity

Initial signs that HOST07if is a low metallicity galaxy include the non-detection of [NII] $\lambda\lambda 6548, 6584$ (below the noise threshold, see value and errorbar in Table 4.1 and 2D spectroscopic image in Figure 4.2), the relatively weak [OII] $\lambda\lambda 3727, 3730$ and [OIII] $\lambda\lambda 4959, 5007$ lines (compared to the strong Balmer lines), and of course its low luminosity. Low-metallicity galaxy abundances are ideally determined using the "direct" method whereby the ratio of the auroral [OIII] $\lambda 4363$ line flux to that of the stronger [OIII] $\lambda\lambda 4959, 5007$ lines is used to constrain the electron temperature T_e in the doubly-ionized oxygen (O^{++}) zone (T_e(OIII)). Because the auroral line is not detected in HOST07if, and the intrinsically stronger [OIII] $\lambda\lambda 4959, 5007$ lines are only weakly detected, the direct method is untenable here.

The question of appropriate metallicity scales will be addressed later in §4.4, but here we derive the metallicity using the R_{23} method of Kobulnicky & Kewley (2004, hereafter KK04). The ratio R_{23} is double valued with metallicity, and the flux ratio [NII]/Hα is typically used to break the degeneracy and select which "branch" of the R_{23} metallicity calibration is appropriate. For HOST07if, [NII]/Hα indicates the lower metallicity branch, so we employ the lower branch of the KK04 calibration of the R_{23} method as updated by Kewley & Ellison (2008). This method is advantageous because it iteratively calculates the metallicity and ionization parameter.

To derive a tighter constraint on the metallicity of HOST07if, we use the higher S/N Hα flux measurement and its error scaled by the fiducial Balmer decrement as proxies for the flux and error of Hβ. As stated above, this is consistent with our assumption of no reddening in HOST07if and results in an Hβ flux only 0.25σ different from that measured, but with an error bar $4\times$ smaller. For HOST07if, we measure a metallicity of $12 + \log(O/H)_{\rm KK04} = 8.01 \pm 0.09$, with an ionization parameter $q = 1.46 \pm 0.48 \times 10^7$. This low value of the ionization parameter is unsurprising given the strength of [OII] $\lambda\lambda 3727, 3730$ and the relative weakness of [OIII] $\lambda\lambda 4959, 5007$. These indicate that the ionizing radiation is dilute and it has been some time since HOST07if's most recent burst of star-formation (consistent with stellar absorption strengths – see below). We note that [NII] $\lambda\lambda 6548, 6584$ is used to break the R_{23} degeneracy, and our measurement of this line predicts the lower branch at only $\approx 69\%$ probability, since [NII] appears to be below the noise level. If we were to choose the upper R_{23} branch, this would make HOST07if a $> 5\sigma$ outlier on the mass-metallicity relation (T04, Kewley & Ellison 2008), an extremely rare event (see e.g. Peeples et al. 2008). Additionally, [NII]/[OII] at such a high metallicity (Kewley & Dopita 2002) would predict an [NII]$\lambda 6584$ flux strong enough to be detected at $> 8\sigma$.

4.3 SN 2007if Host Age and Stellar Mass

Information about the star-formation history (SFH) of HOST07if is desirable for constraining the age of the SN 2007if progenitor. Spectral indices measured from galaxy stellar spectra can be useful in assessing the mean stellar age, likelihood of recent starburst, and stellar mass-to-light ratios (see e.g. Kauffmann et al. 2003; Graves & Schiavon 2008; Gallazzi & Bell 2009). To facilitate the inspection of the SFH of HOST07if, we measure several age-sensitive spectral indices from the emission-subtracted spectrum of HOST07if and compared their values to model spectra generated using stellar population synthesis (SPS) techniques. The details of our analysis are as follows.

We measured the strength of several Balmer absorption features according to their standard definition on the Lick system (Worthey et al. 1994; Worthey & Ottaviani 1997) as well as the strength of the 4000 Å break (D4000, Balogh et al. 1999) in the spectrum of HOST07if after removing emission line features as determined in §4.2. Using the formulae of Cardiel et al. (1998), we measure the values and errors reported in Table 4.2. These indices are known to have strong dependence on stellar age (Vazdekis et al. 2010), with negligible dependence on instrument resolution (and by extension galaxy velocity dispersion). The low D4000 and strong Balmer absorption we measure for HOST07if is indicative of young stellar ages of a few hundred Myr.

Table 4.2 HOST07if Spectral Indices

Index	Value
D4000	1.13 ± 0.05
Hδ_A	3.50 ± 2.33
Hγ_A	7.19 ± 2.36
Hβ	2.34 ± 2.82

To assess the general behavior of the SFH of HOST07if, we generate a library of synthetic galaxy spectra using the BC03 SPS code and a suite of physically-motivated SFHs. We follow the same prescription as Gallazzi et al. (2005) and Gallazzi & Bell (2009, hereafter GB09) to generate models consisting of an exponentially declining continuous SF component superposed with random burst of SF (see GB09 for details). We measured the same spectral indices from our model spectra and plot the location of HOST07if and our model galaxies (blue background) in Hγ_A-$D4000$ space in Figure 4.4. For reference, we also plot the location of SDSS DR7 galaxies whose spectral index values and stellar masses have been measured by the MPA-JHU group[3]. The full sample of galaxies between redshifts $0.005 \leq z \leq 0.25$ are shown as the green contour, while low mass ($\log(M_*/M_\odot) \leq 9.0$) galaxies are shown as the red contour, with the median error bars for each quantity (for each subsample) shown as the crosses in the lower left.

Kauffmann et al. (2003) showed the Balmer-D4000 diagram to be an informative parameter space in which to inspect the SFH of star-forming galaxies, and (GB09) extensively analyzed the properties of galaxies in different regions of this diagram (for Hδ_A). The dense band of model spectra (dark blue) and the majority of the SDSS galaxies form a sequence of galaxies dominated by continuous star-formation ranging from very old (high D4000, low Hγ_A) to very young (low D4000, high Hγ_A) mean stellar ages. Galaxies whose indices are located away from this band have undergone a strong starburst in the past few hundred Myr.

It is evident that HOST07if is located away from the continuous SFH band in this spectral index parameter space, and is even separated from the majority of low mass galaxies whose mean stellar ages are very young. This indicates that HOST07if underwent a major burst of star formation in its recent past. This is perhaps unsurprising given that HOST07if's low luminosity implies a low stellar mass, and low mass dwarf galaxies tend to have SFHs characterized by strong yet intermittent bursts of star-formation (Searle & Sargent 1972). In the case of a strong recent starburst, the light from the burst tends to dominate the galaxy spectral energy distribution (SED), which can make it more difficult to constrain the complete galaxy SFH and mass-to-light ratio (GB09). Thus we will proceed by decoupling the recent burst of SF from the remaining SFH of HOST07if. We will first

[3] http://www.mpa-garching.mpg.de/SDSS/DR7/

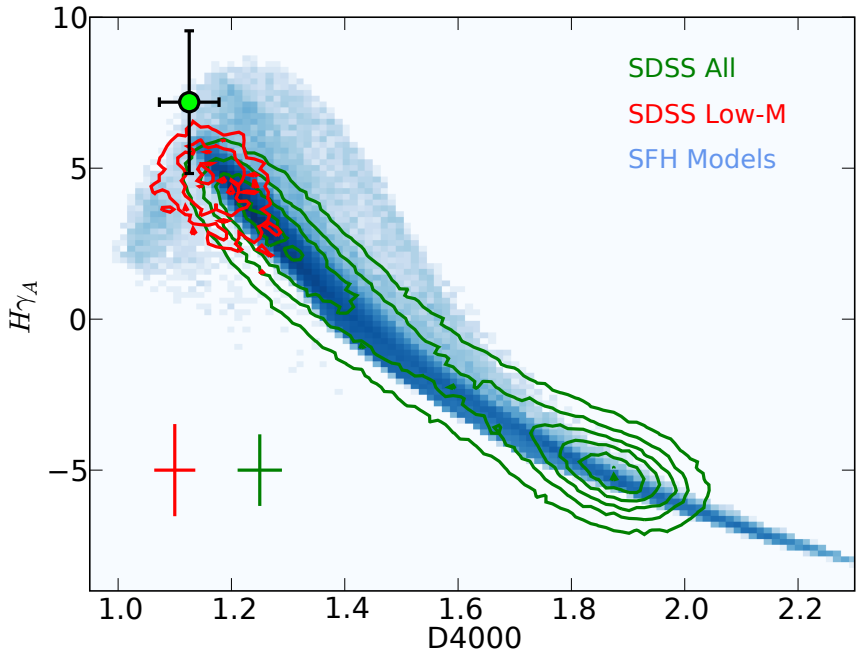

Figure 4.4 Location of HOST07if (green circle) in the $H\gamma_A$-D4000 plane compared to the library of physically motivated SFHs of GB09 (blue background). Overplotted are index values for SDSS galaxies derived by the MPA-JHU group for the full galaxy mass range (green contours) as well as low mass ($\log(M_*/M_\odot) \leq 9.0$) galaxies (red contours), with median measurement errors shown as the colored crosses in the lower left. Galaxies in the densely-populated band spanning the full range of D4000 have SFHs dominated by continuous star-formation, while the galaxies located away from this band have undergone recent burst of star-formation.

assess the age of the most recent starburst, then investigate the potential presence of older stars in HOST07if.

HOST07if Burst Stellar Age

To quantify the age of the most recent starburst in HOST07if, we compare the HOST07if spectral indices to those of a library of starburst model spectra generated from the BC03 SPS models. The burst SFHs are simple boxcar functions in time described only by the start and end time of the burst of star-formation. Burst start times are uniformly distributed between 0 and 13.5 Gyr ago, and durations are uniformly distributed between 10 Myr and 1 Gyr. Metallicities were distributed logarithmically between $0.2 < Z/Z_{\odot} < 2.5$ and distributed as a smoothly decaying function in metallicity ($\propto \log(Z)^{1/3}$) between $0.02 < Z/Z_{\odot} < 0.2$ (in order to not over-represent low-metallicity bursts).

We derive the luminosity-weighted HOST07if starburst age probability distribution function (PDF) in a probabilistic fashion. For each template galaxy in the burst library, we computed the values of the spectral indices measured in the same way as HOST07if. We then derive each template's error-normalized separation from HOST07if in this multi-dimensional parameter space defined by the spectral indices as

$$\chi_i^2 = \sum_{\alpha} \left[\frac{a_{\alpha,i} - a_{\alpha,07if}}{\sigma_{a_{\alpha,07if}}} \right]^2 \tag{4.1}$$

where $a_{\alpha,i}$ is the value of parameter α for template i, and similarly $a_{\alpha,07if}$ and $\sigma_{a_{\alpha,07if}}$ are the value and uncertainty of that same parameter for HOST07if. Each template spectrum is a linear combination of spectra of SSPs of discrete age and metallicity as defined by the BC03 models. We assign a weight to each SSP equal to its integrated optical flux (3500 Å $< \lambda <$ 10000 Å), as the brighter SSPs are more likely to drive the spectral features. Thus each template has a luminosity-weighted age PDF that is the product of the template's coefficients for each SSP multiplied by the luminosity weights for each SSP (and normalized to unity probability). For each age bin in the HOST07if burst age PDF, each template adds probability to the bin that is a product of the template's age PDF value for that age bin and the appropriate weighting ($\exp[-\chi_i^2/2]$) for the template's parameter space separation from HOST07if. The final burst age PDF for HOST07if was renormalized according to the total probability of all templates ($\sum_i \exp[-\chi_i^2/2]$). We use the final HOST07if burst age PDF to derive the median age and $\pm 1\sigma$ errors for the stellar population of HOST07if as derived from the cumulative probability function.

We examined the accuracy of this method by performing the same age measurement with our burst library SEDs where $g - r < 0.5$ mag (thus the youngest subsample of bursts), which we will refer to as the "validation sample". We tested our method for a variety of combinations of spectral indices, and measured the mean offset from the true value (bias) and dispersion (systematic error) for each combination. In general, the bias was much smaller than the dispersion, and the dispersion decreased as more Balmer indices were added but saturated at the dispersion using the combination of Hδ, Hγ, and Hβ. The Hβ absorption strength for HOST07if is roughly the same magnitude as the emission equivalent width ($EW(H\beta) = 5.3 \pm 1.5$Å), so the potential for emission contamination of this index exceeds the reduction in systematic error gained by its inclusion. Additionally, the age sensitivity of the Hβ index is slightly dependent on spectrograph resolution and

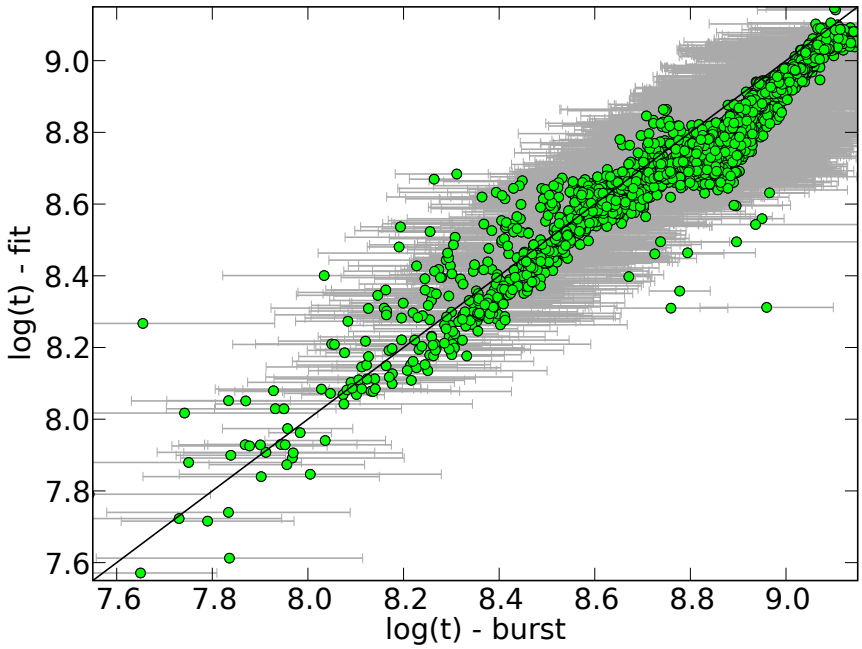

Figure 4.5 Reconstructed starburst age for our selected library galaxies vs. the input time of most recent starburst (green circles), with duration of starburst shown as horizontal grey bars. The scatter about the true value is 0.06 dex.

galaxy velocity dispersion (Vazdekis et al. 2010), whereas the other two Balmer indices are not, and the velocity dispersion of HOST07if is poorly constrained at our spectrum S/N. We thus exclude the Hβ index from our parameter space. We also considered other (non-Balmer) Lick indices, including G4300, but these provided no stronger constraints on the HOST07if age. Given the relative insensitivity of these other indices in the $\sim$100 Myr age range found for HOST07if (Vazdekis et al. 2010), this is unsurprising.

The final set of indices used to define the parameter space for template matching was D4000, Hδ, and Hγ. We show in Figure 4.5 the comparison between the median reconstructed stellar age against the median time (green circles) and duration (grey horizontal bars) of the starburst for each model in the aforementioned validation sample. The final mean offset between input and reconstructed age is $\Delta \log(t) = -0.05$ dex with a scatter of 0.06 dex. We thus consider our reconstruction method to be accurate, with a systematic age uncertainty of $\Delta \log(t) = 0.06$.

The final burst age PDF for HOST07if is shown in Figure 4.6, and we can see that the age constraint is remarkably tight. Our analysis shows the luminosity-weighted stellar age of HOST07if to be $\log(t) = 8.09^{+0.37}_{-0.43}$[stat]$\pm$0.06[sys], or in linear age $t_{\rm burst} = 123^{+165}_{-77}$ Myr (with the addition of statistical and systematic errors in quadrature). For the BC03 tracks at metallicity $Z = 0.004$ (the closest value to our derived galaxy gas-phase metallicity) this corresponds to a main-sequence turn-off mass of $M/M_{\odot} = 4.6^{+2.6}_{-1.4}$.

We also investigated the inclusion of optical colors in constraining stellar age, beginning

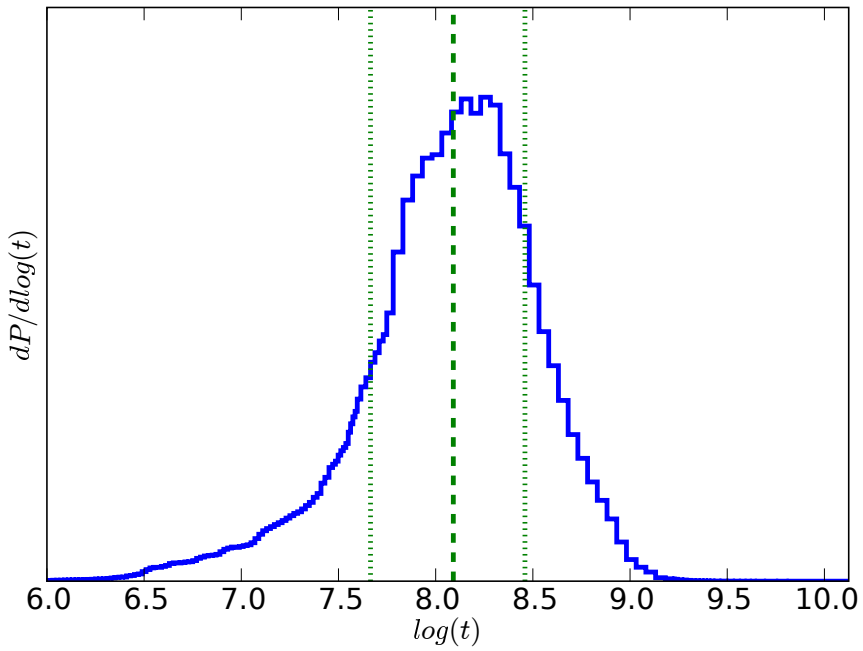

Figure 4.6 Final luminosity-weighted burst age PDF for HOST07if. The solid vertical line represents the median of the cumulative probability distribution, while the two dashed vertical lines represent the 16th and 84 percentile (i.e. 1σ) of the same.

with $g-r$ which is strongly correlated with stellar age and was shown by GB09 to be a good color for constraining M_*/L. The age implied by the HOST07if $g-r$ optical color was somewhat in tension with that implied by the spectral indices ($\log(t) \sim 8.5$ vs. $\log(t) \sim 8.1$). The cause of this discrepancy is likely to be either the presence of some older stars in addition to the recent burst of star-formation (see §4.3), or intrinsic reddening in the galaxy (see §4.4).

It is worth noting that the distribution of ages and metallicities in the model library has a significant impact on the resultant age PDF. Applying the same method to the GB09-like SFH library used in Figure 4.4 yields a very differently shaped PDF, and does not successfully recover burst ages for those SFHs with a dominant recent starburst. This is because the manner in which the library SFHs populate the age-metallicity parameter space effectively acts as a prior on the resultant age PDF, whose final form is especially dependent on the way in which different age bins are coupled to one another by the assumed shape of the SFH. Our burst model library employs the simplest possible SFHs (excepting of course a δ-function SFH) and provides an effectively flat and decoupled prior because it populates age and metallicity bins evenly and only couples adjacent age bins with equal weight and over relatively short (< 1 Gyr) timescales.

Finally, we note that our burst age assessment method also provides corroboration of the low metallicity of HOST07if (measured from emission lines above in §4.2). In addition to tracking the age distribution of each template, we can inspect the distribution of metallicity tracks used in construction of the templates. Thus we can examine the burst age PDF as a function of metallicity, and derive the integrated probability for each BC03 metallicity track. Doing so yields the following probabilities: 25% for $Z = 0.0004$, 40% for $Z = 0.004$, 17% for $Z = 0.008$, 13% for $Z = 0.02$ (solar), and 5% for $Z = 0.05$. This discrete distribution illustrates the strong preference for lower metallicity tracks despite the relatively flat prior (w.r.t. each track). This is a product of the metallicity sensitivity of the spectral indices used in the data-model comparison, and shows that the stellar spectral features favor a low metallicity in agreement with our measurement of the gas phase metallicity above.

Old Stars in HOST07if

Perhaps the greatest limitation in our ability to constrain the age of the SN 2007if progenitor is the uncertainty in the amount of old stars in HOST07if. Low-mass dwarf galaxies such as HOST07if are likely to have a bursty SFH (Searle & Sargent 1972) characterized by intense bursts of star-formation separated by extended quiescent periods of reduced SFR (Sánchez Almeida et al. 2008). Such galaxies may have formed the majority of their stars in the distant past (Zhao et al. 2011), so it is critical to investigate the potential amount of old stars in HOST07if.

The bursty nature of the HOST07if SFH is supported by the comparison of the burst star-formation rate (SFR) implied by our age constraint as compared to that implied by the observed Hα emission. We showed above that the HOST07if spectrum is dominated by stars of age 123 Myr, and we can make a simple approximation of the mass of stars formed during the burst by multiplying the observed g-band flux by the mass-to-light ratio of our estimated burst age (and metallicity). Doing so yields an approximate mass of $10^7 M_\odot$ of stars formed in the burst, and if we assume this was formed in $t \approx 100$ Myr (likely an extreme over-estimate), we can estimate a rough burst SFR of $SFR_{burst} \approx 0.1\ M_\odot\ yr^{-1}$. The presence of H$\alpha$ emission implies some current star-formation, which we can quantify using the formula of Kennicutt (1998) to find $SFR_{H\alpha} = 2.2 \times 10^{-3}\ M_\odot\ yr^{-1}$. Thus, even our crude estimate of the burst SFR shows the ratio of SFR during

the burst to that at the present time to be at least $SFR_{burst}/SFR_{H\alpha} \approx 50$, which implies that the HOST07if SFR is tapering off from its intense value during the recent burst.

To investigate the amount of old stars in HOST07if, we begin by reconstructing the spectrum derived by convolving the burst 2D age-metallicity PDF with the BC03 SSPs. This "reconstructed" stellar spectrum is plotted in the top panel of Figure 4.7 along with the data and stellar background fit from §4.2. Remarkably, information from the Balmer absorption features and D4000 alone are enough to reconstruct much of the HOST07if stellar background with high fidelity, especially in the bluer wavelengths. A slight color discrepancy of $\Delta(g-r) \approx 0.11$ mag is evident here, which could be due to dust in HOST07if (see §4.4) or old stars (see discussion below). In the lower panel of the same figure, we show the ionizing flux below the Lyman limit ($\lambda = 912$ Å) for the reconstructed spectrum as compared to the SSP at the age closest to our median age and metallicity closest to our spectroscopic measurement ($Z = 0.004$). We performed a simple calculation of the Hα flux that would result from this ionizing flux assuming 45% of ionizing photons eventually generate an $H\alpha$ photon (Donahue et al. 1995), and found it to be within a factor of about 2 of the measured value. Thus, our technique not only accurately reproduces the stellar spectrum in the optical regime, but also independently predicts the Balmer emission strength fairly well. This indicates that our age-matching technique is effectively reproducing the tapering SFR in HOST07if, which may indicate we are recovering not only the central burst time, but also some of the morphology of the burst SFH.

We proceed in our investigation of possible old stars in HOST07if by taking our reconstructed burst spectrum as being representative of the true starburst SED. As noted above, the spectrum predicted from our burst PDF is somewhat bluer ($\Delta(g-r) \approx 0.11$ mag) than what we observe for HOST07if, which could be a product of additional old stars. Here we take a conservative approach and explore the implications if the entire color excess arises from an old stellar population. To the burst spectrum we add the SED from an additional mass of old stars injected at a single age ranging from 1 Gyr to 13.5 Gyr. For each age, we fit for the mass of stars that minimizes χ^2 from the $g-r$ and $u-g$ colors, as well as the upper and lower masses that produced a $\Delta\chi^2$ of 1 (i.e. $\pm 1\sigma$) from the optimum value. In Figure 4.8 (top panel) we plot the best mass (and $\pm 1\sigma$ values) of old stars (normalized to the burst mass) as a function of age, as well as the best fitting χ^2 (middle panel). For reference in this plot, we show the best χ^2 obtainable by reddening the burst spectrum with dust (at $R_V = 3.1$), found to be $\chi^2 = 1.14$ at $A_V = 0.22$ mag. At all ages, the spectral features (D4000, Hδ_A, Hγ_A) of the old+burst spectrum differed from the observed values in HOST07if by much less than their measured uncertainties, justifying our approach of examining the starburst and old stellar populations separately.

This test illustrates the aforementioned fact that young bursts of star formation tend to obscure older stellar populations. Half or more of the stars in HOST07if could indeed come from older stars and still be consistent with the observed spectral indices and colors, and we can currently only disfavor old stars in HOST07if by making assumptions about the form of its SFH. However, our age measurement technique showed that old stars alone are inconsistent with the observed spectral features of HOST07if, and a significant amount of young stars dominates the galaxy spectrum. Further observational constraints on old stars in HOST07if must wait for additional data, such as deep imaging in the near infrared.

An old stellar population can be the source of SN 2007if only if its reservoir of potential progenitor systems has not been exhausted. Making the simplest assumptions – that the origi-

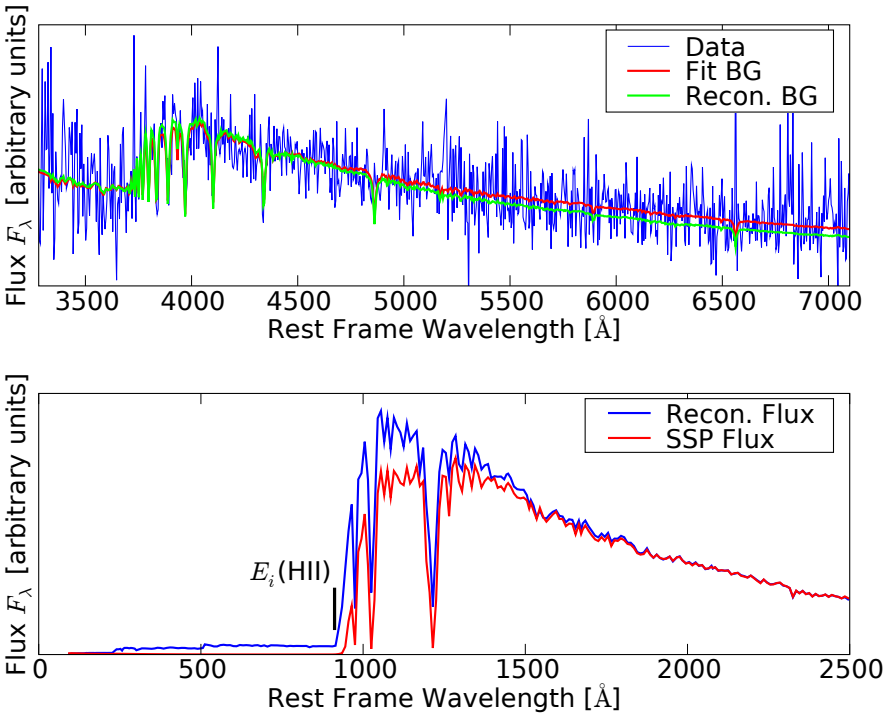

Figure 4.7 *Top:* Comparison of the spectrum reconstructed from the HOST07if age PDF(green) compared to the data (blue) and the background estimate from the emission-line fitting procedure (red). *Bottom:* A comparison of the reconstructed spectrum (blue) and the spectrum of the SSP with age closest to the age estimate for HOST07if. Note the presence of HII ionizing radiation in the reconstructed spectrum while the SSP (as expected) shows none.

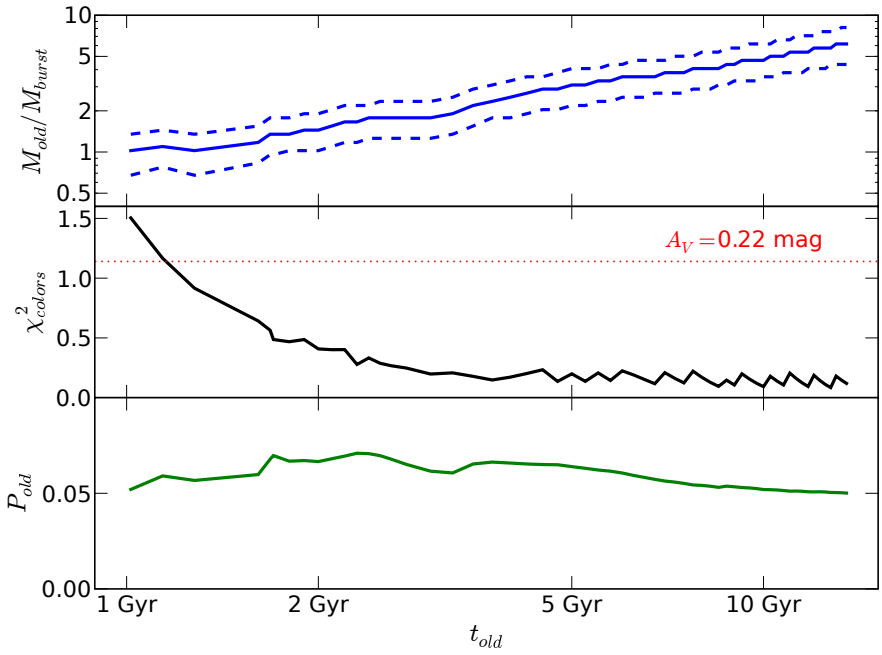

Figure 4.8 *Top:* Best fit value (solid blue line) and $\pm 1\sigma$ values (dashed lines) for mass of old stars at each age that when added to the burst spectrum produce the best matching colors ($g-r$ and $u-g$), scaled to the mass of the burst spectrum. *Middle:* χ^2 of colors for best-fit mass value as a function of age (solid black line), with the best possible χ^2 obtainable by reddening the burst spectrum (dotted red line) which is found at $A_V = 0.22$ mag. *Bottom:* Final probability of SN 2007if arising from old stars injected at a given age, derived from the product of the SN production likelihood with the color-matching likehood (from the above χ^2 values).

nal reservoir of progenitor systems is proportional to initial stellar mass, M_{old}, and that the delay time distribution (DTD) of SN 20007if-like events is not an increasing function of the delay, t_{old}, for populations older than $\sim$100 Myr – we can define a maximum relative rate today, given by $(M_{old}/t_{old})/(M_{burst}/t_{burst})$, arising from any ancient burst of star formation. Coupling this relative rate with the best-fit value of M_{old} for each age, and scaling by the χ^2 probability from the color matching, we derive the total probability of SN 2007if having been born from an old stellar population as a function of age. The results are shown in the bottom panel of Figure 4.8, where one sees that the likelihood of SN 2007if arising from an older stellar population never exceeds about 7% (note that this could be even lower if there is some reddening due to dust). We therefore conclude there is a high likelihood that SN 2007if was born in the recent burst of stars whose age was constrained in §4.3. We note that mathematically this consumption-timescale constraint gives the same relative factor as for old stellar populations distributed equally at multiple ages – where consistency requires a fixed DTD normalization across ages – and then assuming a t^{-1} power law for the DTD. This case is of particular interest because a t^{-1} power law is similar to the DTD observed for normal SNe Ia (Maoz 2010; Barbary et al. 2010), and expected in most DD models.

HOST07if Stellar Mass

The SPS models used above to constrain the luminosity-weighted age of the HOST07if stellar population can also be used to constrain the HOST07if mass-to-light ratio. Though spectral indices can in principle be used to constrain the mass-to-light ratio (e.g. GB09), the S/N of our spectral indices results in a large uncertainty ($\sim$ 1 dex) in the index-based mass-to-light ratio. Instead, a much tighter constraint can be obtained using optical color. We thus compare the $g-r$ color of HOST07if to that of our SFH models, as this color was shown by GB09 to be a good color for constraining mass-to-light ratios.

Which SFH models are appropriate for determining mass-to-light ratios is a deeper question than can be addressed here. Instead we follow the prescription generally favored in the literature, which is to use exponentially-declining SFHs similar to those of Kauffmann et al. (2003) and GB09. Though the SFHs of dwarf galaxies such as HOST07if are likely to be bursty, a long period of intermittent burst of SF can be well-approximated by a continuous SFH. We thus use the aforementioned suite of model spectra built following the prescriptions of GB09 to constrain the HOST07if mass-to-light ratio using $g-r$ color in the following way. Each model galaxy SED is normalized to $M = 1M_{\odot}$, and we measure the g-band luminosity for each template. Using color-based χ^2 weights, we measure the weighted mean stellar mass of a burst of unit g-band luminosity as:

$$\langle M \rangle = \frac{\sum_i w_i M_i}{\sum_i w_i} \tag{4.2}$$

and its uncertainty:

$$\sigma_M = \left(\langle M^2 \rangle - \langle M \rangle^2 \right)^{1/2} \tag{4.3}$$

where the weight $w_j = \exp -\chi_j^2/2$ for each template is computed from the template's $g-r$ color χ^2 as:

$$\chi_j^2 = \left[\frac{(g-r)_{HOST07if} - (g-r)_j}{\sigma_{(g-r)_{HOST07if}}} \right]^2 \tag{4.4}$$

Assuming a solar g-band absolute magnitude of $M_{\odot,g} = 5.15$ (Bell & de Jong 2001), we derive a mass-to-light ratio for HOST07if of $\log(M_*/L)_{\rm model} = -0.50 \pm 0.17$. With the absolute magnitude derived in §4.1 and the aforementioned mass-to-light ratio, this implies a galaxy stellar mass for HOST07if of $\log(M_*/M_\odot) = 7.32 \pm 0.17$.

As a comparison, we inspect the mass-to-light ratios for SDSS galaxies as determined by the MPA-JHU team. We find their M_*/L values to be well represented as a linear function in both optical $g-r$ color and more weakly in absolute magnitude M_g. From their data, we estimate the HOST07if mass-to-light ratio to be $\log(M_*/L)_{\rm SDSS} = -0.52 \pm 0.15$, which is consistent with our value within the error bars (as would be expected since our SFH models are essentially the same). In a similar vein, we use the color-based M_*/L formulae (appropriately corrected for our choice of IMF) from Bell & de Jong (2001) along with the color measured from HOST07if to estimate a mass-to-light ratio of $\log(M_*/L) = -0.55$, again consistent with our estimate.

4.4 HOST07if Analysis Cross-Checks

We now discuss several cross-checks we performed in order to estimate systematic effects in our parameter estimations. The possible effects of dust in HOST07if, systematic uncertainties in metallicity scales, and the limitations of our particular choice of stellar population synthesis (SPS) models will be addressed in turn.

The Effect of Uncertain Reddening

In typical applications the Balmer decrement is used to estimate reddening due to dust and correct emission line metallicity diagnostics. Our detection of Hβ is consistent with no reddening, however it is of sufficiently low S/N that a large range of reddening is allowed by this measurement. Several lines of evidence suggest that the reddening should be low. In Scalzo et al. (2010) we set strong upper limits on the column of Na I, suggesting little enriched material is available in the ISM for the formation of dust. Given that HOST07if is in a post-starburst phase, the HII regions and molecular clouds associated with this burst will have dissipated long ago, and thus it is quite plausible that the extinction limit derived for SN 2007if is not atypical of that for the emitting gas and stars. Because dust requires metals to form, the expected low metallicity based on the low luminosity of HOST07if also leads to the expectation of low extinction. Lee et al. (2009) and Garn & Best (2010) measure the Balmer decrement as a function of galaxy luminosity and do indeed find that low-luminosity galaxies typically have extinction of only $A_V \sim 0.1$.

The emission line fluxes of HOST07if also favor low reddening. Correction for reddening will increase R_{23} and lead to a higher predicted O/H. However, N2O2 (=[NII]λ6584/[OII] $\lambda\lambda 3727, 3730$) works in the opposite sense. Indeed, at the lowest metallicities ($12 + \log(O/H) < 8.1$), N2O2 is expected to saturate at primary N/O nucleosythesis ratio of $\log(N/O) = -1.43^{0.07}_{-0.08}$ (Nava et al. 2006), giving N2O2$= -1.32^{+0.08}_{-0.09}$. Thus, our non-detection of [NII]λ6584 provides an upper limit on N2O2 that can be used to constrain the amount of reddening. In the upper left panel of Figure 4.9 we show these complementary constraints in the A_V–(O/H) plane. These constraints alone disfavor any reddening greater than $A_V \sim 1.8$, and the metallicity prediction would have been 0.21 dex higher than that derived with fixed $A_V = 0$.

The very blue color and strong Balmer absorption of the stellar continuum in HOST07if

place additional constraints on reddening. It was noted above that the reconstructed spectrum from our age-metallicity PDF was slightly bluer (by ~ 0.11 mag in $g-r$ and 0.06 mag in $u-g$, corresponding to a best-fit extinction of $A_V = 0.22$ mag) than the observed color of HOST07if. While this could be caused by reddening due to dust, it could also be indicative of the presence of older stars (see §4.3). However, the Balmer absorption of the HOST07if stellar continuum and its optical colors can be combined to place an *upper* limit on the amount of reddening that is consistent with the observed color of HOST07if. This can be understood as a disagreement between the extreme blue stellar color implied by large reddening and the Balmer absorption strengths; if the reddening was large and HOST07if was intrinsically much bluer, its implied age would be younger and thus its Balmer absorption strengths would have been shallower than observed. We can quantify this constraint by examining the effect of reddening on the $g-r$ and $u-g$ colors of HOST07if and the subsequent agreement with our model spectra used in constraining the burst age. For each value of A_V, we sum the probability of matching to each of the 150,000 burst templates using the χ^2 method described above with the $g-r$ and $u-g$ colors included in the χ^2. Shown in the upper right panel of Figure 4.9, the A_V PDF from this method shows a sharp drop at $A_V \sim 0.5$. With the constraints from the stellar features added to our PDF, the metallicity we would have measured is only 0.08 dex higher than the $A_V = 0$ value. With the 1σ reddening of $A_V \sim 0.5$, our mass estimate for HOST07if would have increased by ∼0.3 dex (accounting for both the luminosity and mass-to-light ratio changes), only slightly larger than the measurement error for that quantity.

Finally we show the result of including the SN 2007if reddening constraint of Scalzo et al. (2010) as an assumed constraint on the global host reddening. We show the resultant 2D PDF in the lower left panel of Figure 4.9, and find that the resultant metallicity would have been 0.02 dex higher than the $A_V = 0$ value. Marginalizing our 2D PDFs in A_V gives the (O/H) PDFs for each scenario described above, and we show these in the lower right panel. The values we reported for each scenario represent the metallicity of maximum likelihood for the PDFs shown. Thus, while there is some uncertainty in the amount of reddening in HOST07if because we cannot strongly constrain the Balmer decrement, ultimately it has little effect on our final results, which robustly show a low metallicity. Additionally, the spectral indices used in our age measurement are measured across short wavelength ranges and thus are relatively insensitive to reddening, making our age estimate also robust against possible reddening in HOST07if.

Metallicity Calibration

Strong emission-line methods such as the R_{23} method (McGaugh 1991; Zaritsky et al. 1994, KK04) produce oxygen abundance values that are systematically higher than those derived with the direct method by $0.2-0.5$ dex (Kennicutt et al. 2003). In galaxies like HOST07if where [OIII] $\lambda 4363$ is not detected with sufficient S/N but strong line fluxes indicate low metallicity, this poses a challenge for deriving the correct absolute metallicity. Placing our metallicity estimate on the correct absolute scale is subject to the uncertainty as to which metallicity calibration is correct in an absolute sense. This is a subject much debated, and while the final scale remains undecided, Kewley & Ellison (2008) provided an excellent analysis of the discrepancies between various scales and means of converting between them. The scatter in these relations (0.06 dex systematic error, see analysis below) is smaller than the measurement errors from our spectrum. Placement of our measurements on a common scale with those of other SN Ia hosts in the literature suffices for comparison purposes, and will be employed in the discussion of §4.5.

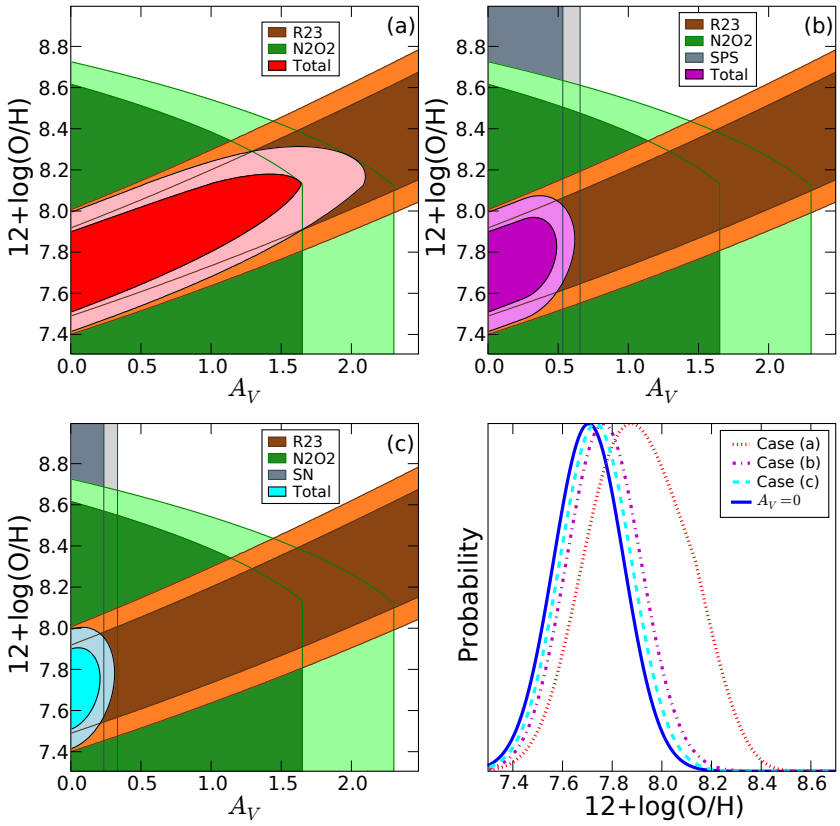

Figure 4.9 *Upper Left:* Two-dimensional probability distribution function of O/H vs. A_V combining constraints from the R_{23} ratio and N2O2 ratio from emissions lines. The two filled contours represent the 1σ and 2σ probability levels for each constraint, with the red and pink contours corresponding to the 1σ and 2σ final combined constraints. *Upper Right:* Same as left, but with additional constraint from SPS matching (see text). Magenta and fuscia contours are final 1σ and 2σ combined constraints. *Lower Left:* Same as upper left, but with addition of SN reddening constraint from Scalzo et al. (2010). Cyan and light blue contours are final 1σ and 2σ combined constraints. *Lower Right:* Metallicity PDF (marginalizing in A_V) for the three above cases (Case a - emission line constraints only, red dotted line; Case b - emission line plus SPS constraints, magenta dash-dotted line; Case c - emission line plus SN constraints, cyan dashed line) as well as the simple case assuming $A_V = 0$ (blue solid line).

Systematics in Stellar Population Synthesis

Next, we consider the impact of our particular choice of SPS models. It is a well-known problem that different stellar evolution and population synthesis codes produce different results due to different treatment of uncertain stages of stellar evolution, extinction due to dust, and the IMF (see e.g. Conroy et al. 2009). Assessment of the full impact of these uncertainties is beyond the scope of this work, but we inspected the impact of employing a Salpeter (1955) IMF instead of the Chabrier (2003) IMF used in our primary analysis. The age constraint for HOST07if remained unchanged, as the Salpeter IMF increases the amount of low-mass stars (relative the Chabrier IMF) which negligibly affect the spectrum of young starbursts similar to HOST07if which are dominated by bright massive stars. The mass-to-light ratio, however, is ≈ 0.16 dex higher for the Salpeter IMF, again a product of the increased proportion of low mass stars. Thus while our host mass is (as expected) dependent on the IMF chosen, the age constraint is robust against different IMFs.

To place our results in a more general stellar population context, we inspected the stellar spectra catalog of Gunn & Stryker (1983) and measured the Balmer absorption strengths in the same manner as for HOST07if. We then analyzed which single star spectra had the closest absorption strengths to HOST07if, and found the majority of these to be late B-type or early A-type stars. This is consistent with the age and main-sequence turnoff mass derived for HOST07if. Thus we find that our age measurement for the stellar population dominating the light of HOST07if is consistent with single-star spectra, indicating that our results are unlikely to be strongly dependent on the choice of SPS models.

Summary

In summary, the possible systematic errors or biases on our measurements of the metallicity and age of HOST07if are small compared to measurement errors. Our classification of HOST07if as metal-poor is confirmed for a wide variety of assumptions about reddening by dust in the host, and is true regardless of the metallicity calibration chosen. Our measurement of the young age of the stellar populations in HOST07if is not an artifact of our choice of SPS models or template SFHs. One important subtlety to note is that our age PDF for the stellar populations in HOST07if does not constitute a direct measurement of the progenitor age of SN 2007if, as the SN progenitor system was drawn from a single epoch in the SFH of its host galaxy. Our estimate of the stellar ages of the host represents the distribution of ages from which the progenitor was drawn, rather than a constraint on the age of the single progenitor system. The statistics of the host age distribution strongly favor a young age for the progenitor system of SN 2007if. Our assertion that HOST07if is young and metal-poor is robust, and serves as appropriate context for considering the properties of the progenitor of SN 2007if.

4.5 Implications of HOST07if Properties

In this section we discuss HOST07if in the context of previous SN Ia host galaxy studies, as well as the implications for progenitor scenarios for SN 2007if suggested by our data. Our assumption is that the properties of the host galaxy stellar population are good indicators of the properties of the progenitor system of SN 2007if. We showed above that this argument is statistically sound, as the recent major starburst dominates the galaxy light. Below we will show that our results

are consistent with regions of progenitor parameter space believed to produce SNe Ia, and our results thus provide important constraints on what portions of that parameter space are likely to produce super-Chandrasekhar SN Ia.

Metallicity of SN 2007if host - Comparison to other SN Ia hosts

Metallicity is a key parameter affecting the evolution of SN Ia progenitors. In the SD scenario (Hachisu et al. 2008), accretion is stabilized by a strong wind from the WD whose strength is driven by Fe opacity. Lower metallicity decreases the allowable regions of WD mass - orbital period parameter space in which the wind is strong enough to stabilize the accretion (Kobayashi & Nomoto 2009). In general, metallicity will affect the relation between initial main-sequence mass and final WD mass, as well as the time to evolve off the main sequence (Umeda et al. 1999b). For WDs of the same mass, a lower metallicity produces a slightly lower C/O ratio (a product of the aforementioned evolution time effect), which has been proposed as a possible source of the diversity in SN Ia brightnesses (Umeda et al. 1999a).

Placing our metallicity measurement in the context of previously published spectroscopic SN Ia host metallicities requires using a common scale, as different metallicity calibrations produce significantly different results (see the excellent discussion in Kewley & Ellison 2008). To our knowledge, the lowest spectroscopic SN Ia host metallicities to-date are those of SN 1972E at $12+\log(O/H) = 8.14$ (Hamuy et al. 2000), and SN 2004hw at $12+\log(O/H) = 8.23$ (Prieto et al. 2008). The original metallicity of the host of SN 1972E is drawn from Kobulnicky et al. (1999), who use the "direct" method to measure the oxygen abundance. As noted above, the "direct" method values are typically lower than strong line values by at least 0.2 dex. Therefore we collected the galaxy emission line fluxes from Kobulnicky et al. (1999) and measured its abundance using the KK04 technique employed for HOST07if, finding $12 + \log(O/H)_{72E,KK04} = 8.35 \pm 0.03$. The metallicities of Prieto et al. (2008) come from SN Ia hosts in the T04 sample, where metallicities where derived in a Bayesian manner by comparing emission line fluxes to photoionization models of Charlot & Longhetti (2001). While the means to reproduce their metallicity analysis are not available, the absorption-corrected emission line fluxes are available from the MPA-JHU group. Using the fluxes for the host of SN 2004hw, we find $12 + \log(O/H)_{04hw,KK04} = 8.24 \pm 0.03$. After placing all these metallicities on a common scale, our value of $12 + \log(O/H)_{KK04} = 8.01 \pm 0.09$ for the metallicity of HOST07if is $\approx 2\sigma$ lower than the lowest metallicity from these previous samples, and far below the metallicities of typical SN Ia host galaxies.

Interpretation of the metallicity of HOST07if on an absolute scale is subject to the intercalibration issues described above. The T04 scale is a popular one in the literature, as the mass-metallicity relation they derive is often invoked to use host mass as a proxy for metallicity. As stated above, the algorithm for this scale is not accessible, but we can convert our values to this scale using the conversion formulae of Kewley & Ellison (2008). Doing so yields a metallicity for HOST07if of $12+\log(O/H)_{T04} = 7.71\pm0.14$[stat]$\pm0.06$[sys], and for the host of SN 1972E yields $12 + \log(O/H)_{72E,T04} = 8.22$, while the value for SN 2004hw of $12 + \log(O/H)_{04hw,T04} = 8.23$ was derived in the T04 data set. On this scale HOST07if is nearly 3σ lower metallicity than the other SN Ia hosts.

We can place the metallicity of HOST07if on a solar abundance scale by comparing our measurements of the oxygen abundance to the solar value of $12+\log(O/H)_{\odot} = 8.86$ (Delahaye et al. 2010). On the KK04 scale, HOST07if has metallicity $Z_{KK04} \approx Z_{\odot}/5$, while on the T04 scale it has

$Z_{\rm T04} \approx Z_{\odot}/9$. The T04 value is perhaps in better agreement with the stellar metallicity preferred by our template matching (see §4.3) where 40% of the probability is in the $Z = 0.004$ ($Z_{\odot}/5$) track and 25% in the $Z = 0.0004$ ($Z_{\odot}/50$), though the coarse metallicity binning of the BC03 models makes this difficult to quantify precisely. While the absolute scale is somewhat uncertain, the metallicity of HOST07if is significantly sub-solar on several reasonable metallicity scales.

Finally we note that the gas-phase metallicity measured for HOST07if at the present epoch may be higher than the metallicity at the time of the birth of the progenitor of SN 2007if, presumably during the major starburst 123 Myr before the SN. The massive stars formed during that burst have exploded as core collapse SNe and enriched the ISM of HOST07if with their ejecta. Sánchez Almeida et al. (2009) found that dwarf galaxies with bursty SFHs showed gas-phase metallicities enriched by ≈ 0.35 dex (as compared to stellar metallicities) during the periods between bursts of star-formation. Thus the metallicity of the progenitor system of SN 2007if could possibly be even lower than the extremely low gas-phase metallicity measured for HOST07if at the time of the SN itself.

SNe Ia in low luminosity hosts

SN 2007if is part of a large and continually growing list of unusual SNe Ia discovered in low-luminosity host galaxies. Though low-luminosity galaxies have a higher number density than high-luminosity galaxies due to the steep faint-end slope of the galaxy luminosity function (e.g. Schechter 1976), high-luminosity galaxies retain the majority of stellar mass and thus are likely to produce the large majority of supernovae. Despite this fact, the number of supernovae in low-luminosity hosts is now significant, and includes a number of peculiar SNe such as SN 2007if.

The SN 2002cx-like supernova SN 2008ha (Foley et al. 2009) was found in a faint ($M_B = -18.2$ for $h = 0.7$) irregular galaxy. SN 2002ic (Wood-Vasey et al. 2002; Hamuy et al. 2003; Wood-Vasey et al. 2004) and SN 2005gj (Aldering et al. 2006; Prieto et al. 2007), both of which demonstrated features consistent with interaction with circumstellar material, were found in low-luminosity hosts (as-yet undetected for SN 2002ic and $M_B = -17.4$ for SN 2005gj; Aldering et al. 2006). At the most extreme, SN 1999aw was found in a host galaxy of brightness $M_B = -11.9 \pm 0.2$ (Strolger et al. 2002). The prototype of the possible super-Chandrasekhar class, SN 2003fg, was discovered in a low luminosity galaxy whose mass was estimated at $\log(M_*/M_{\odot}) = 8.93$ (Howell et al. 2006), though it is possible this is a tidal feature of a larger morphologically-disturbed galaxy nearby.

While the prevalence of unusual SNe Ia in low-luminosity galaxies is intriguing, it is by no means a one-to-one relationship. Most of the SN 2002cx-like host galaxies are spirals of moderate stellar mass (Foley et al. 2009), and other super-Chandrasekhar candidates have been found in more massive galaxies. SN 2006gz was found in a bright Scd galaxy (Hicken et al. 2007), and SN 2009dc appeared to be located in a massive S0 galaxy (UGC 10064) but may be associated with a nearby blue companion (UGC 10063) at the same redshift which may be interacting with the fiducial host of SN 2009dc (Silverman et al. 2011; Taubenberger et al. 2011).

There have also been relatively normal SNe Ia in low luminosity galaxies. The host galaxy of SN 2006an has an extremely low luminosity ($M_g = -15.3$, SDSS) and stellar mass ($\log(M_*/M_{\odot}) = 7.7$, Kelly et al. 2010) but was matched spectroscopically to the normal SN Ia SN 1994D (Quimby et al. 2006). The Catalina Real-Time Transient Survey (Drake et al. 2009) discovered SN 2008hp in a very faint ($M_g = -12.7$) host galaxy, but matched it spectroscopically to

a normal SN Ia (Drake et al. 2008). Additionally, the SNfactory discovered a number of relatively normal SNe Ia in low luminosity galaxies (see below).

To summarize, we note that low luminosity SN Ia hosts do not exclusively produce unusual SNe Ia, but there appears to be a higher frequency of these peculiar SNe Ia, including SN 2007if, in lower luminosity hosts.

Host Galaxies of the Probable super-Chandrasekhar SN Ia Sample

The properties of the full sample of probable super-Chandrasekhar SNe Ia is crucial for narrowing down the range of possible explosion scenarios for these exceptional SNe. Though there exist four SNe Ia whose classification as super-Chandrasekhar is generally agreed upon (SN 2003fg, SN 2006gz, SN 2007if, and SN 2009dc), three additional SNe Ia showed possible spectroscopic similarity to the four confirmed super-Chandrasekhar SNe Ia or photometric indication of exceeding M_{Ch} (SNF20080723-012, SN 2004gu, and SN 2009dr).

In Taubenberger et al. (2011) we derived stellar masses for the super-Chandrasekhar SN Ia host galaxies, as well as gas-phase metallicities for those where spectroscopic observations were available. In Figure 4.10 we show the location of the super-Chandrasekhar SN Ia hosts in the galaxy mass-metallicity (MZ) diagram, as well as their distribution compared to that of SDSS (Lampeitl et al. 2010) and SNLS (Sullivan et al. 2010) host galaxies. For the hosts of SNe 2003fg and 2009dr, as well as for UGC 10063, no metallicities could be determined, so these galaxies are plotted as vertical lines; for the SN 2009dr host the upper mass limit is shown. There seems to be a tendency of the hosts of super-Chandrasekhar SNe Ia to have (on average) lower masses than the SDSS galaxies. This trend also holds in the histograms in the lower two panels, where the host mass distribution of super-Chandrasekhar SNe Ia is compared to those of SNe Ia from the non-targeted SDSS (Lampeitl et al. 2010) and SNLS (Sullivan et al. 2010) surveys. In the middle panel UGC 10064 has been assumed to be the host of SN 2009dc, in the bottom panel UGC 10063.

The host mass distribution of super-Chandrasekhar SNe Ia has a mean and dispersion of $\log(M_*/M_\odot) = 9.2 \pm 1.3$ or $\log(M_*/M_\odot) = 9.0 \pm 1.1$, depending on whether UGC 10064 or UGC 10063 is considered as the host of SN 2009dc. These numbers are conspicuously lower than the $\log(M_*/M_\odot) = 9.8 \pm 1.0$ and $\log(M_*/M_\odot) = 10.0 \pm 0.9$ obtained for all SNLS and SDSS SN Ia hosts, respectively. To verify whether the observed distributions differ to a statistically significant degree, we ran a Kolmogorov-Smirnov test, using the SDSS and SNLS host mass distributions as a reference, and assuming in our null hypothesis that the hosts of the super-Chandrasekhar SNe Ia have been drawn from the same distributions. At a customary significance level of $\alpha = 0.05$, this null hypothesis is not rejected for both reference distributions. If, however, the significance is relaxed to $\alpha = 0.10$, the null hypothesis is rejected for the SDSS reference distribution (but not yet for the SNLS reference distribution).

This outcome is independent of which galaxy is adopted as the host of SN 2009dc, since it is driven by the high frequency of low-mass dwarf galaxies among the hosts of the super-Chandrasekhar SNe Ia. Of course, this is all low number ($n = 7$) statistics, and one should note that the addition of a single event might change the result considerably. Nevertheless, we tentatively claim weak evidence for an excess of low mass galaxies as hosts of the super-Chandrasekhar SNe Ia. Recent work by Khan et al. (2011) has extended this analysis to inspect the metallicity at the sites of SN 2009dc, SN 2003fg, and SN 2006gz. They showed that these SNe occur far from the core of their potential hosts, implying a lower SN progenitor metallicity than implied by these galaxies' lo-

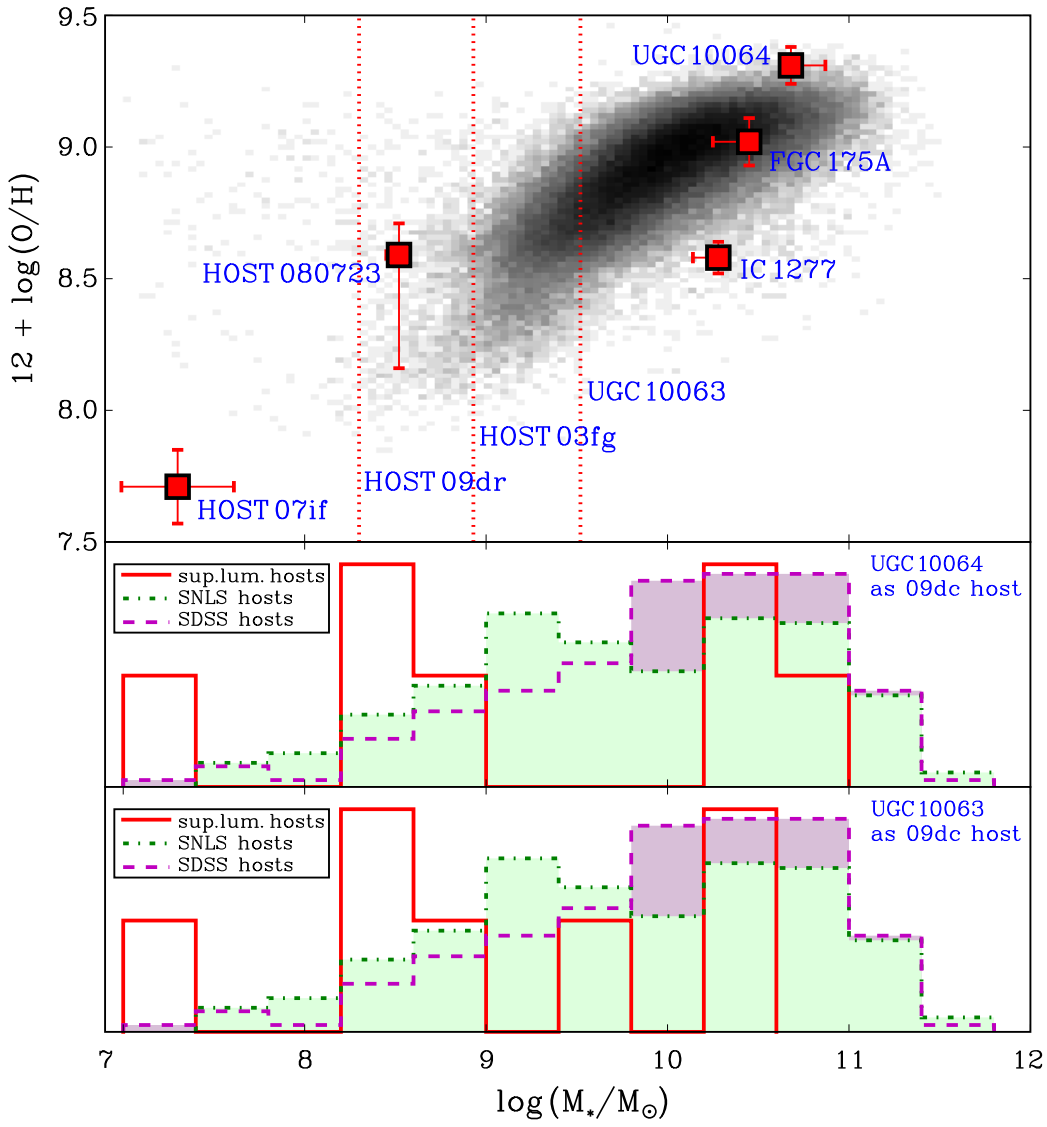

Figure 4.10 Top panel: masses and metallicities of the hosts of super-Chandrasekhar SNe Ia, compared to SDSS galaxies. Whenever no spectroscopic metallicity was available, a vertical line was drawn. The mass reported for the SN 2009dr host is an upper limit, following the non-detection in SDSS images. Middle and bottom panels: binned mass distribution of super-Chandrasekhar SN Ia hosts, compared to 162 SN Ia hosts from SDSS and 231 SN Ia hosts from SNLS. In the middle panel UGC 10064 is considered to be the host of SN 2009dc, in the lower panel UGC 10063. The distributions are scaled by arbitrary amounts to enable a comparison by eye.

cation on the MZ diagram. Thus low metallicity may be a common quality of super-Chandrasekhar SN Ia progenitors.

Host Age Constraint - Implications for SN 2007if Progenitor Scenarios

A consistent picture for the progenitor of any supernova should be able to explain not only the energetics of the explosion itself, but also the rates and timescales of such events. For normal SNe Ia, the correlation of SN rates with host galaxy mass and star-formation rate (Mannucci et al. 2005; Sullivan et al. 2006) indicated the likelihood of two progenitor components (the "A+B" model Scannapieco & Bildsten 2005) with different time scales. This is most directly encapsulated in the SN Ia delay time distribution (DTD; Mannucci et al. 2006). While the DTD of SNe Ia is still debated (see e.g. Mennekens et al. 2010), the predictions of various scenarios for normal SNe Ia serve as a useful baseline for placing our age constraint for HOST07if in the context of progenitor scenarios for SN 2007if.

Though the presence of SNe Ia in elliptical galaxies and the decline of the SN Ia rate at high redshift argue for progenitors with long delay times (Strolger et al. 2004, 2005), the correlation of SNe Ia with star-formation indicates the need for short-lived SN Ia progenitors (Aubourg et al. 2008) with delay times of order a few hundred Myr. Such short timescales have indeed been obtained in models of SD progenitor scenarios (e.g. Hachisu et al. 2008, their WD+MS channel), and DD scenarios (e.g. Ruiter et al. 2009).

As an example, Mennekens et al. (2010) describe a particular DD channel (dubbed the "CE" channel) in which two stars, with initially large separation and orbital period of several hundred days, undergo two common-envelope phases at the end of the main sequence lifetime of the more massive star. Following the MS evolution and the CE episodes, the orbital period of the system is reduced to a few hundred seconds and rapidly decays by gravitational radiation over a few hundred kyr. Finally the two WDs merge after a total period of order a few hundred Myr from the initial birth of the stars. This binary evolution channel has delay times consistent with our age estimate for the stellar population of HOST07if.

Liu et al. (2010) proposed a stellar evolution channel for super-Chandrasekhar SNe Ia involving a CO-WD primary and He secondary. This system is born from a binary with initial masses of $M_1 = 7.5 M_\odot$ and $M_2 = 4.0 M_\odot$ (at solar metallicity) that undergoes rapid rotation and explodes as a super-Chandrasekhar SN Ia with a delay time of approximately $t_{super-Ch} \approx 65$ Myr. Though the initial masses and timescales would be different at the sub-solar metallicity of HOST07if, the timescale of this scenario is roughly the same order of magnitude as our age constraint from the host spectrum.

Blais & Nelson (2011) proposed a new binary evolution scenario which could lead to an SN Ia through the DD channel. In their "single CE" scenario, two stars of very similar mass ($M_1/M_2 > 0.95$) fill their Roche lobes almost simultaneously, leading to a common envelope episode that brings the remnant WDs to a much tighter orbital separation followed by the standard DD merger as a result of orbital energy dissipation due to gravitational radiation losses. Their scenario manifests a large range of timescales, from less than 100 Myr to greater than a Hubble time, which allows for the timescale that we estimate for the age of HOST07if. Indeed, a non-negligible fraction of the short timescale ($\log(t) \leq 8.2$) realizations of this scenario show a total WD system mass in the range $2.1\ M_\odot \leq M_{WD,tot} \leq 2.3\ M_\odot$ (L. Nelson, private communication), in line with to the total system mass estimate we derived for SN 2007if in Scalzo et al. (2010).

Short timescales similar to the age of HOST07if are allowed in some SD scenarios [e.g. the "WD+MS" channel ofHachisu et al. (2008), see also Han & Podsiadlowski (2004), Greggio (2005) and references therein], but are especially common in DD scenarios (Yungelson & Livio 2000; Greggio 2005; Ruiter et al. 2009; Mennekens et al. 2010). While our age constraint does not definitely establish whether one of the traditional SN Ia progenitor scenarios or a new scenario is more favored for SN 2007if, our determination that SN 2007if was likely born from a young stellar population disfavors some scenarios, such as the WD+RG channel of the SD scenario from Hachisu et al. (2008) in which the WD accretes matter from a red giant companion, or the "RLOF" channel of the DD scenario described by Mennekens et al. (2010) in which early mass transfer in the binary proceeds by slow Roche lobe overflow (RLOF) and requires a significantly longer delay time than the age we measure for HOST07if.

Another interesting consequence of our age constraint is the resultant progenitor WD mass constraint for SN 2007if. If we assume SN 2007if originated from the merger of two WDs born in the dominant HOST07if starburst that have evolved off the main sequence prior to merger, we can use models connecting initial MS and final WD mass to derive a crude lower limit for the total system mass prior to SN Ia explosion. Using the models of Umeda et al. (1999b, see their Fig. 6) at $Z = 0.004$, we roughly estimate that a $M/M_{\odot} = 4.6$ main sequence star (corresponding to the MS turnoff mass derived above for HOST07if) would produce a $M_{WD} = 0.85\ M_{\odot}$ white dwarf. Thus in this toy model SN 2007if should have originated from the merger of two WDs whose total mass can be no less than $M_{tot} = 1.70\ M_{\odot}$, clearly in excess of M_{Ch}. There must some dynamical orbital decay time for a double WD merger, so this approximation should be considered an extreme lower limit. Though the evolution of post-MS stars in binary systems is far more complicated than the single star evolutionary scenarios of Umeda et al. (1999b), these models provide a good approximate scale of the available C/O material at the time of WD merger. Thus, our age estimate for HOST07if implies that even if stars just leaving the main sequence in HOST07if merge immediately, their mass must exceed the Chandrasekhar mass by a fair margin, reinforcing the model of SN 2007if as a super-Chandrasekhar SN Ia we derived in Scalzo et al. (2010).

4.6 Summary

In this Chapter we have presented Keck photometry and spectroscopy of the faint host galaxy of the super-Chandrasekhar SN Ia SN 2007if. HOST07if has very low stellar mass ($\log(M_*/M_{\odot}) = 7.32 \pm 0.17$), and has the lowest-reported spectroscopically-measured metallicity ($12+\log(O/H)_{\rm KK04} = 8.01 \pm 0.09$ or $12+\log(O/H)_{\rm T04} = 7.71 \pm 0.14$[stat]$\pm 0.06$[sys]) of any SN Ia host galaxy. We used the Balmer absorption line strengths in conjunction with the 4000Å break to constrain the age of the dominant starburst in the galaxy to be $t_{\rm burst} = 123^{+165}_{-77}$ Myr, corresponding to a main-sequence turn-off mass of $M/M_{\odot} = 4.6^{+2.6}_{-1.4}$.

This host galaxy is an ideal system for measuring SN progenitor properties. Dwarf galaxies such as HOST07if typically have a well-mixed ISM, lacking the large-scale abundance gradients found in larger galaxies. Like other low-mass dwarf galaxies, HOST07if shows indications of a bursty star-formation history, as its recent star-formation is dominated by the large starburst approximately 123 Myr in its past which presumably gave birth to the progenitor system of SN 2007if. We note, however, that bright recent starbursts are efficient at obscuring the light of older stellar populations, and HOST07if could possibly have a significant amount of mass in older stars (c.f. §4.3).

However, we also showed that with the decreased probability of SN 2007if arising from progressively older stars, the allowable amount of old stars in HOST07if leaves only a small probability that the SN was not born in the most recent starburst. Our constraints on the age and metallicity of the host of SN 2007if do not constitute direct constraints on the properties of its progenitor, but rather characterize the distribution of stars from which its progenitor was drawn. Nonetheless, the low metallicity and young stellar age of HOST07if are robust measurements (c.f. §4.4), and strengthen our interpretation that the properties of HOST07if are good indicators of the properties of the SN 2007if progenitor itself.

Our results provide key properties that should be reproduced by any proposed progenitor scenarios for SN 2007if. The low host metallicity can be used as input to stellar evolutionary tracks chosen for progenitor modeling, and will be particularly important in the mass loss stages of the progenitor. The relatively short timescale for the explosion of SN 2007if provides constraints on the binary evolution of the progenitor system. While development of a consistent progenitor scenario for super-Chandrasekhar SNe Ia is beyond the scope of this work, we have shown that a key member of this subclass, SN 2007if, is very likely to have originated from a low-metallicity young progenitor. Future inspection of the hosts of other super-Chandrasekhar SNe Ia as more are discovered will be critical for assessing the frequency of these characteristics for super-Chandrasekhar SN Ia progenitors.

Chapter 5

Masses and Metallicities of SN Ia Host Galaxies

Inferring the likely progenitor properties of an individual SN Ia from the properties of its host galaxy is a difficult task. Most galaxies have billions of stars of varying ages and metallicities (and multiplicities), formed in numerous episodes of star formation throughout a typically complex history consisting of infall and consumption of pristine gas, injection of metals into the inter-stellar medium from SNe, and dynamical interactions within the galaxy and with its neighbors. To characterize this complex amalgam of material by a few parameters (e.g. stellar mass, metallicity, current star-formation rate) is often a generous simplification, and may not necessarily be characteristic of every stellar system therein.

Instead the study of SN Ia host galaxies is a *statistical* endeavor in which we try to constrain the properties of the distribution from which the SN Ia progenitor was drawn. In some special cases, such as a chemically well-mixed dwarf galaxy (e.g. the host of SN 2007if, as shown in Chapter 4), or a galaxy that formed a majority of its stars in a short period and can be well modeled by a simple stellar population, the properties of potential SN Ia progenitors are more tightly constrained by the inherently narrow distribution of stellar properties within the galaxy. However, in a more complex galaxy with broad age and metallicity distributions, the nature of the progenitors of its SNe Ia remains more uncertain.

The study of the full distribution of SN Ia host galaxy properties partially mitigates this concern by averaging over a large ensemble of SN Ia host galaxies. If the difference between SN progenitor and average host properties is randomly distributed, then a large statistical sample of the two should have consistent averages. That is, the statistical distribution of SN Ia host galaxy properties, such as age and metallicity, should track the underlying distribution of SN properties. Thus we can use full samples of SN Ia hosts to learn more about the SN progenitors. The SNfactory sample is ideal in this regard, as our untargeted search technique provided an impartial sample (see Section 3.1.5) of SNe Ia in host galaxies of all types.

In this Chapter we use the SNfactory host galaxy stellar masses and gas-phase metallicities to perform three key investigations into the nature of SN Ia progenitors. First we calculate the level of agreement of SN Ia host galaxies with the fiducial galaxy mass-metallicity relation, a key assumption of many authors which has yet to be tested rigorously with a large statistical sample. Next we inspect the distribution of SN Ia host galaxy stellar masses – which is a product of the

average star formation history of galaxies as a function of stellar mass, the statistical distribution of stellar mass in all galaxies, and the SN Ia delay time distribution – and examine its utility in constraining the SN Ia delay time distribution. Finally we confront the theoretical low-metallicity inhibition prediction of Kobayashi & Nomoto (2009) with the observed metallicities of SNfactory SN Ia host galaxies, and determine the level to which our sample can confirm or refute this theory.

5.1 SN Ia Host Galaxies and the Galaxy Mass-Metallicity Relation

The level of agreement of SN Ia host galaxies with the normal galaxy mass-metallicity (MZ) relation can provide important insight into preferred SN Ia progenitor environments. Discrepancies between the SN Ia MZ distribution and that of normal galaxies could potentially indicate metallicity preferences for SNe Ia, which would have important implications for high-z SN Ia surveys. Alternatively, disagreement with the MZ relation could have other interpretations, as was the case with long-duration gamma ray burst host galaxies.

Some recent studies of the host galaxies of long-duration gamma ray bursts (LGRBs) found that they tended to have systematically lower metallicities than those predicted by fiducial galaxy MZ relation (Modjaz et al. 2008; Levesque et al. 2010). Initial interpretations of this trend speculated on a preference for lower metallicity environments in the production of LGRBs. The key insight, however, came from considering the effect of galaxy star-formation rate (SFR) on the galaxy MZ relation (Mannucci et al. 2010). Accounting for this effect, it was found that LGRB hosts indeed agreed with the SFR-adjusted MZ relation (or equivalently the M-Z-SFR relation) but merely appeared in the region of galaxy parameter space populated by the most intensely star-forming galaxies (Kocevski & West 2011; Mannucci et al. 2011). Thus this trend showed the preference for LGRBs to form in very young stellar environments.

The SN Ia host galaxy agreement with the MZ relation has been an implicit assumption of previous authors who interpreted SN Ia brightness trends with host galaxy stellar mass in terms of SN Ia progenitor metallicity. The SNfactory sample is ideal for testing this assumption, as our untargeted search found SNe Ia in an unbiased sample of host galaxies. In this Section we present our method for inspecting the consistency of SN Ia host galaxies with the galaxy MZ relation and the results from the hosts of SNe Ia discovered by SNfactory.

5.1.1 The Fiducial Galaxy Mass-Metallicity Relation

The correlation of galaxy luminosity and stellar mass with metallicity has been known for several decades (Lequeux et al. 1979), but has been quantitatively refined only recently with the advent of major galaxy spectroscopic surveys at low (SDSS York et al. 2000) and intermediate (Zahid et al. 2011) redshifts. Of particular interest for this work is the correlation of galaxy stellar mass with gas-phase metallicity, which for simplicity we will refer to simply as "metallicity" in this Chapter. For SDSS the MZ relation was studied by the MPA-JHU SDSS team in Tremonti et al. (2004) for the fourth SDSS data release and subsequently for future data releases. Tremonti et al. (2004) found that for a sample of ≈45,000 galaxies, gas-phase metallicities followed a tight relation in the stellar mass range of $8.5 \leq \log(M_*/M_\odot) \leq 11.0$ with a dispersion of about 0.1 dex at high stellar masses. The dispersion in the MZ relation increases at lower stellar mass, up to about 0.3 dex at $\log(M_*/M_\odot) = 8.5$.

Reduction of dispersion in the MZ relation through the study of other galaxy observables has been a key point of interest for galaxy astrophysics. Cooper et al. (2005) showed that the residual deviation from the galaxy MZ relation correlated with the local overdensity of galaxies, such that galaxies in regions of high density tended to have metallicities slightly higher that the values predicted by the MZ relation.

More importantly, Mannucci et al. (2010) found that galaxy SFR shifts the MZ relation, such that more strongly star forming galaxies have lower metallicities than less active galaxies of the same mass. They thus introduced a relation in the three-dimensional galaxy parameter space defined by stellar mass, gas-phase metallicity, and star formation rate which they dubbed the "fundamental metallicity relation." This relation has an even tighter dispersion than the MZ relation alone, generally 0.05 dex across the full range of galaxy stellar masses and SFRs.

5.1.2 SNfactory SN Ia Hosts and the MZ Relation

For this analysis we wish to inspect how much SN Ia hosts deviate from the fiducial MZ relation and whether those deviations are consistent with the observed dispersion in the MZ relation. To do so we use derived stellar masses and metallicities from the MPA-JHU SDSS team analysis of the SDSS DR7 (Abazajian et al. 2009) data. They derive galaxy stellar masses from broadband photometry using the stellar population synthesis library of Kauffmann et al. (2003), and calculate gas phase metallicities from emission line fluxes according to the method outlined in Tremonti et al. (2004). To facilitate the appropriate comparison, we use the SNfactory host stellar masses and metallicities derived in Chapter 3, with masses converted to the same IMF (Chabrier 2003) as the MPA-JHU values and metallicities converted to the Tremonti et al. (2004) scale using the metallicity cross-calibration relations of Kewley & Ellison (2008). The full SNfactory host MZ diagram is shown in Figure 5.1.

In order to assess the agreement of SNfactory host masses and metallicities with the SDSS MZ relation, we first compare the observed SN Ia host metallicities with the values predicted by the MZ relation for their observed mass. In practice, we sum the metallicities of all neighboring (in mass) SDSS galaxies, weighted by their distance from the observed host mass (i.e. $\exp[-\chi^2/2]$ where $\chi^2 = ((M_i - M_{host})/\sigma_M)^2$) with proper accounting for the number of SDSS hosts as a function of mass. Thus for each SN Ia host we can calculate the difference between its observed metallicity and that predicted from the MZ relation as $\Delta Z = Z_{host} - Z_{MZ}$, with an uncertainty equal to the quadrature sum of the host metallicity measurement error and the dispersion of the MZ relation at that host mass (i.e. the RMS of the metallicity values of its stellar mass neighbors from SDSS).

Performing this calculation for all 130 SN Ia hosts in the SNfactory sample in the stellar mass range over which the MZ relation is well populated by SDSS (the aforementioned $8.5 \leq \log(M_*/M_\odot) \leq 11.0$), we find the weighted mean and RMS deviation of SN Ia host metallicities from the MZ relation to be:

$$\langle \Delta Z \rangle = -0.003 \pm 0.012 \tag{5.1}$$

Similarly, if we rephrase the MZ deviation in terms of pull values:

$$\left\langle \frac{\Delta Z}{\sigma_Z} \right\rangle = -0.10 \pm 1.00 \tag{5.2}$$

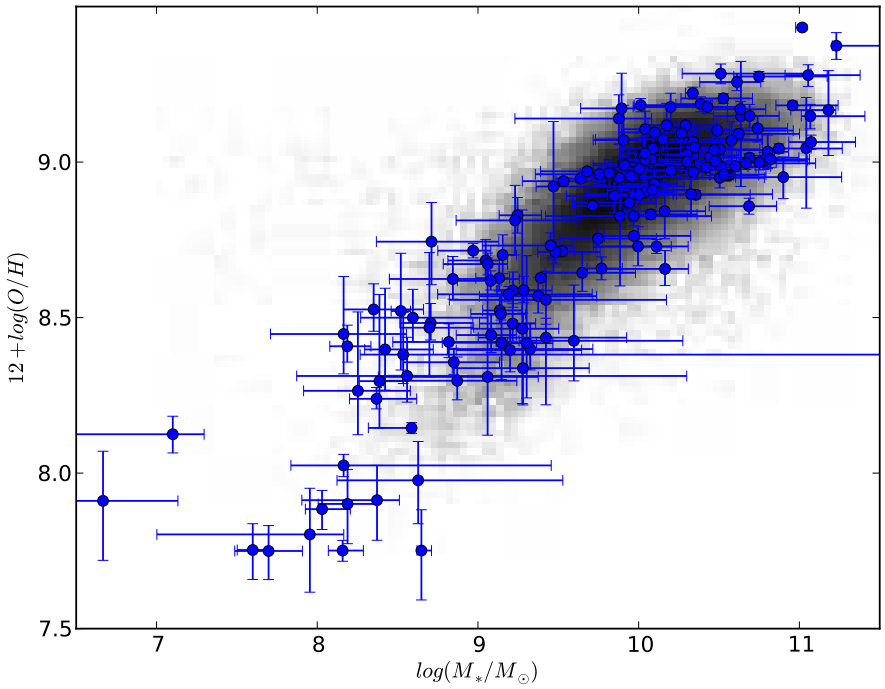

Figure 5.1 Location of SNfactory host galaxies in the MZ plane. The grey background is a density plot of the galaxies in the SDSS DR7 sample analysis from the MPA-JHU team.

Again we note that the errors quoted for these two quantities are the RMS, not the error on the mean. Thus we can see that SN Ia host galaxy metallicities are, on average, remarkably consistent with the values predicted for their host masses by the galaxy mass-metallicity relation. The fact that the RMS of our pull values is exactly 1.00 (with no tuning of measurement errors) implies agreement of SN Ia hosts with the MZ relation for not only the average metallicity values, but also the observed dispersion. This also implies that our measurement errorbars are not misestimated.

To calculate each individual host galaxy's deviation from the SDSS MZ relation in further detail, we derive the metallicity cumulative distribution function (CDF) at each value of stellar mass, again using the weighted metallicities of each host's neighbors in stellar mass. The host is then assigned a score corresponding to where its metallicity is placed in the CDF of metallicities at its mass. This principle is illustrated in Figure 5.2.

Thus for each SN Ia host galaxy, we have a measure of where its metallicity lies in the distribution of metallicities at its stellar mass, which we will call its MZ agreement score. If SN Ia hosts obey the MZ relation, then the ensemble distribution of these scores should be distributed uniformly between 0 and 1. We show in Figure 5.3 this distribution of MZ agreement scores for the 130 SNfactory SN Ia host galaxies whose mass falls within the aforementioned range. From this histogram we can see that the scores are relatively uniform. In the right panel of the same Figure, we plot the cumulative distribution function of the MZ agreement scores as compared to a line of unit slope (i.e. the CDF for a flat distribution). We can see from this plot that indeed our distribution is very close to a flat (uniform) distribution, and the cumulative distribution is reasonably close to unity. This would imply that not only are the mean and RMS metallicity deviation for SN Ia hosts consistent with the MZ relation, but the shape of their distribution is also similar.

5.2 SN Ia Host Galaxy Mass Distributions

In this section we show how the distributions of SN Ia host galaxy stellar masses can be used to discriminate between various SN Ia delay time distributions. The distribution of SN Ia host galaxy masses can be predicted from theory as follows. First let us denote the average star-formation history (SFH) of galaxies of stellar mass M_* as $\psi(M_*, t)$. This we combine with the SN Ia delay time distribution (DTD) $\eta(t; Z(M_*))$, which in principle could be a function of metallicity, to derive the number of SNe Ia expected in a mass interval of width dM:

$$\frac{dN}{dM}(M_*) = \int_0^{t_0} \psi(M_*, t)\eta(t; Z(M_*))\, dt \tag{5.3}$$

In practice, these two quantities, ψ and η, are difficult to measure. It is possible to predict the approximate SFH density from hierarchical galaxy assembly models, and the DTD is often predicted as a product of SN Ia progenitor models. Indeed this method was invoked by KN09 to derive a predicted SN Ia host metallicity distribution. Here we describe a simpler method to arrive at similar results.

5.2.1 Simplified "A+B" Model

Instead of a complex form for η, we may invoke a simpler parametrization of the SN Ia DTD as:

$$\eta(t) = a + b\delta(t) \tag{5.4}$$

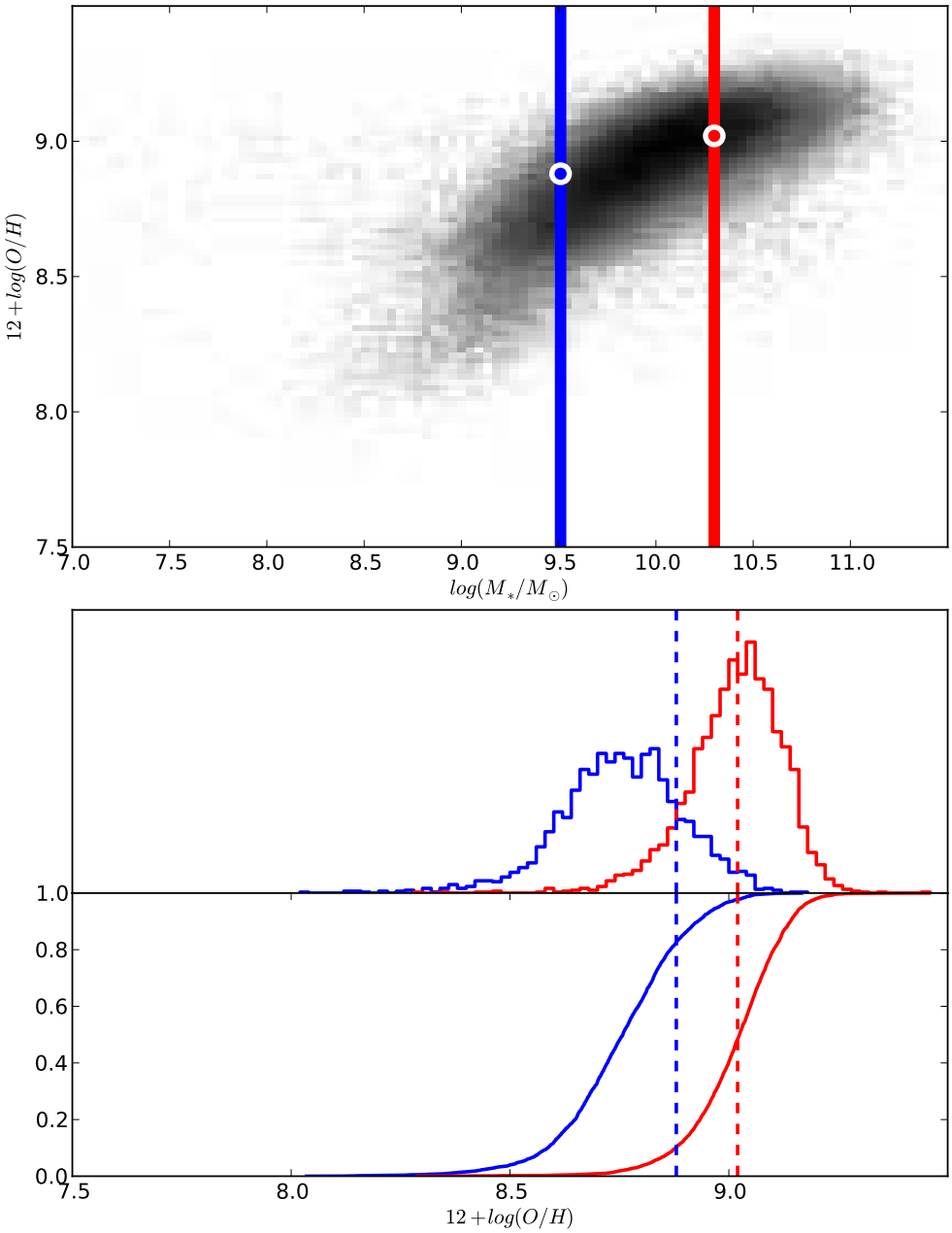

Figure 5.2 Example method for calculating the MZ agreement score for each SN Ia host in the SNfactory sample. In the top panel, the blue and red boxes correspond to the $\pm 1\sigma$ mass values for two hosts, with the white circles showing their mass and metallicity values. The middle panel shows the (unweighted) histogram of metallicities within ± 0.05 dex of each host mass, and the bottom panel shows the (weighted) cumulative distribution function (CDF) for metallicities at each host's mass. The score for each host is the intersection of its metallicity value (vertical lines) with the metallicity CDF at its mass.

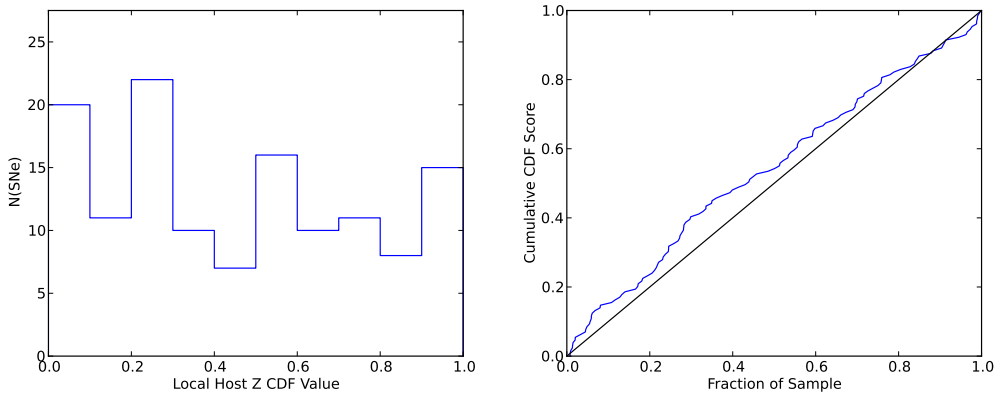

Figure 5.3 Left: distribution of MZ scores for SN Ia hosts from SNfactory. Right: CDF comparison of the SN Ia host MZ score distribution to a uniform (flat) distribution.

which simplifies our host mass distribution to

$$\frac{dN}{dM}(M_*) = a \cdot \left[\int_0^{t_0} \psi(M_*, t)\, dt\right] + b \cdot [\psi(M_*, 0)] \tag{5.5}$$

Thus one component of the rate (the first term) is proportional to the total stellar mass available, and another component (the second term) is proportional to the current instantaneous star-formation rate. This reduces precisely to the popular "A+B" (Scannapieco & Bildsten 2005) formulation proposed from studies of the SN Ia rate as a function of host mass and SFR (Mannucci et al. 2005, 2006; Sullivan et al. 2006):

$$\mathrm{SNR} = A \cdot M_* + B \cdot \mathrm{SFR} \tag{5.6}$$

where the SNe Ia associated with stellar mass are assumed to have long delay times (called "delayed", "tardy", or "extended") and the SNe Ia associated with current SFR (typically dubbed "prompt") are assumed to have very short delay times (e.g. Aubourg et al. 2008).

More broadly speaking, our functional form for the DTD could have invoked a less sharply-peaked function than our δ-function to parametrize the "prompt" component and would have resulted in a similar breakdown of the final SN Ia rate. In fact, most of the aforementioned rates studies reported SFRs averaged over some recent interval (e.g. 0.5 Gyr), so this form would be more general. In general the "A+B" model is a convenient simplification of the DTD to reflect two coarse age bins representing young and old progenitor populations. The ratio of "prompt" to "tardy" SNe Ia crudely captures the slope of the DTD, so "A+B" represents the 0th and 1st order terms in the expansion of the DTD as a power series. For simplicity in some of the subsequent analyses, we will perform simulations using this simple yet effective parametrization.

If we consider this dependence of the SN Ia rate on galaxy mass and star-formation rate, it follows that the SN Ia galaxy mass distribution will be dependent on the distribution of those quantities as a function of galaxy mass. Thus to construct our models for the distribution of SN Ia host galaxy masses, it is necessary to have a functional form for these two distributions. These have

been well measured in the local universe from observational data, and we describe their derivation and functional forms below.

Galaxy Mass and SFR Distributions

In the local universe, the number density of galaxies in a luminosity interval dL is represented by the well-known Schechter (1976) function:

$$\phi(L)dL = \phi_0(L/L_*)^\alpha \exp(-L/L_*)d(L/L*) \tag{5.7}$$

In terms of magnitudes (to avoid confusion we use m for magnitudes and M for galaxy mass) this becomes:

$$\phi(m) = \phi_1 10^{-0.4(m-m_*)(\alpha+1)} \exp(-10^{-0.4(m-m_*)}) \tag{5.8}$$

Most observational constraints on Schechter function parameters are reported in terms of m_* and $\alpha + 1$. In the low-redshift universe, these parameters in $ugriz$ were well measured for the SDSS by Blanton et al. (2003) and will be utilized in our analysis below.

Connecting galaxy luminosities to stellar masses requires a galaxy mass-to-light ratio. Mass-to-light ratios are typically a strong function of galaxy color and a weaker function of galaxy absolute magnitude (Kauffmann et al. 2003), and they are driven largely by the average age of the galaxy's stellar population and less strongly by the details of the galaxy star-formation history. Over a large sample, one can derive the average M_*/L as a function of absolute magnitude, as was done in Kauffmann et al. (2003). Coupling this measurement to the Schechter luminosity function parameters in i-band from Blanton et al. (2003) provides us with the desired stellar mass distribution $dN/dlog(M)$ shown as the dash-dotted green curve in Figure 5.4.

Next we want to derive a similar distribution function for the star-formation rate density in the local universe. This requires additional information about the average star-formation activity as a function of galaxy stellar mass. Fortunately, Salim et al. (2007) measured the SFR in the local universe and found that the galaxy specific SFR (sSFR - the SFR per unit mass) strongly correlates with galaxy stellar mass. Interestingly, the $sSFR$-M_* relation is well fit by a Schechter function, such that lower mass galaxies have more intense star formation (higher sSFR) and the star formation intensity experiences a sharp drop off around $\log(M_*/M_\odot) \sim 11$. Coupling this function for sSFR with the previous Schechter function for stellar mass, we can derive a functional form for the star-formation rate density in the local universe, which is plotted as the dashed magenta curve in Figure 5.4.

In Figure 5.4 we plot the distribution of stellar mass and star formation in the local universe, as well as the host galaxy mass distribution for SN Ia hosts from SNfactory. It is evident from these distributions that the mass and SFR in the local universe peak at different galaxy mass scales, and the SN Ia host mass distribution peaks somewhere between the peaks of these two distributions. It can also be seen that the SN Ia host mass distribution follows the SFR distribution at low mass scales, and the stellar mass distribution at high mass scales. As we will show below, this is because the SN Ia host mass distribution can be modeled as a linear combination of the two distributions, and the SFR distribution is dominant at low mass scales (and the stellar mass distribution is dominant at high mass scales) for almost any possible linear combination of the two distributions.

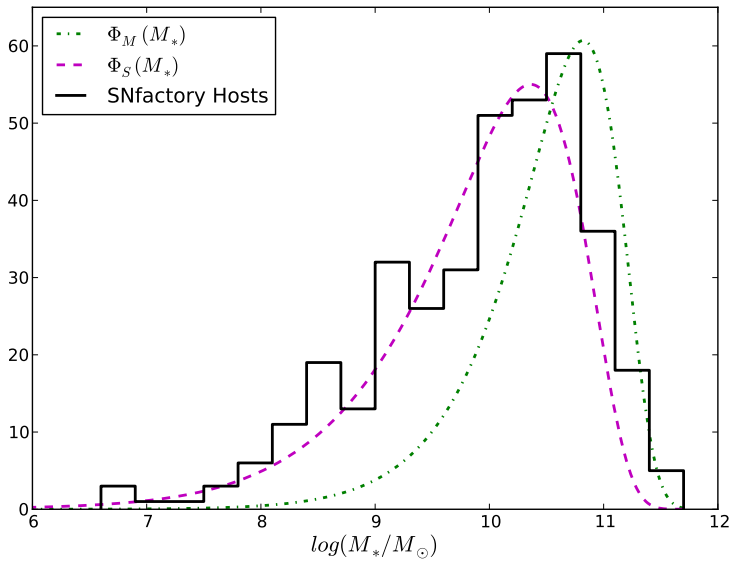

Figure 5.4 Distributions of stellar mass (dash-dotted green curve) and star formation (dashed magenta curve) in the local universe, using Schechter function parameters fitted from SDSS data (Blanton et al. 2003) and sSFR measurements from GALEX (Salim et al. 2007). Also plotted is the host mass distribution from SNfactory (solid black histogram).

Fitting the SN Ia Host Mass Distribution

If we label the distribution of galaxy stellar mass in the local universe as $\Phi_M(M_*)$ and the distribution of star formation as $\Phi_S(M_*)$, these can be related to the aforementioned SFH density as:

$$\Phi_M(M_*) = \int_0^{t_0} \psi(M_*, t)\, dt$$
$$\Phi_S(M_*) = \psi(M_*, t = 0)$$

which thus transforms our previous host mass distribution (Eq. 5.3) to become:

$$\frac{dN}{dM}(M_*) = a \cdot \Phi_M(M_*) + b \cdot \Phi_S(M_*) \tag{5.9}$$

Thus we see that the distribution of SN Ia host galaxy masses under the "A+B" formalism is merely a linear combination of the distributions of stellar mass and star formation in the local universe. Since both of these are known quantities, we can fit the observed SN Ia host mass distribution to find the best fitting coefficients a and b (which are related to the rate coefficients A and B through the normalization factors of Φ_M and Φ_S).

From these fitted values we can determine the total number of "prompt" and "tardy" SNe Ia implied by the host galaxy mass distribution as:

$$N_P = b \int \Phi_S(M_*) dM$$
$$N_T = a \int \Phi_M(M_*) dM$$

In the analysis below, it will be useful to define the fraction of the total number of SNe Ia arising from the prompt channel, which we will call the prompt fraction ρ defined as:

$$\rho \equiv \frac{N_P}{N_P + N_T} \tag{5.10}$$

This fraction is dependent on the ratio of A to B, or equivalently the slope of the SN Ia DTD, which we can roughly estimate from observations. Using A and B from Scannapieco & Bildsten (2005) we find a currently best favored value of $\rho = 0.68 \pm 0.28$.

We now wish to utilize the observed SN Ia host galaxy mass distribution from SNfactory to constrain the prompt fraction ρ. To do so, we calculate a theoretical SN Ia host mass distribution function for an input value of ρ and calculate a probability value for each observed SNfactory host mass, treating the model host mass distribution as a normalized probability distribution function. We then calculate the likelihood of the model as a product of all the probabilities for the observed SNfactory host masses. Marginalizing over all values of ρ between 0 and 1, we find the maximum likelihood prompt fraction (and its $\pm 1\sigma$ uncertainty) of $\rho = 0.83 \pm 0.06$. This falls within the 1σ error bars for the value calculated from the Scannapieco & Bildsten (2005) rate coefficients but is much more precise.

We show this best fit in Figure 5.6 along with the SNfactory host mass distribution. Performing a Kolmogorov-Smirnov (KS) test comparing this predicted host mass distribution with that

observed by SNfactory, we obtain a KS score of $D = 0.065$. Given the sample size of $N \approx 400$, the KS test gives a probability of the observed SN Ia mass distribution being drawn from the best fit theoretical distribution with a probability of approximately 6%. The low agreement probability is likely due to the insufficiency of the simplified "A+B" to encapsulate the true SN Ia DTD, and we will investigate more complex DTDs in the next section.

5.2.2 General Power Law DTD

The above simplification of splitting the galaxy SFH into two age bins allowed us to characterize the SN Ia DTD by only two coefficients "A" and "B", which effectively capture the overall normalization of the DTD and a first order slope. In our analysis of SNfactory hosts, this effectively reduced to a constraint on the DTD slope (A/B) because we do not have a global normalization of the SN Ia rate. However, our data have the power to constrain more complicated functional forms of the SN Ia DTD. Here we inspect the use of a simple power law DTD of the form $\eta(t) \propto t^s$ with a lower age cutoff of t_{prompt} (representing the youngest age allowed for an SN Ia progenitor). Such a functional form has been fit by previous authors (Totani et al. 2008; Barbary et al. 2010; Maoz 2010), and would be a reasonable expectation for the DTD form in DD scenarios (e.g. Ruiter et al. 2009). We now use our SNfactory host galaxy mass distribution to constrain the power law slope DTD s and lower age cutoff t_{prompt}.

To use the above formula (5.3) with a power law SN Ia DTD, we cannot use the integral simplifications of the "A+B" approximation. Instead we must have a functional form for the galaxy star-formation history as a function of galaxy stellar mass (i.e. $\psi(M_*, t)$). To accomplish this we utilize the SFHs measured for SDSS galaxies by Tojeiro et al. (2009) using the code VESPA (Tojeiro et al. 2007). VESPA compares the observed galaxy SED to SPS models and constrains the contributions of stellar populations in various age bins, thus deriving a SFH for a given spectrum. Binning the SFHs of galaxies by their stellar masses, we successfully obtained an empirical form of $\psi(M_*, t)$ based on SDSS data (defined in discrete bins of age and stellar mass). Combining this with a SN Ia DTD lets us calculate a theoretical SN Ia host galaxy mass distribution.

For this analysis, let us assume that the SN Ia DTD is a power law with a lower age cutoff of t_{prompt}:

$$\eta(t) = \begin{array}{ll} \eta_0 t^s & ; t \geq t_{prompt} \\ 0 & ; t < t_{prompt} \end{array} \tag{5.11}$$

Using the above galaxy SFH as a function of stellar mass with this DTD, we can derive the predicted SN Ia host galaxy stellar mass distribution for a given value of the DTD slope s and lower age cutoff t_{prompt}.

In Figure 5.5 we plot the observed SNfactory host galaxy stellar mass distribution against the predicted host mass distribution for our VESPA-derived galaxy SFHs and power law SN Ia DTD for several values of the DTD slope s and lower age cutoff t_{prompt} (rescaled to the normalization of the SNfactory distribution). This figure illustrates how these DTD parameters affect the host mass distribution: (a) a flatter SN Ia DTD (i.e. lower $|s|$) produces a host mass distribution that peaks at higher galaxy masses, and (b) a younger low age cutoff t_{prompt} serves to extend the lower mass end of the SN Ia host mass distribution.

To derive quantitative constraints on the DTD power law slope s and lower age cutoff t_{prompt} from the SNfactory host galaxy mass distribution, we marginalize over the two parameters

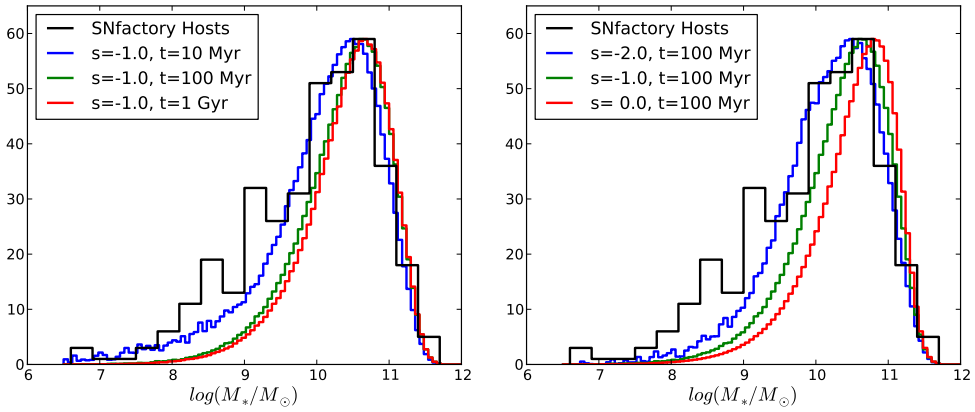

Figure 5.5 Predicted SN Ia host mass distribution given a power law DTD of slope s and lower age cutoff t_{prompt}. The effects of varying the power law slope s (left panel) or the lower age cutoff t_{prompt} (right panel) are shown here, with the observed SNfactory SN Ia host mass distribution shown for reference.

in the ranges $-2 < s < 0$ and $10\ \mathrm{Myr} < t_{prompt} < 1\ \mathrm{Gyr}$ (which corresponds to a main sequence turn-off mass range of $17M_\odot > M_{MS} > 2M_\odot$ at solar metallicity) and again calculate the agreement by maximizing the likelihood function. Our calculations show the best fit DTD slope to be $s = -1.17 \pm 0.10$ and best lower age cutoff to be $t_{prompt} = 18 \pm 7$ Myr, and the host mass distribution predicted by these best parameters is show in Figure 5.6. Our best fit model has a KS score of $D = 0.059$ and probability of 14%, an improvement over the best "A+B" fit but still not a strong agreement. This leaves room for the possibility that the SN Ia DTD shape is more complicated than a simple power law with a sharp lower age cutoff.

Our value for s is consistent with that recently estimated from high-redshift cluster SN Ia rates by Barbary et al. (2010), who found a best fit DTD power law slope of $s = -1.3^{+0.55}_{-0.40}$, and Maoz (2010) who used numerous data sets to show the SN Ia DTD is likely to have a power law slope of $s \approx -1$. Interestingly, the best fit lower age cutoff corresponds to the main sequence turn off timescale (at solar metallicity) for stars of mass $M \sim 10M_\odot$ (Bruzual & Charlot 2003), which is close to the typical upper mass limit for expected progenitors of white dwarfs of $M_{MS,WD} \lesssim 8M_\odot$.

5.2.3 Results and Future Work

In this section we showed how the SN Ia host galaxy stellar mass distribution can be modeled from observations of galaxy physical parameters (stellar mass and star formation rate distributions, or more detailed star formation histories) coupled to a theoretical SN Ia delay time distribution. Using the observed SN Ia host mass distribution, we showed that the ratio of "prompt" to "tardy" SNe Ia (i.e A/B) can be constrained by the host mass distribution using only the distributions of stellar mass and star formation in the local universe as additional input. We also showed how the host mass distribution can provide constraints on DTD model parameters when information about galaxy star formation histories is available. Our results show stronger agreement of the SNfactory host mass distribution with a power law DTD, as compared to the simple two-component

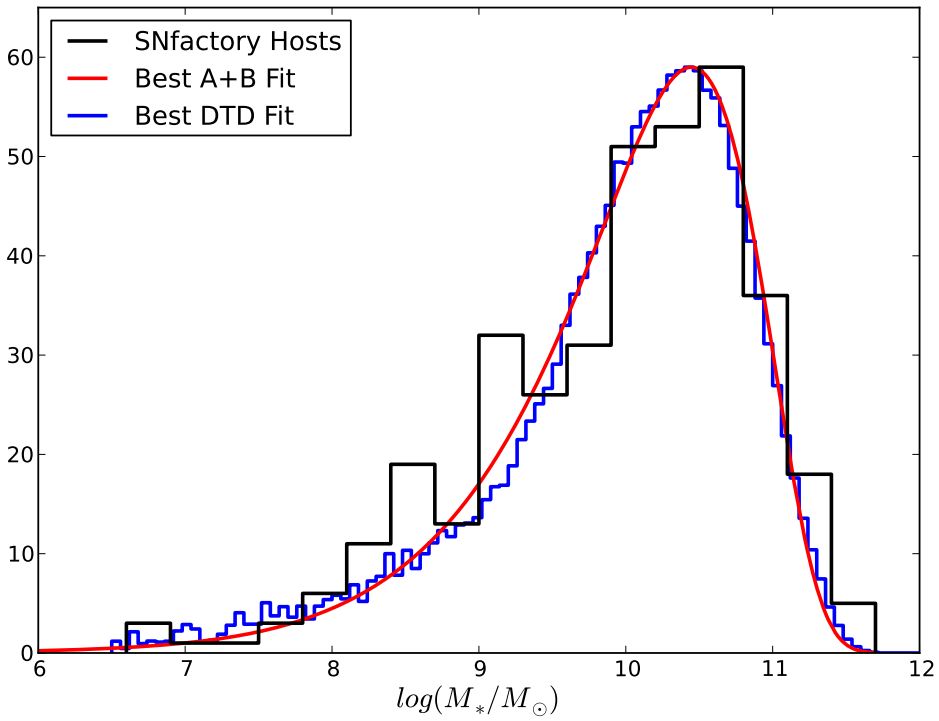

Figure 5.6 Host mass distribution predicted by the best fit "A+B" model from above (red curve), the best fit power law DTD model (blue) curve, and the observed SNfactory SN Ia host mass distribution.

"A+B" DTD. Though our analysis shows only modest agreement with the model DTD, this may be improved with the future detailed inspection of SNfactory search biases (which will enable bias corrections for the observed host mass distribution) and more sophisticated DTD modeling.

Our work shows the power of SN Ia host observables in constraining SN Ia models. We investigated only simple DTD models here, but there exist more detailed models for SN Ia DTD in the literature (e.g. Hachisu et al. 2008; Ruiter et al. 2009; Blais & Nelson 2011). Additional constraints on DTD models using host mass distributions can be derived by leveraging higher redshift data, such as those of SDSS-SN (Lampeitl et al. 2010) or SNLS (Sullivan et al. 2010), where the galaxy star formation characteristics will differ from those in the local universe. In future work, we will investigate a wider variety of SN Ia DTDs and explore the use of high-redshift SN Ia host properties to reinforce the constraints of the SNfactory host mass distribution on SN Ia progenitors.

5.3 Low Luminosity SN Ia Host Galaxies

The study of SNe Ia in low luminosity hosts is of interest for several reasons. First, the low metallicities and young stellar ages expected in low luminosity hosts provide the best local analogs to the low metallicities and young ages of high redshift SN Ia environments. Second, comparatively few lower-redshift SNe Ia have been found in low luminosity hosts due to the targeted nature of many nearby SN Ia searches. Third, as noted above (see Section 4.5), a large number of unusual SNe Ia have been found in low luminosity hosts. Finally, low luminosity hosts provide the best tool for testing the proposed low-metallicity SN Ia inhibition predicted by Kobayashi et al. (1998); Kobayashi & Nomoto (2009, hereafter KN09).

Here we use the SNfactory sample of SN Ia hosts to observationally test the KN09 low-metallicity cutoff prediction. There exist several key challenges in performing such a test. Firstly, the metallicity of the particular SN Ia progenitor is drawn from the distribution of stellar metallicities within its host galaxy. Though low-luminosity galaxies (where violators of the KN09 theory are most probable) are typically well-mixed chemically, the internal galaxy metallicity distribution is still non-negligible. The most reliable observable signature of a low metallicity cutoff would be evident in the statistical behavior of SN Ia hosts at low metallicity.

A second challenge in this endeavor arises from the uncertainty of determining galaxy stellar metallicities on an absolute scale. The KN09 cutoff is cast in terms of iron abundance with respect to the solar value, whereas metallicities in galaxies are most easily derived from gas-phase oxygen abundance (with respect to hydrogen). Connecting the observed gas-phase oxygen abundance to the stellar iron abundance with respect to solar requires several critical quantities: (i) the solar oxygen abundance, (ii) a conversion from gas-phase oxygen abundance to stellar iron abundance, and (iii) a correct estimation of the galaxy oxygen abundance from emission lines. All three of these quantities are currently subjects of vigorous research, with their final values not definitively settled. Thus our search for violators of the KN09 threshold lacks a precisely defined gas-phase metallicity value (or more appropriately a combination of emission line fluxes) to target. Our analysis then must find a lack of low-metallicity hosts where more would be expected. The prediction of the expected number is a key objective in this analysis.

The third and final challenge in the search for SN Ia hosts whose metallicity lies below the KN09 prediction (or alternatively for a clear signature of the lack of such hosts) arises from SNe Ia whose host stellar populations cannot be identified. Several SNe Ia from the SNfactory have

no clearly defined host, even with the aid of very deep imaging. The parent stellar population of these SNe Ia remains a mystery, and the relation of these SNe Ia with respect to the KN09 theory is left ambiguous.

In this Section we present the first attempt to confront the KN09 low-metallicity inhibition theory with observations of SN Ia host galaxies using the SNfactory host sample. We will address in turn our methods for confronting the aforementioned difficulties in this endeavor, and ultimately will show that we indeed find a paucity of low metallicity hosts that represents provisional support for the KN09 theory.

5.3.1 Low-Luminosity SN Ia Host Sample

The most likely candidate host galaxies of low metallicity SN Ia progenitors are those galaxies of very low luminosity, as these faint galaxies are likely to be low mass and thus low metallicity (e.g. Tremonti et al. 2004). We thus developed a focused observing program targeting likely KN09 violator hosts, and utilized primarily Keck LRIS observations to assess the gas-phase metallicity of low-luminosity hosts. Here we briefly outline the target selection and properties of the SNe Ia found in these low luminosity hosts.

Target Selection

Despite the uncertainty in the physical quantities needed to convert the KN09 prediction to observable galactic properties, the fiducial values of these quantities can provide a reasonable estimate for the galaxy luminosity scale at which KN09 violators are most likely. The current best estimate for the solar oxygen abundance is $12+\log(O/H)_{\odot} = 8.86$, as measured by Delahaye et al. (2010) using asteroseismology techniques. At low metallicities ($[Fe/H] \approx -1$) the stellar $[O/Fe]$ ratio is about 0.3 dex (McWilliam 1997) in the Milky Way, but is likely to be closer to 0 in dwarf galaxies (Tolstoy et al. 2009). Combining these quantities implies that the target gas-phase oxygen abundance where inhibition sets in should be $12 + \log(O/H)_{KN09} \approx 7.7$.

We can use the galaxy mass-metallicity (MZ) relation (Tremonti et al. 2004) to find the galaxy stellar mass scales on which to search for KN09 violators. The median galaxy mass corresponding to the cutoff gas-phase metallicity calculated above is about $\log(M_{KN09}/M_{\odot}) \approx 7.3$. However, the MZ relation has some dispersion (about 0.3 dex in metallicity at the aforementioned mass scale), so that a higher mass galaxy could still have a metallicity low enough to produce KN09 violators. Thus we use a mass cutoff of $\log(M_*/M_{\odot}) = 9.0$ as a nominal cut for our study. At this mass, a galaxy at the KN09 cutoff metallicity would be a 3.8σ outlier of the MZ relation. Using a simple solar mass-to-light ratio (Blanton et al. 2003), this cutoff mass corresponds to an absolute host galaxy magnitude of $M_g = -17.35$ in g-band.

Most of the data for this study come from observations taken over three nights with Keck LRIS. The goal of these observations was to obtain emission line flux strengths from the (longslit) spectra of these low-luminosity SN Ia host galaxies. Because the strength of emission was not known prior to observations, our standard observing strategy was to obtain 30 minutes of spectroscopic observations for each target. Thus our resulting signal-to-noise (and thus metallicity error) are variable, but the majority of our observations yielded high S/N ($\sigma_Z \sim 0.1$ dex) metallicity measurements. The implications of our observational completeness and metallicity success rate will be addressed later in this study.

Table 5.1. Low-luminosity SN Ia hosts from SNfactory.

SN Name	$z_{\rm helio}$	Host $\log(M_*/M_\odot)$	Host $12+\log(O/H)$	SN SALT2 $x1$	SN SALT2 c
SNF20070429-003	0.0672	6.63 ± 0.60	···	···	···
SNF20080910-007	0.0791	6.67 ± 0.56	7.91 ± 0.18	0.02 ± 0.11	-0.01 ± 0.01
SNF20070504-012	0.1000	6.83 ± 1.55	···	···	···
SNF20051004-001	0.0088	7.10 ± 0.44	8.12 ± 0.06	···	···
SNF20070825-001	0.0742	7.32 ± 0.17	7.71 ± 0.15	···	···
SNF20080512-008	0.0774	7.60 ± 0.10	7.75 ± 0.09	0.79 ± 0.16	0.03 ± 0.02
SNF20080510-001	0.0717	7.70 ± 0.21	7.75 ± 0.09	-0.16 ± 0.16	-0.00 ± 0.01
SNF20061101-003	0.1000	7.74 ± 0.33	···	···	···
SNF20060514-003	0.0880	7.80 ± 0.52	···	0.30 ± 0.19	-0.02 ± 0.02
SNF20060622-020	0.1136	7.90 ± 0.61	···	···	···
SNF20080516-000	0.0732	7.95 ± 0.58	7.80 ± 0.17	1.05 ± 0.23	0.01 ± 0.02
SNF20061024-012	0.0430	8.03 ± 0.14	7.88 ± 0.06	···	···
SNF20050925-010	0.0376	8.05 ± 0.23	···	···	···
SNF20050824-002	0.1242	8.07 ± 1.06	7.92 ± 0.02	···	···
SNF20050822-000	0.1374	8.16 ± 0.42	8.45 ± 0.16	···	···
SNF20070424-006	0.0702	8.16 ± 0.11	7.75 ± 0.03	···	···
SNF20080908-000	0.0525	8.16 ± 0.81	8.02 ± 0.04	-0.40 ± 0.19	-0.07 ± 0.02
SNF20070420-001	0.0948	8.19 ± 0.13	8.41 ± 0.06	0.38 ± 0.13	0.00 ± 0.01
SNF20080606-012	0.0750	8.19 ± 0.18	7.90 ± 0.12	···	···
SNF20070422-003	0.0382	8.25 ± 0.33	8.26 ± 0.20	···	···
SNF20051113-000	0.0824	8.35 ± 0.25	8.53 ± 0.08	-1.02 ± 0.20	0.05 ± 0.02
SNF20080706-004	0.0399	8.36 ± 0.48	8.42 ± 0.02	···	···
SNF20061108-004	0.0889	8.37 ± 0.45	···	···	···
SNF20070331-013	0.0598	8.37 ± 0.21	8.24 ± 0.03	···	···
SNF20071117-006	0.0770	8.37 ± 0.30	7.91 ± 0.12	···	···
SNF20070824-001	0.0293	8.40 ± 0.81	8.46 ± 0.12	···	···
SNF20050731-005	0.0675	8.42 ± 0.21	8.40 ± 0.16	···	···
SNF20051020-000	0.0650	8.43 ± 0.40	···	···	···
SNF20070419-011	0.1095	8.47 ± 0.50	···	···	···
SNF20080610-003	0.0954	8.49 ± 0.07	8.63 ± 0.10	···	···
SNF20070528-003	0.1167	8.51 ± 0.44	···	···	···
SNF20071019-003	0.0326	8.51 ± 0.20	8.59 ± 0.03	···	···
SNF20080909-024	0.1294	8.51 ± 0.66	···	···	···
SNF20080723-012	0.0793	8.52 ± 0.06	8.52 ± 0.19	···	···
SNF20061107-004	0.0900	8.54 ± 1.82	8.38 ± 0.11	···	···
SNF20070712-002	0.0921	8.56 ± 1.21	8.31 ± 0.10	···	···

Table 5.1 (cont'd)

SN Name	$z_{\rm helio}$	Host $\log(M_*/M_\odot)$	Host $12+\log(O/H)$	SN SALT2 $x1$	SN SALT2 c
SNF20050903-000	0.0882	8.59 ± 1.13	8.40 ± 0.27	···	···
SNF20070730-002	0.0407	8.59 ± 0.14	8.15 ± 0.02	···	···
SNF20060618-014	0.0638	8.60 ± 0.40	8.50 ± 0.08	0.42 ± 0.18	0.04 ± 0.02
SNF20070425-010	0.0800	8.62 ± 0.79	···	···	···
SNF20080919-001	0.0420	8.63 ± 0.70	7.98 ± 0.13	0.29 ± 0.18	0.06 ± 0.02
SNF20070712-003	0.0739	8.65 ± 0.04	7.75 ± 0.15	-0.17 ± 0.16	-0.05 ± 0.01
SNF20080510-000	0.0346	8.66 ± 0.22	···	···	···
SNF20050919-000	0.0372	8.70 ± 0.23	8.47 ± 0.20	···	···
SNF20050821-007	0.0595	8.71 ± 0.23	8.48 ± 0.06	0.15 ± 0.29	0.01 ± 0.02
SNF20080909-030	0.0311	8.71 ± 0.38	8.74 ± 0.13	0.88 ± 0.16	0.09 ± 0.02
SNF20070427-010	0.1400	8.75 ± 0.12	···	···	···
SNF20070418-019	0.0880	8.76 ± 0.19	···	···	···
SNF20070717-003	0.0860	8.80 ± 0.53	8.98 ± 0.01	-0.85 ± 0.14	0.12 ± 0.01
SNF20061019-019	0.0855	8.82 ± 0.32	8.42 ± 0.05	···	···
SNF20060921-006	0.0527	8.84 ± 0.40	8.62 ± 0.07	···	···
SNF20061011-005	0.0230	8.85 ± 0.30	8.36 ± 0.04	0.37 ± 0.20	-0.09 ± 0.02
SNF20071012-004	0.0710	8.85 ± 0.43	···	···	···
SNF20060916-002	0.0721	8.87 ± 0.42	8.30 ± 0.07	1.07 ± 0.29	0.03 ± 0.02
SNF20051119-004	0.0734	8.94 ± 0.39	···	···	···
SNF20080620-000	0.0330	8.97 ± 0.17	8.72 ± 0.02	-1.04 ± 0.18	0.12 ± 0.02
SNF20060906-011	0.0649	8.99 ± 0.67	···	···	···

Properties of SNe Ia in Low Luminosity Hosts

Of the 396 SNe Ia discovered by SNfactory, 57 were discovered in hosts whose stellar masses were less than $\log(M_*/M_\odot) = 9.0$. These SNe Ia are listed in Table 5.3.1 along with the host galaxy masses and metallicities, and SN light curve parameters (where available).

As previously noted, low-luminosity galaxies have produced some interesting SNe Ia. To gauge how unusual (or not) these low-luminosity-hosted SNe Ia are, we plot in Figure 5.7 the scatter plots and normalized histograms of the light curve width (SALT2 $x1$) and color (SALT2 c) distributions of the low-luminosity-hosted SNe Ia from the SNfactory cosmology sample against the distributions from the full cosmology sample. As expected, the light curves of these SNe Ia tend to be (on average) wider than the full SN Ia sample (higher stretch), consistent with the trend of light curve width with galaxy mass previously noted by other authors.

Interestingly, the light curve color distribution of the low-luminosity-hosted SNfactory SNe Ia shows a paucity of highly-reddened colors. The implication here is that low-luminosity galaxies do not produce highly extincted SNe Ia. This is to be expected if SN Ia reddening is generated exclusively by dust in the interstellar medium (ISM) of the SN Ia host galaxy, as low-

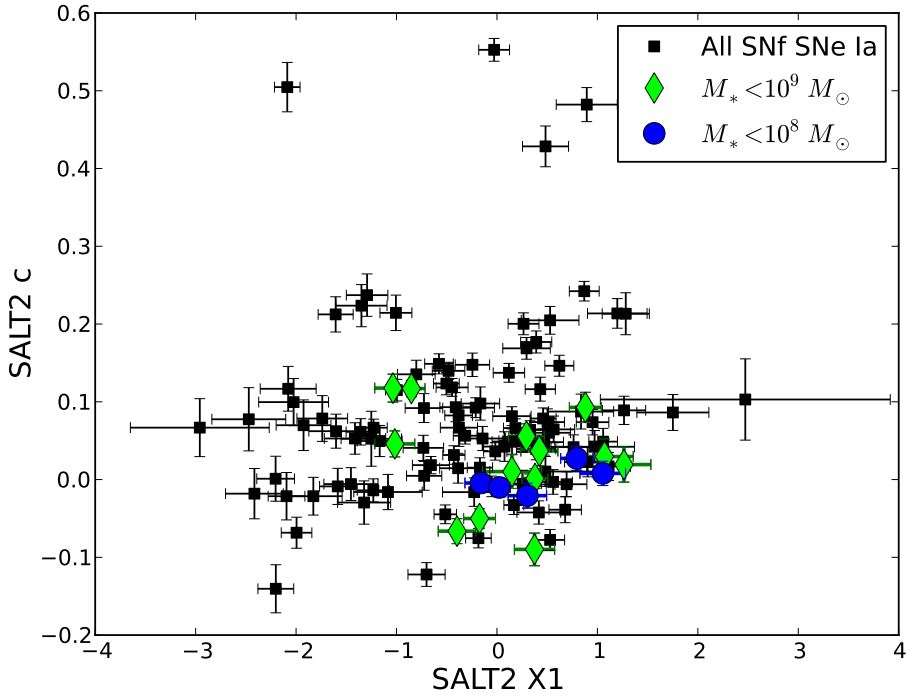

Figure 5.7 Light curve width (SALT2 x_1) and color (SALT2 c) properties for all SNe Ia from SNfactory (black squares) compared to those hosted in low mass galaxies (green diamonds: $\log(M_*/M_\odot) < 9$, blue circles: $\log(M_*/M_\odot) < 8$).

luminosity galaxies are expected to have low metal content and thus have a small dust content. Similarly, the smaller physical size of low-mass galaxies would imply a low column density of gas, and thus a low foreground extinction even under higher dust-to-gas ratios. If reddening in SNe Ia is produced by the circum-stellar medium (CSM) surrounding the SN Ia progenitor system (presumably originating from previous mass-loss episodes) then one would expect highly CSM-extincted SNe Ia to be present in all environments.

5.3.2 Hostless SNe Ia

Our spectroscopic observations of low-luminosity SN Ia hosts targeted the nearest object which was expected to be the host. In several cases, the nearest object proved to be either faint foreground Milky Way stars, or background high-redshift galaxies. In these cases, we obtained deep imaging with LRIS afterward to identify other potential hosts and place limits on the possible mass of host galaxy candidates in the SN vicinity.

In two such cases, for the hosts of SNF20050728-012 and SNF20070901-016, subsequent deep imaging showed tidal tails emanating from nearby galaxy groups (see Figure 5.8). In these instances, the SNe Ia are unlikely to be of low enough metallicity to be KN09 violators, as tidal material stripped from larger galaxies is more likely to share metallicity with its larger parent galaxy (see, e.g., Croxall et al. 2009). While such SNe Ia could be interesting in studies of SNe Ia in extreme environments, they are not useful in our search for KN09 violators.

More perplexing in our search for extremely low-metallicity SN Ia host galaxies are those SNe Ia without any identifiable host galaxy. For 8 SNe Ia, no viable host galaxy candidates were found even with very deep imaging, and no evident tidal structures from large galaxy groups were evident. For these SNe Ia, all possible host candidates within 15 kpc were spectroscopically screened and confirmed to be either foreground Milky Way stars or background high-redshift galaxies. We also confirmed that no distant galaxies in the field were within 10 effective radii of the SN location. Similarly, we searched the NED database for nearby known galaxy clusters, and found only one candidate (for SNF20080905-005) whose redshift was too discrepant (by 3000 km s^{-1}) to be a viable source of this SN.

We show in Table 5.2 the magnitude limits from deep photometry for our hostless SNe Ia, along with the corresponding galaxy stellar mass upper limits assuming a solar mass-to-light ratio. This mass-to-light ratio choice is appropriate for normal intermediate mass ($\log(M_*/M_\odot) \sim 9.0$) galaxies with somewhat older stellar populations and redder colors than lower mass galaxies, and thus can be considered a conservatively high upper limit for the mass-to-light ratio for any extreme low mass galaxy.

Since our primary objective in this study is to identify low metallicity SN Ia host galaxies, we inspect the likelihood of these potentially hostless SNe Ia originating from extremely low mass galaxies. We first examine whether the presence of SN Ia hosts with masses at or below our observational upper limits for the hostless SNe Ia might be consistent with expectations for the number of low mass SN Ia hosts. To do so, we repeat the host mass distribution maximum likelihood analysis of the previous Section, this time including the hostless SNe Ia by using their host mass upper limits as placeholder values for their host masses. Since the host mass distribution function (and

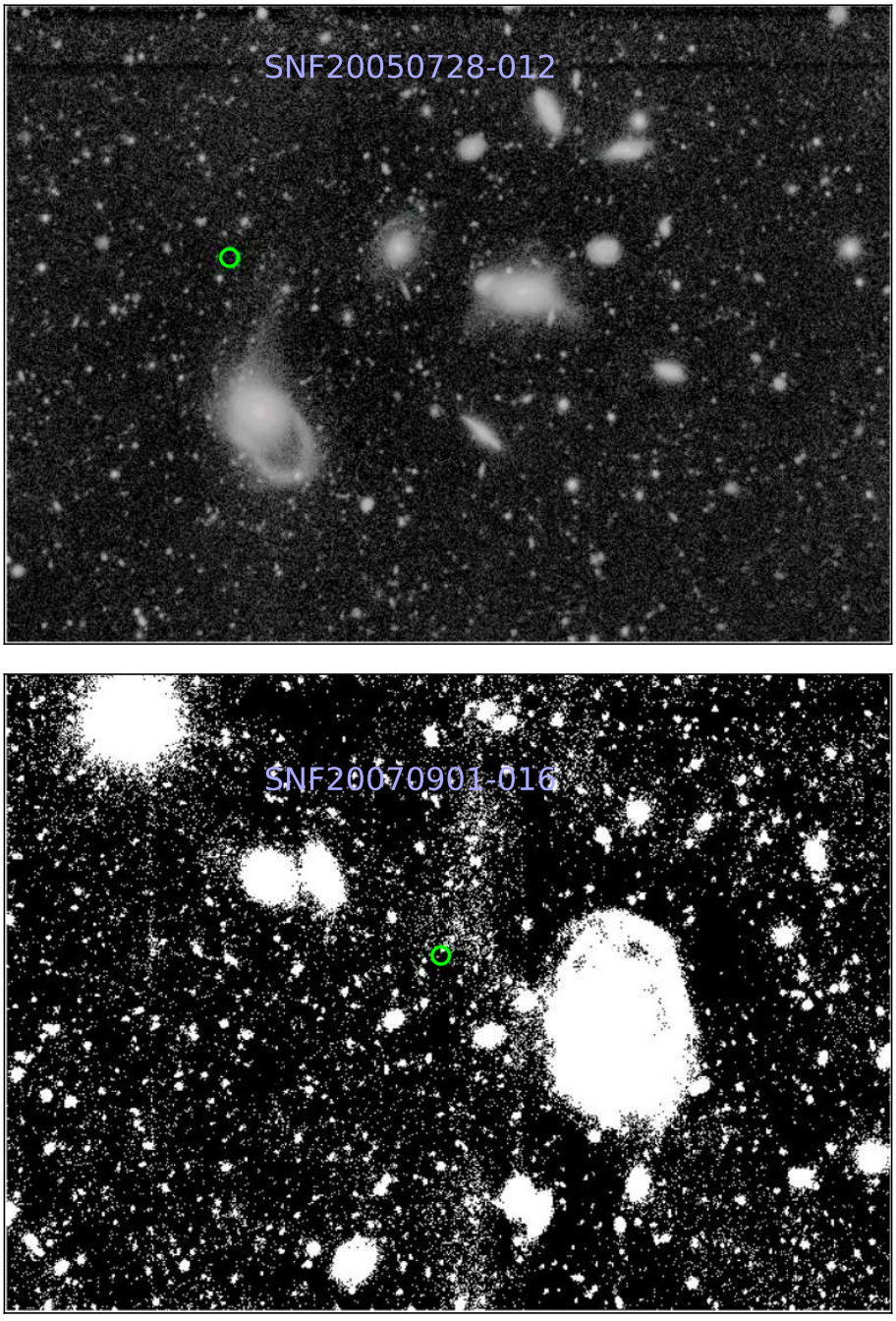

Figure 5.8 SNfactory SNe Ia in tidal tails of large interacting galaxy groups, SNF20050728-012 (top) and SNF20070901-016 (bottom).

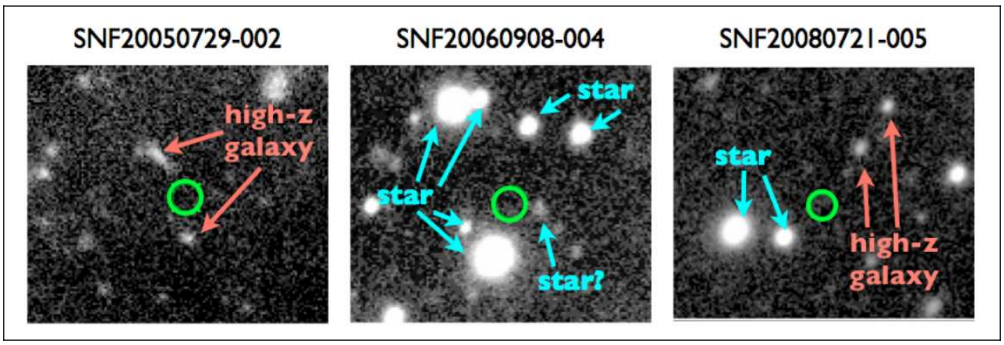

Figure 5.9 SN vicinity for several hostless SNe Ia from SNfactory. All potential host candidates within a reasonable distance from the SN location have been spectroscopically classified as either foreground stars or background galaxies.

Table 5.2 Hostless SNe Ia from SNfactory.

SN	$m_{\mathrm{g,lim}}$ [a]	z_{SN}	$M_{\mathrm{g,lim}}$	$\log(M_*/M_\odot)_{\mathrm{lim}}$ [b]	Source
SNF20050729-002	27.07	0.0934	−11.09	6.50	SNIFS
SNF20060601-005	25.91	0.0948	−12.28	6.97	LRIS
SNF20060908-004	27.97	0.0492	−8.73	5.55	LRIS
SNF20061110-006	26.57	0.1330	−12.41	7.02	LRIS
SNF20071108-018	26.10	0.1005	−12.23	6.95	LRIS
SNF20080721-005	27.99	0.0565	−9.02	5.67	LRIS
SNF20080905-005	26.56	0.0585	−10.53	6.27	LRIS
SNF20080918-004	24.80	0.0546	−12.13	6.91	SNIFS

[a] 3σ limiting apparent magnitude in g-band

[b] Corresponding host stellar mass 3σ upper limit given solar mass-to-light ratio.

thus the PDF for our likelihood analysis) decreases toward lower masses, using the upper limits for this calculation is appropriate for estimating an upper limit of the likelihood of finding so many low mass systems. The resultant likelihood for our SNfactory host mass distribution with hostless SNe Ia included is a factor of about 10^{-12} smaller than the likelihood without the hostless SNe Ia (after appropriate rescaling for the altered sample size). The implication of this result is that the presence of so many low mass SN Ia hosts strongly disagrees with our model based on the distribution of stellar mass and star formation in normal galaxies. This could imply that these hostless SNe Ia come from stellar systems not formed in the typical galaxy evolution sequence that drives the observed stellar mass and SFR distributions in the local universe. For the purpose of testing the KN09 theory, we wish to know the likelihood of these SNe Ia originating from progenitors below the proposed metallicity cutoff. While arguments based on galaxy stellar mass limits and the galaxy MZ relation would point to the likelihood of these hostless SNe Ia being KN09 violators, their disagreement with the galaxy mass distribution function hints that the MZ relation may not be applicable in these systems. Thus while we cannot conclusively show that these hostless SNe Ia do not violate the KN09 cutoff, we cannot confidently invoke galaxy mass assembly arguments to argue that they do have metallicities below the cutoff.

The origin of these apparently hostless SNe Ia is an intriguing mystery. While we have ruled out any normal host candidates within a reasonable distance from these SNe, there remain several alternate (yet highly irregular) possible explanations for their origin. It is still possible that these SNe Ia could be associated with normal size host galaxies that are extremely far away (i.e. > 25 kpc), and were possibly ejected from the galaxy in the distant past (enough to exceed our effective radius cut). Though such events are expected to be rare (since only small fractions of galaxy mass are typically lost in such ejections) at least one strong contender for such a case has been found in the unusual SN PTF09dav (Sullivan et al. 2011b). Indeed if a SN Ia progenitor system was ejected from its host with a terminal velocity of only 100 km s^{-1}, then a distance of 25 kpc could be traversed in only 250 Myr. Thus tidally ejected SNe Ia with long delay times could severely confuse host association. In a similar situation, the progenitors of these hostless SNe Ia could have been ejected from their host galaxy with a high velocity along the observer line of sight, thereby complicating host identification due to a redshift mismatch. This however, is somewhat unlikely, as a large velocity discrepancy would result in a significant deviation from the brightness predicted by normal Hubble expansion (i.e. a large Hubble residual), and this is not the case for those SNe Ia with available Hubble residuals. Additionally, we found no clear host candidates nearby with even modestly close velocities (< 2000 km s^{-1}). Similarly, these hostless SNe Ia are not analogous to the two obvious tidal ejection SNe Ia presented above. Though an ejection origin of these hostless SNe Ia is still remotely possible, we have carefully excluded any obvious scenarios of this sort.

If these hostless SNe Ia are not dynamically stripped from larger galaxies, it is most likely that they originated from extremely faint stellar groups. Perhaps the best candidate systems would be very old and compact dwarf galaxies which quenched all their gas and ceased star formation in the distant past. As noted in the HOST07if analysis above (see Chapter 4), older stellar populations have a higher mass-to-light ratio, meaning a very old stellar system even of modest mass would have a very low luminosity. These would be the extreme analogs of the quiescent dwarf galaxies (Sánchez Almeida et al. 2008) which become fainter between episodes of star formation. Though some very faint dwarfs have been identified in the Local Group and nearby galaxy clusters (see Tolstoy et al. 2009, for a review), none have yet been identified in distant isolated regions. Assess-

ment of the prevalence of such faint stellar systems is a challenging endeavor yet to be undertaken, and thus cannot be pointed to as a clear source for our potentially hostless SNe Ia.

Perhaps the most extreme potential explanation for the origin of these SNe Ia is the possibility that their progenitors formed from the inter-galactic medium. Star-formation in the space between galaxies is a poorly understood subject, as might be expected given the difficulty of identifying the low luminosity star-formation the IGM would be likely to produce. If these SNe Ia did indeed originate from IGM stars, they would serve as an excellent probe of this under-examined medium. While the origin of these hostless SNe Ia is a conundrum for SN Ia progenitor studies, they present a unique opportunity to study exotic realms of star formation and stellar dynamics, and we hope they will be examined in greater depth in the future.

5.3.3 KN09 Threshold with SNfactory Data

The primary objective of this study is to examine whether the metallicities of SN Ia host galaxies from the SNfactory provide evidence in support of or contradictory to the KN09 low-metallicity SN Ia inhibition theory. As shown in Table 5.3.1 and in Figure 5.10, none of the SNfactory host galaxies has a measured metallicity significantly below the fiducial predicted KN09 cutoff metallicity. Thus we must turn to an inspection of the statistical behavior of all SNfactory hosts and whether their metallicities show significant support for a low metallicity cutoff.

A critical component of this analysis is to predict the number of SN Ia hosts that should have metallicity below the KN09 cutoff if the cutoff is not present. This method will rely heavily on the SN Ia host galaxy mass distribution modeling techniques of the previous section. Below we will describe the particular adaptation of our previous methods to this low metallicity cutoff analysis, including our use of Monte Carlo techniques to simulate the expected metallicity distribution for our sample. We then discuss the observational completeness for our host metallicity measurements and the final significance of our data's support for the KN09 theory.

Low Metallicity SN Ia Host Expectations

In order to evaluate the agreement of our data with a low-metallicity SN Ia cutoff, we must first answer the question of how many SN Ia hosts we should have expected below the fiducial cutoff gas-phase oxygen abundance (given our sample size). More generally, since the exact value of the cutoff is somewhat uncertain, we investigate the likelihood of observing no hosts below the observed minimum metallicity of our sample.

To predict the expected metallicity values for the SNfactory sample, we begin with the host galaxy mass distribution. For the purposes of this analysis, we will model the SN Ia host galaxy mass distribution using the "A+B" models of the previous section, which were parametrized by the "prompt fraction" ρ (i.e. the fraction of SNe Ia associated with star-formation, see discussion above). This model serves as a good approximation of the shape of the SN Ia host mass distribution and provides an analytical means of calculating expected host metallicity statistics.

Let us start with a simple calculation of the expected number of SN Ia hosts whose metallicity violates the KN09 threshold. We first calculate the amount of stellar mass and star formation in the local universe that occurs on galaxy mass scales below the expected KN09 mass scale (calculated above) using the integrals of the distribution functions for these two quantities. We find that p_M =0.08% of stellar mass and p_S =1.58% of star formation in the local universe can be found in

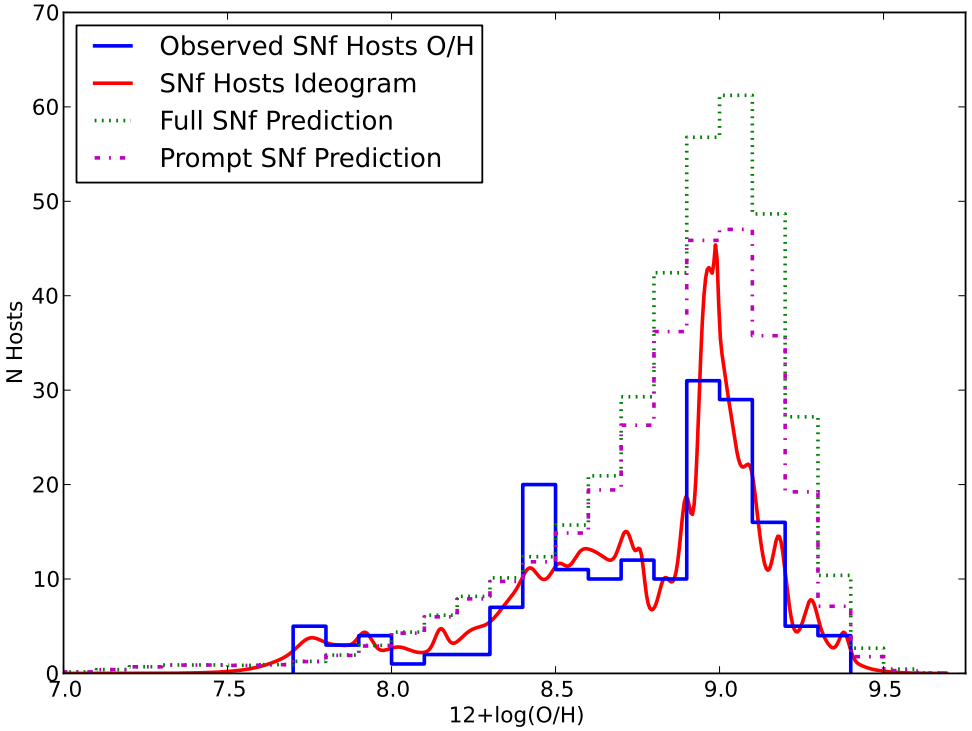

Figure 5.10 Observed SN Ia host metallicities for SNfactory hosts (solid blue histogram), compared to the predicted total distribution based on SNfactory host masses coupled with the MZ relation (dash-dotted green curve), and the predicted number of star-forming hosts for which we might have measured a gas-phase metallicity (dotted magenta curve). For reference, we also plot an ideogram of the SNfactory host metallicities as the (unbinned) red curve.

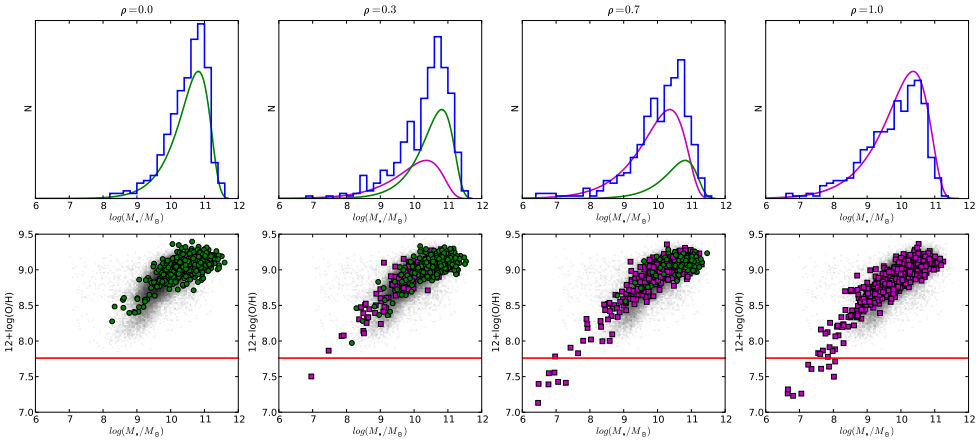

Figure 5.11 Top: Host galaxy mass histograms for example Monte-Carlo realizations for various values of ρ. Bottom: Host galaxy locations in MZ space for the same realizations. Prompt SN Ia hosts are represented as magenta squares, while tardy SN Ia hosts are green circles.

galaxies whose masses are below M_{KN09}. A SN Ia host galaxy mass distribution paramtrized by ρ then has a predicted fraction of KN09 violators that is merely the weighted sum of these two fractions $p_V = \rho p_S + (1-\rho)p_M$. For a sample of size N, the likelihood of finding N_V violators then is just described by a binomial distribution parametrized by N and p_V. For the best fit prompt fraction from above $\rho = 0.83$ with the full SNfactory sample size $N = 396$, this gives a violator fraction of p_V =1.3%, with a probability of finding no KN09 violators (i.e. $N_V = 0$) of $P = 0.0058$. Thus if we confidently determine all SNfactory hosts to not be KN09 violators, this would constitute a strong confirmation of the KN09 theory.

Because there exists some spread in the galaxy mass-metallicity relation (which is not constant in metallicity), the above simple calculation could be subtly different than the real SN Ia host metallicity distribution. To examine this effect, we perform Monte-Carlo simulations of the expected SN Ia host galaxy mass and metallicity distributions for numerous values of the prompt fraction ρ. For a given ρ, we randomly generate $N_g \approx 100000$ galaxy mass values distributed according to Φ_S and Φ_M appropriately weighted (by ρ and $1-\rho$, respectively). From these we randomly selected $N_{SN} = 396$ mock SN Ia host galaxies, and to these mock galaxies we assigned gas-phase oxygen abundances according to the MZ relation of Tremonti et al. (2004) with random offsets gaussianly distributed according to the observed dispersion about the MZ relation (as estimated from MPA-JHU metallicities for SDSS data). This procedure was repeated $N_{sample} = 10000$ times for each value of ρ, which was sampled from 0 to 1 in steps of 0.1.

In Figure 5.11 we present examples of simulated host mass distributions and locations of mock hosts in MZ space for several values of ρ. These examples clearly illustrate the general trend: "tardy" SNe Ia occur more frequently in galaxies of much higher mass, and thus rarely occur in low-metallicity hosts, while "prompt" SNe Ia have a fair number in low-metallicity hosts.

For each ρ, we evaluated the distribution of two quantities: (i) the number of SN Ia hosts with metallicity below the fiducial cutoff in each realization, labeled N_V (number of "violators"

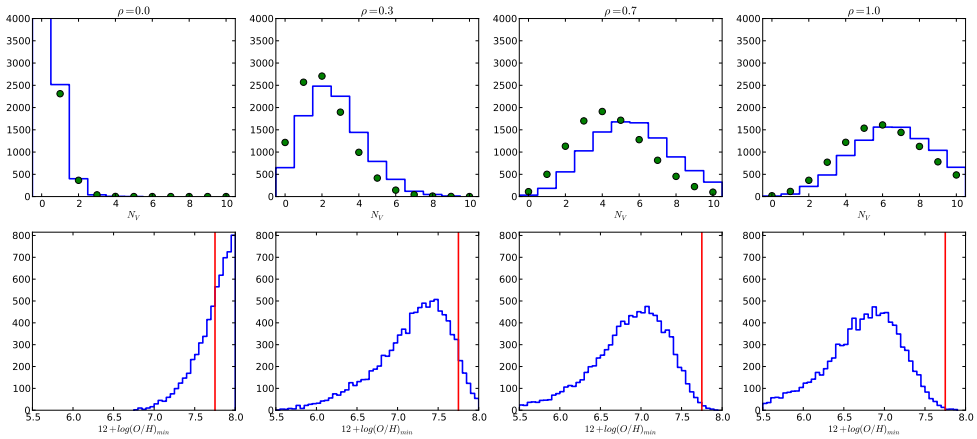

Figure 5.12 Top: Histogram of the number of KN09 violators N_V with metallicities below the fiducial threshold value (solid blue histogram) in our Monte-Carlo simulations. The green points represent the predictions from a binomial distribution for our given sample size and the expected fraction of galaxies below the KN09 mass cutoff value. Bottom: Histogram of the lowest metallicity values from Monte-Carlo simulations (blue histogram), along with the observed lowest spectroscopic metallicity (vertical red line) from SNfactory.

of the prediction); and (ii) the minimum metallicity in each realization Z_{min}. In Figure 5.12 we show the distributions of these two quantities across all realizations at a given ρ for several values of ρ. With the N_V distributions we also plot the values predicted by our simple binomial distribution calculation above. As we can see, our simple calculation comes very close to the simulated distribution, meaning it is reasonable to perform our significance tests using this simplified model based on a binomial distribution parametrized by the calculated violator fraction.

From the above plots it is evident that if all SNe Ia originated from the tardy channel then it would be unsurprising to find no violators of the KN09 threshold given our sample size ($N_V = 0$ for 75% of realizations at $\rho = 0$). Indeed, the fraction of hosts whose mass lies below the value corresponding to the KN09 cutoff is 0.03% when $\rho = 0$ (i.e. the sub-KN09 stellar mass fraction p_M from above), indicating the need for a sample size of several thousand before a violator would be observed, or substantially more SNe Ia before a significant non-detection could be observed. The number of violators rapidly increases as even a small number of prompt SNe Ia appear (at $\rho = 0.1$ more than half of the realizations have violators). For example, at $\rho = 0.8$ (close to the best fit value of $\rho = 0.83$), the fraction of realizations without violators is 0.31%, and the number of realizations whose Z_{min} exceeds our observed value is equally small (0.34%)

Observational Completeness and Final Results

To correctly assess the statistical power of the observed SNfactory sample in analyzing the KN09 cutoff prediction, we must first inspect our observational completeness. In the top panel of Figure 5.13 we show the total number of SNfactory hosts in (coarse) bins of stellar mass, as well as the counts for spectroscopic observations and successful metallicity measurements. In the

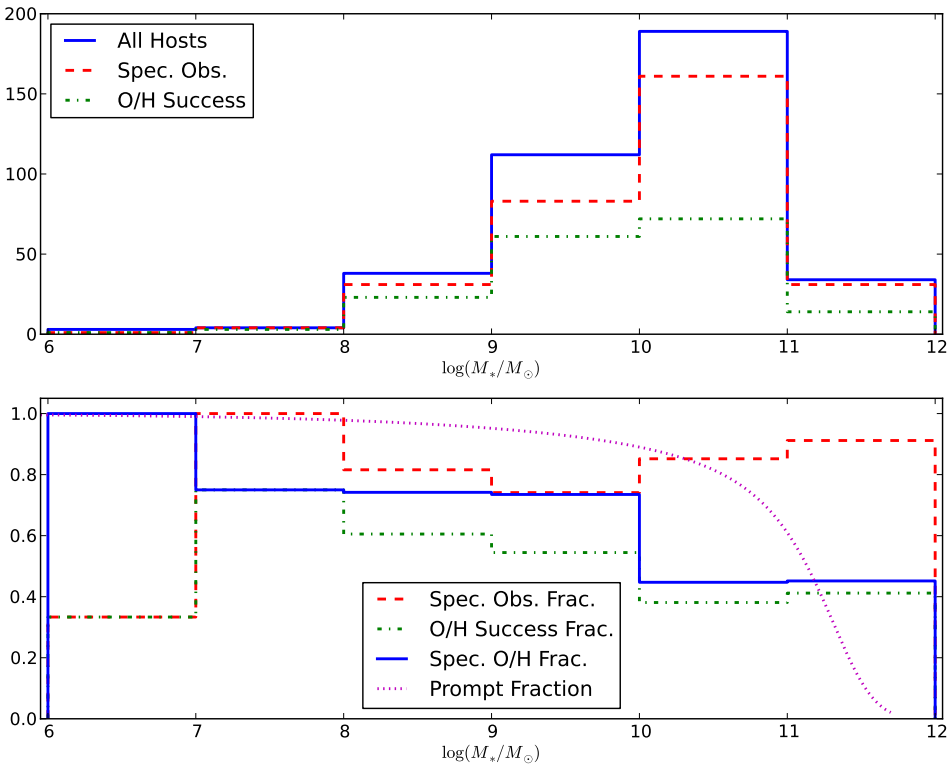

Figure 5.13 Top: Counts of all SNfactory host galaxies, all those hosts observed spectroscopically, and those with successful metallicities measurements. Bottom: The same quantities, but plotted as completeness fractions rather than raw counts. The coarse bins in stellar mass are employed to mitigate low statistics at small mass scales.

bottom panel of the same Figure we show the completeness fractions for spectroscopic observations, metallicity measurements, and also the spectroscopic metallicity success fraction (i.e. the number of metallicities divided by the number of spectroscopic observations rather than the total number of hosts). Our spectroscopic observation fraction actually *improves* as host mass decreases, a product of our heightened priority for low mass host observations and the dominance of star-forming hosts at low mass scales. Our metallicity success fraction (with respect to the number of observations) is roughly constant at about 80% at lower mass scales.

In the bottom panel of Figure 5.13 we also show for reference the expected prompt fraction as a function of stellar mass for the fiducial global prompt fraction of $\rho = 0.83$ (this is merely the ratio of the galaxy SFR distribution divided by the combined SFR and stellar mass distributions). This shows that the decrease in metallicity success at higher masses is almost certainly a product of more tardy SNe Ia associated with old stars, which are more likely to be found in passive galaxies without emission lines needed for calculating gas phase metallicities. This curve also illustrates a very important consideration when calculating our effective sample size: the rate of metallicity

completeness at high mass scales is not important in calculating our average completeness, as it is driven by the presence of tardy SNe Ia in passive systems rather than observational incompleteness.

Thus we propose that it is reasonable to estimate that the effective number of observed metallicities corresponds to 80% of the total sample size, since this is the value of our metallicitiy success rate at low mass scales where we might have expected to see emission in all hosts (and interestingly is also close to our measured prompt fraction). This corresponds to $N_{eff} = 317$, which interestingly is close to the total number of spectroscopically observed hosts $N_{obs} = 312$.

With this, let us finally return to our previous model using a binomial distribution to predict the likelihood of observing a given number of KN09 violators. For the aforementioned KN09 violator fraction of $p_V = 0.013$ and an effective sample size of $N_{eff} = 317$, the probability of finding no violators ($N_V = 0$) is P =1.6%. Thus with the observed sample of SNfactory host galaxies, our discovery of no KN09 violators amounts to provisional observational support for their low-metallicity inhibition theory.

5.3.4 Discussion

In this Section we sought to examine the theorized low metallicity inhibition of SNe Ia proposed by Kobayashi & Nomoto (2009) by inspecting the SN Ia host galaxy sample from SNfactory. We first sought to rephrase the KN09 prediction of minimum progenitor iron abundance in terms of host galaxy gas-phase oxygen abundance, and found that their prediction likely indicates a minimum host metallicity expectation of $12 + \log(O/H) \approx 7.7$. Because none of the observed SNfactory host galaxies had metallicities significantly below this value, and because the exact value of the cutoff has some uncertainty, we then turned to the proper means of interpreting the number of low-metallicity hosts and the minimum observed SN Ia host metallicity in the context of the KN09 prediction.

Using the host galaxy stellar mass distribution modeling of Section 5.2 coupled to Monte-Carlo techniques, we showed that the number of predicted KN09 violators, as well as the expectation value of the lowest observed SN Ia host metallicity, could be predicted as a function of the "prompt" SN Ia fraction, i.e. the fraction of SN Ia progenitors from young stellar populations. Because the distribution of star formation density in the local universe is dominant over the distribution of stellar mass at low galaxy stellar mass values, we found that nearly all possible KN09 violators would need to arise from the "prompt" population. Indeed, the predicted number of violators, as well as the distribution of minimum observed host metallicities, from our simulations show that for a "prompt" fraction close to that measured from SN Ia rates (i.e. $\rho = 0.83$, see Section 5.2), the mean number of KN09 violators for our full sample size should have been about $N_V \approx 6$ with a minimum observed metallicity of about $12 + \log(O/H) \approx 7.0$. After inspecting our observational completeness to determine the effective sample size of our data, we calculated that the likelihood of observing no KN09 violators was 1.6%, meaning our observations constitute a moderately strong confirmation of low metallicity inhibition of SN Ia hosts.

The lack of SN Ia host galaxies of such low metallicity is certainly not an artifact of our metallicity calculations or the lack of such low metallicity galaxies in the local universe. To confirm this assertion, we took emission line fluxes for several known low metallicity galaxies from van Zee & Haynes (2006) and Izotov & Thuan (2007) and calculated metallicities in the same manner as for our SNfactory hosts (namely the KK04 R23 method converted to T04 using the KE08 formulae). We then calculated masses from SDSS photometry using color-based mass-to-light ratios

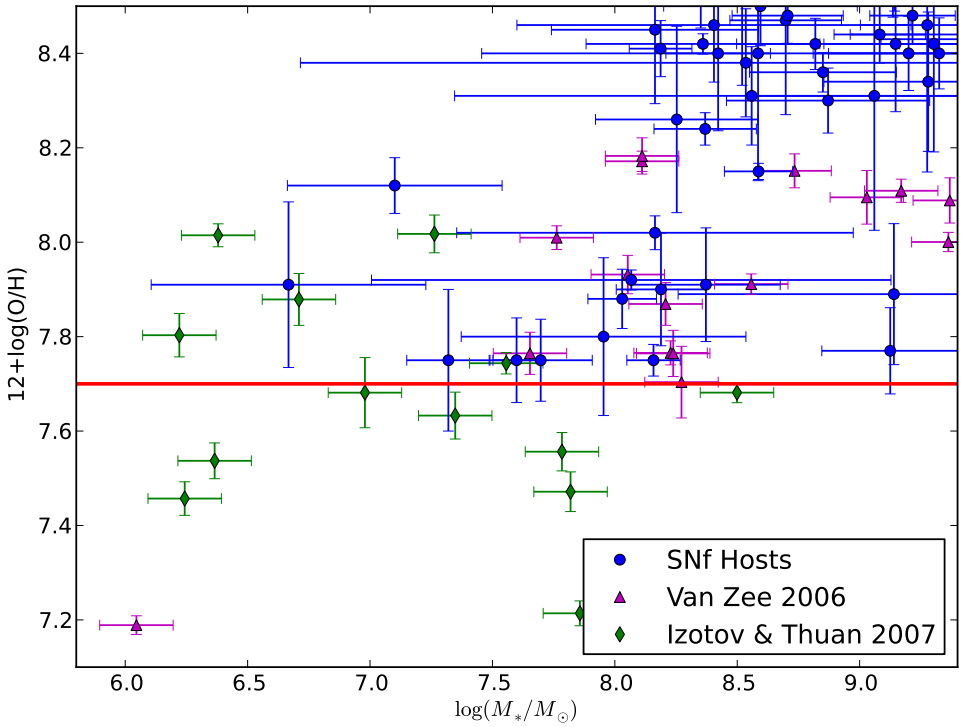

Figure 5.14 MZ diagram of SNfactory low metallicity hosts (blue circles) and several samples of known low metallicity galaxies from van Zee & Haynes (2006) (magenta triangles) and Izotov & Thuan (2007) (green diamonds). We also plot the KN09 cutoff as the horizontal red line.

derived from the MPA-JHU SDSS database. We plot these in Figure 5.14 along with the SNfactory hosts. As we can see, these galaxies show general agreement with the MZ relation and extend to lower metallicities than the KN09 cutoff.

However, several factors could leave open the possibility of there being an as-yet undetected KN09 violator in the SNfactory sample. First and foremost is the lack of spectroscopic completeness in our low-mass host galaxy sample. In particular, several of our lowest mass hosts have yet to be observed spectroscopically. It is still possible that some SNfactory hosts have metallicity lower than the fiducial cutoff value, and indeed a few would be strong outliers on the galaxy mass-metallicity relation if they do not. The final word on SNfactory agreement (or disagreement) with the KN09 low metallicity inhibition would be significantly enhanced by spectroscopic observation of these lowest mass SN Ia hosts.

Further complication arises from the SNe Ia with no identifiable hosts. We rigorously inspected host galaxy candidates in the vicinity of these SNe Ia and confirmed that no nearby objects could be the SN host, with very stringent limits on possible host mass (see Table 5.2). While the origin of these SNe Ia remains an intriguing mystery, it complicates the investigation of potential low-metallicity SN Ia hosts. If indeed these SNe were born in extremely low-mass hosts that obey the typical galaxy MZ relation, all of these would almost certainly violate the fiducial KN09 cutoff.

However, we showed that the galaxy mass values implied by our observations (even the upper limits) would be strongly discrepant with our model for the SN Ia host mass distribution. Thus we cannot immediately conclude that hostless SNe Ia come from low mass systems that obey the MZ relation and thus must violate KN09. Instead the origin of these fascinating SNe Ia may fall outside the usual regime of galaxy mass assembly, likely precluding any arguments about their potentially metallicity based on normal galaxy models.

Finally difficulties still remain in identifying the exact metallicity values below which no SNe Ia (or almost none) should occur, as several conversions must take place between the proposed number and the observational quantities. Even if we definitively identified an SN Ia host with metallicity significantly below our predicted value, these factors would leave ambiguity in its identification as a true KN09 violator. Indeed, the authors have stated that the rate below their threshold would be extremely small but possibly non-zero, so a single violator would not necessarily negate their theory. Furthermore, recent comments by Hachisu et al. (2011) have suggested that any non-zero iron abundance, even as low as that found in Population II stars, could be sufficient to allow the formation of a SN Ia. Since the number of galaxies at even lower metallicities is very small, a decrease in the predicted threshold value would make the likelihood of our finding KN09 violators in the SNfactory sample much smaller. Fortunately our analysis is not strongly dependent on the exact value of the threshold, but instead uses predictions of the SN Ia host metallicity distribution to show that the observed paucity of very low metallicity hosts is contradictory to models without low metallicity inhibition.

Our inspection of the KN09 low metallicity SN Ia inhibition theory with SNfactory host galaxy metallicity represents the first major observational attempt to test this theory. Despite the fact that we might have expected several (≈ 6) host galaxies to have metallicity below the fiducial value predicted by KN09, we found the surprising result that none of the observed SNfactory SN Ia hosts had metallicity below this value. This tentative observational confirmation of their theory is a tantalizing result that could be further strengthened by additional samples of SN Ia host galaxies. A fair number of low luminosity SN Ia hosts have also been found by both the Palomar Transient Factory and the Catalina Real-Time Transient Survey, with several hosts likely to have masses lower than the mass scale expected for the KN09 cutoff. Thus additional SN Ia samples exist which could significantly augment the statistics for our SNfactory sample. We wish to encourage the spectroscopic observation of these very low mass hosts, which could provide significant strengthening of the results we presented here.

Chapter 6

The Dependence of SN Ia Brightnesses on the Properties of Their Host Galaxies

In this Chapter we investigate the correlation of SN Ia host galaxy properties with the brightnesses of the SNe Ia they host, using SN Ia and host galaxy data from the SNfactory. Several recent studies (Kelly et al. 2010; Sullivan et al. 2010; Lampeitl et al. 2010) observed that the stretch- and color-corrected brightnesses of SNe Ia correlated with the stellar mass of their host galaxies, such that SNe Ia in high-mass host galaxies were brighter than SNe Ia in low-mass galaxies after application of the usual stretch- and color-based brightness correction techniques. In this work we investigate the same trend with SNfactory data, as well as analogous trends with host galaxy gas-phase metallicity and star-formation rate, and finally with SN Ia brightnesses corrected using unique spectroscopic standardization techniques developed by SNfactory.

The recently observed correlation of corrected SN Ia brightnesses with the mass of their host galaxies is of great concern for future cosmological SN Ia surveys. Though this trend is not strong enough to negate the dark energy signature in current SN Ia samples, it could potentially bias estimation of cosmological parameters, especially the dark energy equation of state parameter w. Galaxy mass correlates with metallicity (Tremonti et al. 2004) and stellar age (Gallazzi et al. 2005), properties whose average values evolve with redshift, implying that the average corrected SN Ia brightnesses at higher redshift will be fainter than the average corrected SN Ia brightnesses in the local universe.

The origin of this trend is of paramount concern for SN Ia cosmologists. Some authors have speculated on the possibility of the SN progenitor metallicity driving the SN luminosity, since galaxy mass correlates with metallicity. However the correlation of galaxy stellar ages with mass and the possible influence of progenitor ages has thus far been neglected in the literature. If this trend is indeed progenitor driven then its driving feature is still unidentified. Additional consideration must be given for the fact that SN Ia light curve width is known to correlate with galaxy stellar mass, and the amount of dust in galaxies scales with mass (and metallicity). The observed trend with galaxy mass could be an artifact of deficiency in the standard brightness correction techniques that leaves certain regions of SN Ia parameter space under- or over-corrected.

Coincident with the concern for biased cosmological results generated by this trend is the desire to find a means to correct for it. Some of the aforementioned authors have suggested using host galaxy mass as a third SN Ia brightness correction parameter (after stretch and color),

but this proposal has several critical limitations. Firstly, requiring galaxy photometry for host mass estimates may require either an extended host followup program (which may tax the resources of some search programs, especially low-redshift all-sky surveys) or the cut of SNe Ia in faint hosts from cosmological analyses. Secondly, and more importantly, the measurement of the properties of an SN Ia host galaxy does not constitute a measurement of the progenitor properties. Distributions of stellar age and metallicity exist within individual galaxies, so a host-based SN Ia brightness correction (for e.g. metallicity) would introduce a random error whose magnitude is proportional to the difference between the true SN progenitor metallicity and the value averaged over its entire host galaxy. This error then is completely unrelated to the properties of the SN itself, and the remaining brightness diversity is no longer representative of only SN physics. While such a host-based correction may be useful in the short term to empirically correct an observed source of bias, it cannot directly recover the true SN Ia luminosity.

Thus it is desirable to find an unbiased SN Ia luminosity indicator derived only from observations of the SN itself, and galaxies should be used only to confirm that our choice of luminosity indicators is indeed unbiased with respect to host properties. To begin this endeavor, we will investigate alternate SN Ia standardization techniques developed by the SNfactory in our analysis below and examine whether this observed host bias remains.

6.1 Stretch- and Color-Corrected SN Ia Brightnesses and Host Properties from SNfactory

Using the SN Ia and host galaxy data described above (see Chapter 3), we first investigate the correlation of SN Ia host galaxy properties with the brightnesses of SNe Ia after the application of the standard stretch- and color-based luminosity corrections. Here we will use the SN Ia light curve parameters fit from SNfactory data using the SALT2 (Guy et al. 2007) code. Host galaxy masses and specific star formation rates are derived using ZPEG as described above, while gas phase metallicities are derived from host spectra. We note that the Hubble residual errors were slightly padded in order to force the Hubble Diagram fit to have $\chi^2_\nu = 1$.

For reference, we plot the SN Ia light curve parameters against the properties of their host galaxies in Figure 6.1. As has been noted by previous authors, light curve width has a clear trend with host galaxy mass. We also show trends of light curve width with galaxy sSFR and metallicity, which are unsurprising given that these quantities correlate with stellar mass in galaxies. Interestingly, we see that highly reddened SNe Ia (e.g. $c \gtrsim 0.2$) only occur in high mass (and high metallicity) hosts. This too is to be expected as these highly reddened SNe Ia are predicted to suffer from extinction by foreground dust, which is more abundant in high mass star-forming (and high metallicity) galaxies.

6.1.1 Hubble Residuals vs. Galaxy Properties

In this analysis we use the Hubble residuals for 119 SNe Ia from SNfactory after corrections have been made for light curve width (SALT2 X1) and color (SALT2 c). Of these 119 SNe Ia, 116 have good host stellar mass estimates from photometry, 2 are hostless (see discussion in Section 5.3.2), and 1 is lacking photometry data. For these 116 SNe Ia with good host masses, the same fits from ZPEG also provide specific star formation rates. Of the 119 SNe Ia considered here,

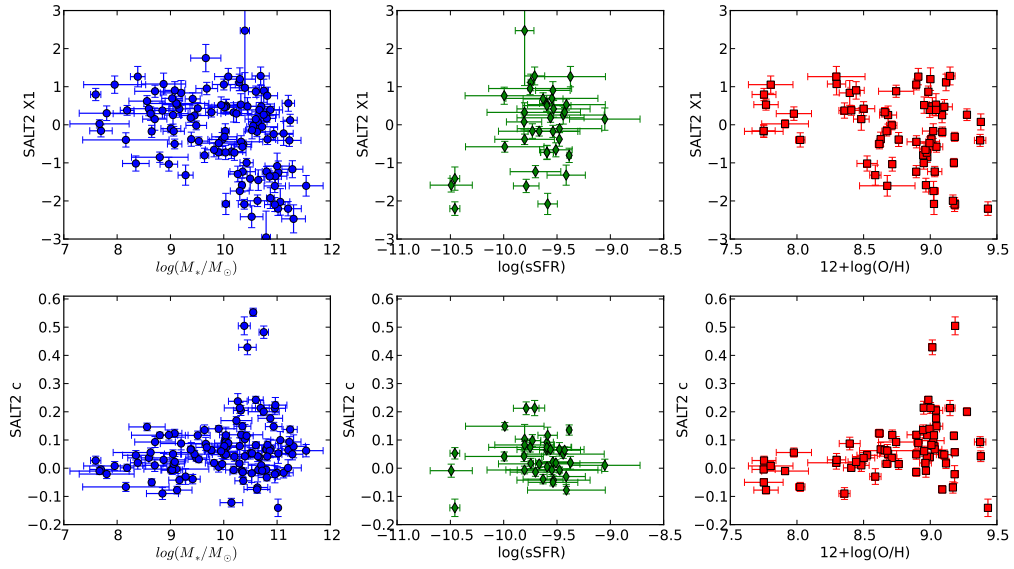

Figure 6.1 Light curve width (SALT2 X1 - top row) and color (SALT2 c - bottom row) for our SNe Ia as compared to the properties of their hosts: stellar mass (left column), specific star formation rate (middle column), and gas phase metallicity (right column).

67 have good gas-phase metallicities (i.e. are star forming and have emission line fluxes consistent with star formation rather than AGN activity – see Chapter 3 for details). In Figures 6.2, 6.3, and 6.4, we plot the SALT2 Hubble residuals against host galaxy stellar mass, sSFR, and metallicity respectively. For visual aid we show the bin-averaged values of the SN Ia Hubble residuals in bins corresponding to 1.0 dex in galaxy stellar mass. The best fit linear trend and mean residuals split by host mass (sSFR, metallicity) are shown as well, and will be described in detail below.

As was noted by previous authors, our data indicate a correlation of SN Ia Hubble residuals with host galaxy mass. Our data also indicate for the first time confirmation of a similar trend with host gas-phase metallicity, which was to be expected given that these parameters are correlated in normal galaxies (and in SN Ia hosts - see Section 5.1). We quantify this observed trend with two metrics: a linear trend in Hubble residuals vs. host stellar mass (sSFR, metallicity), and the difference between the average Hubble residuals when SNe Ia are split into two bins corresponding to high- and low-mass (sSFR, metallicity) hosts. We summarize the results of these fits in Table 6.1.

While the linear trend fits were typically of low significance ($\lesssim 1\sigma$), the difference in Hubble residuals between high-and low-mass-hosted SNe Ia show a significant step in corrected SN Ia brightnesses. Similar to previous authors' findings, we find that low- and high-mass-hosted SNe Ia have brightnesses that differ by 0.071 ± 0.030 magnitudes *after* stretch- and color corrections have been applied, such that SNe Ia in high mass hosts are brighter after correction than those in low mass hosts. Our data also confirm that corrected SN Ia brightnesses differ for SNe Ia in hosts

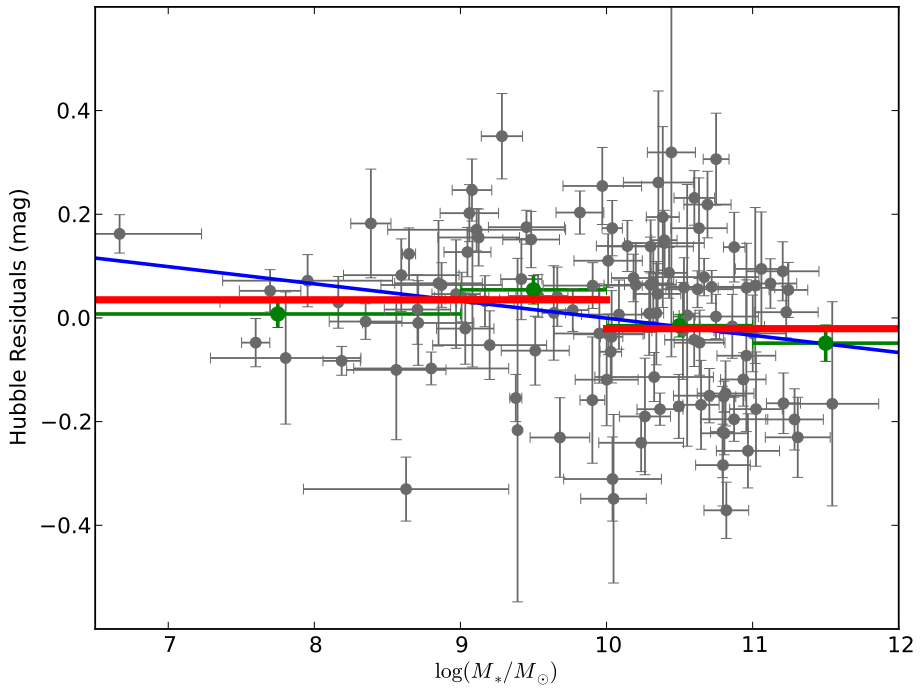

Figure 6.2 SALT2 Hubble residuals for SNfactory SNe Ia plotted versus host galaxy stellar mass (grey points). The blue line represents the best fit linear trend, the green points represent binned averages, and the thick red lines represent the averages for Hubble residuals split into high and low mass bins.

Table 6.1 Hubble Residual Trends with Host Properties

Host Property	Residual Type	N_{SNe}	Linear Trend (mag/dex)	Split Value	Hubble Residual Step (mag)
Mass	Stretch+Color	116	-0.033 ± 0.015	10.0	0.071 ± 0.030
sSFR	Stretch+Color	116	0.031 ± 0.044	-10.0	0.057 ± 0.039
Metallicity	Stretch+Color	67	-0.026 ± 0.043	8.8	0.044 ± 0.031
Mass	Flux Ratio	95	-0.014 ± 0.014	10.0	0.033 ± 0.028

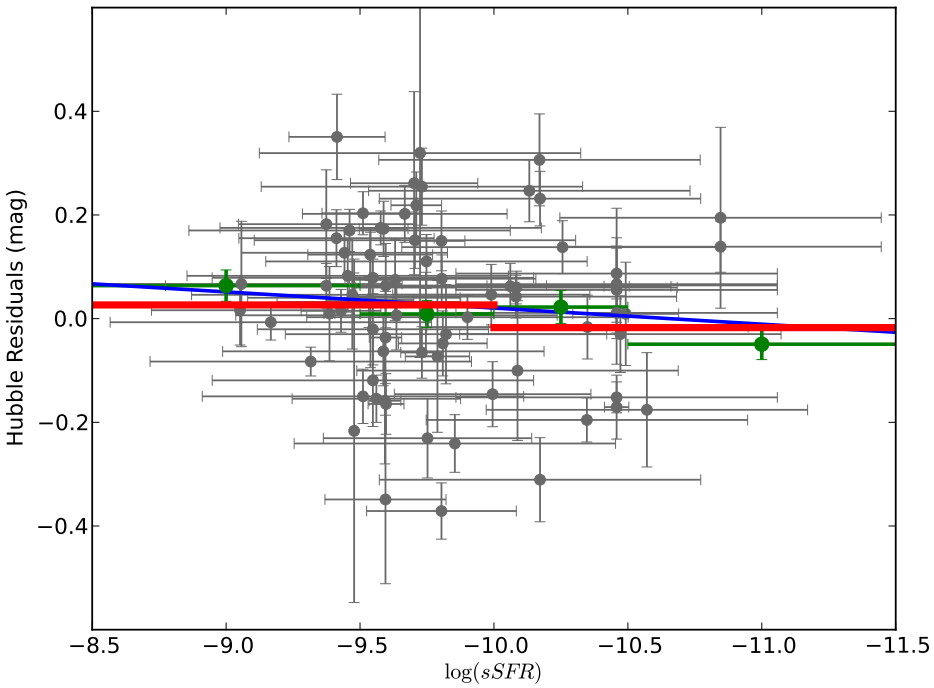

Figure 6.3 Same as Figure 6.2, but for host sSFR.

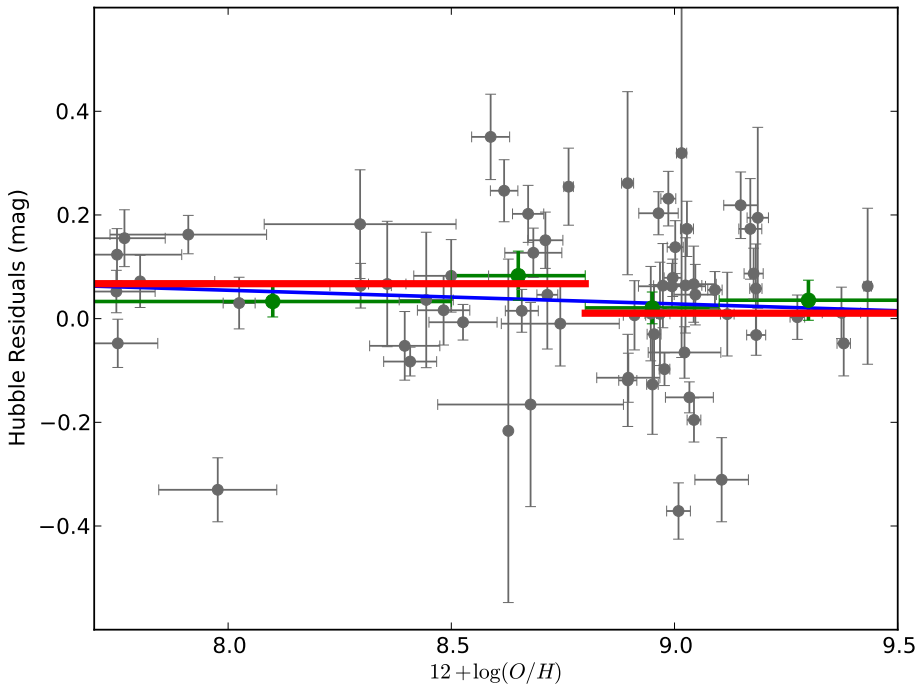

Figure 6.4 Same as Figure 6.2, but for host metallicity.

with different metallicity or star-formation intensity. Regardless of the driving factor behind this trend, this result indicates that applying the canonical SN Ia standardization techniques to SNe Ia at all redshifts will result in biased cosmological parameters as the SN Ia environments evolve in metallicity and star-formation activity as we probe to higher redshifts. This concern, along with our thoughts on the appropriate course of action for SN Ia cosmology, will be revisited and discussed thoroughly in Section 6.3.

6.1.2 SN Ia Cosmology Fits Split By Galaxy Properties

In light of the apparently different corrected brightnesses of SNe Ia in high and low mass host galaxies, it has been proposed that one means of correcting for this trend is to split the SN data sets by host mass and fit for separate sets of light curve correction parameters α, β, and M_B. Such an analysis was undertaken for the SNLS host sample by Sullivan et al. (2010), who noted several results from this investigation. First, they found that the scatter about the Hubble diagram (i.e. Hubble residual RMS) was only marginally improved (from about 0.148 mag to 0.142 mag) by splitting the sample by host mass (at $\log(M_*/M_\odot) = 10.0$). Second, they found that when fit separately high mass hosts had a lower (brighter) M_B (by $\Delta M_B = 0.085$), lower β (by $\Delta\beta = 0.55$), and essentially equal α ($\Delta\alpha = 0.08$) when compared to the parameters fitted for the low-mass hosted SN Ia sample.

We conducted a similar analysis with the SNfactory sample, splitting the sample by host mass and fitting separately for α, β, and M_B parameters for each subsample. As with the Sullivan et al. (2010) analysis, we found only marginal improvement in the Hubble diagram residuals, going from 0.153 mag RMS to 0.148 mag RMS. Because the main SNfactory cosmology analysis is not yet published, we have kept the nominal α, β, and M_B values blinded in order to preserve the integrity of that future analysis. Thus we examine the effect of our split cosmology fit by inspecting the *change* in these fit parameters. We found that the values of α for the two subsets are nearly identical ($\Delta\alpha = 0.05$, with SNLS typical $\alpha = 0.139$). We found that M_B for the high-mass hosts was lower (brighter) by $\Delta M_B = 0.107$ (typical $M_B \approx -19.0$), similar to the SNLS result. And finally, we found that the high-mass β was lower than the low-mass value ($\Delta\beta = 0.99$, with typical SNLS $\beta = 3.2$). Similar results were found when splitting SNe Ia by host sSFR or metallicity.

The above cosmology fits split by host properties appear to give slightly better SN Ia standardization, but it has been known for some time that SN Ia properties (particularly stretch) correlate with the properties of their host galaxies. Thus we investigate an alternate technique whereby we split the SN Ia sample by stretch (SALT2 $x1$) and repeat the above analysis steps. We found very similar results to our mass split fit, with stretch-split fit parameters differing as: $\Delta\alpha = 0.075$, $\Delta M_B = 0.119$, and $\Delta\beta = 0.62$. This calls into question the notion that splitting SN Ia standardization parameters by host properties is truly correcting a progenitor-driven diversity. Instead it may be that the color behavior of SNe Ia with different stretches cannot be effectively corrected with a single color correction parameter β. We will revisit this possibility in the Discussion below.

6.2 Flux Ratio-Corrected SN Ia Brightness and Host Properties

We now revisit the above analyses with an alternate SN Ia standardization technique developed by Bailey et al. (2009) which employs spectral flux ratios to standardize SNe Ia. In that work we showed that the spectral flux ratio $\mathcal{R}_{642/443}$, defined as the ratio of the SN Ia flux at 642 nm divided by the flux at 443 nm (smoothed with 2000 km/s binning), correlated very strongly with the raw SN Ia Hubble residuals (i.e. without stretch and color corrections). We now wish to examine whether the bias in corrected Hubble residuals persists when using this alternate standardization technique.

The SN Ia data set for this analysis consists of the subset of the 119 SNe Ia from the previous sample for which we can apply the correction method of Bailey et al. (2009). This method requires a spectrophotometric observation of the SN within ± 2.5 days of B-band maximum light (as estimated from the full light curve). This requirement brings the parent sample of SNe Ia down to 98, of which we have host stellar masses for 95. As with the previous Section, Hubble residual error bars were again padded to force the Hubble Diagram to have $\chi^2_\nu = 1$.

For simplicity in this section, we inspect only the trend of Hubble residuals with stellar mass, since the sSFR trend is very similar, and the sample attrition for a metallicity analysis is rather significant. In Figure 6.5 we show the flux-ratio-corrected SN Ia Hubble residuals for our 95 SNe Ia plotted against the stellar masses of their host galaxies. Similarly to Figure 6.2, we plot the binned average Hubble residuals, best fit linear trend, and average Hubble residual when splitting the sample by host mass.

The results of our analysis show a similar trend with host mass, but with a marked decrease in magnitude. The high- to low-mass magnitude step after flux-ratio correction is 0.033 ± 0.028 magnitudes, versus 0.071 ± 0.030 magnitudes from stretch- and color-corrected SN Ia brightnesses. Similarly, the linear best-fit trend of flux ratio Hubble residuals with host mass is -0.014 ± 0.014 magnitudes (of SN brightness) per dex (in host mass), compared to -0.033 ± 0.015 mag/dex for stretch- and color-based Hubble residuals for the same sample. Indeed our data could be consistent with there being no trend (at 1.0σ) or step (at 1.2σ) in flux-ratio corrected SN Ia Hubble residuals. Though Bailey et al. (2009) showed that the flux-ratio standardization method results in lower dispersion on the Hubble diagram, the decreased bias in corrected SN Ia magnitudes shown here cannot be a result of that decreased dispersion. The possible cause for this improved reduction in host bias will be a key point of interest in the Discussion that follows.

6.3 Discussion

Recent studies of SN Ia Hubble residuals and the properties of their host galaxies have uncovered the disturbing result that SN Ia brightnesses corrected using the standard light curve width and color corrections show a residual correlation with the masses, and thus presumably the metallicities and mean stellar ages, of their host galaxies. Such a trend is quite distressing for future SN Ia cosmology missions which will hunt for SNe Ia at very high redshifts where the mean stellar age and metallicity are quite different from their values in the local universe. The discovery of this SN Ia host bias has motivated two critical questions: what is the true cause of this bias, and what should be done to correct it? We will address each of these questions in turn, as well as the impact our analysis of SNfactory data on their answers.

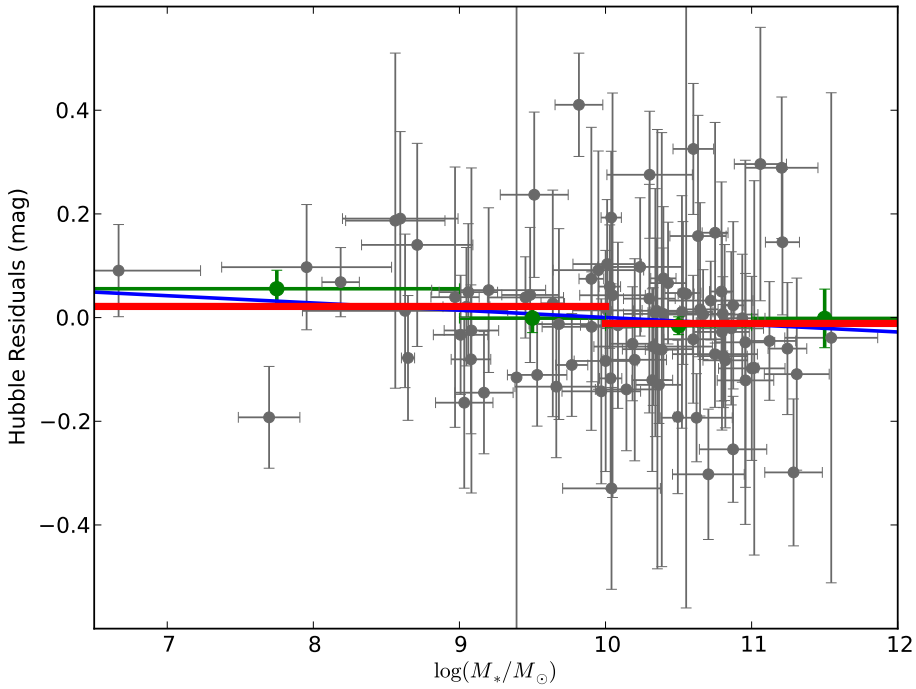

Figure 6.5 Same as Figure 6.2, but with Hubble residuals obtained using spectral flux ratio brightness corrections following the method described by Bailey et al. (2009).

6.3.1 Comparison To Previous Studies

Before discussing the potential origins of the observed host bias and possible means of correcting it, let us first summarize the results presented here and compare those to the findings of previous studies. For simplicity we will focus only on the studies with respect to host stellar mass, since that is the only common host property across all such studies. Using the standard light curve width and color correction techniques for SNe Ia, we found the Hubble residuals for our 116 SNe Ia using SALT2 had a best fit linear trend with mass of $dm/d\log(M_*) = -0.033 \pm 0.015$ mag/dex. When splitting the sample by host mass at $\log(M_*/M_\odot) = 10.0$, we found the mean corrected brightnesses of high-mass-hosted SNe Ia were $\Delta m_{corr} = 0.071 \pm 0.030$ magnitudes brighter than the mean corrected brightnesses of low-mass-hosted SNe Ia. The median redshift for SNfactory SNe Ia is approximately $z = 0.06$. Conducting the same analysis with SN Ia brightnesses corrected using the technique of Bailey et al. (2009), we found a linear trend in mass consistent with zero ($dm/d\log(M_*) = -0.014 \pm 0.014$ mag/dex) at 1σ, and a markedly smaller step in the average corrected magnitudes of high- versus low-mass-hosted SNe Ia ($\Delta m_{corr} = 0.033 \pm 0.028$).

The first major study of SN Ia Hubble residuals as a function of their host galaxy masses came from Kelly et al. (2010), who studied the hosts of low redshift ($z \sim 0.02$) SNe Ia discovered mostly from targeted nearby searches. Their host mass range was significantly higher (median $\log(M_*/M_\odot) = 10.67$) than other similar studies, so their analysis was restricted only to high mass hosts ($\log(M_*/M_\odot) \geq 9.5$). They found a linear trend of corrected brightnesses with host mass of $dm/d\log(M_*) \approx -0.15$ mag/dex with a 2.4σ significance for a sample size of 60 SN Ia hosts. When splitting their sample at $\log(M_*/M_\odot) = 10.8$, they find a bin average magnitude difference of $\Delta m_{corr} = 0.094 \pm 0.045$. Our SNfactory data (and indeed the SDSS-SN and SNLS samples) show a much shallower trend of brightness with host mass than the Kelly sample, and this may be an artifact of the shortened mass range (≈ 2 dex) of the Kelly sample. Our SNfactory sample goes to three orders of magnitude lower in host mass and doubles the sample size of the Kelly sample. Thus we have the first sample of low redshift SNe Ia to detect this host bias across the full mass range sampled by higher redshift surveys.

Similar analyses were conducted by Sullivan et al. (2010) for the SNLS 3rd year sample of SNe Ia and by Lampeitl et al. (2010) for the SDSS-SN survey. Sullivan et al. (2010) found a best fit linear trend of Hubble residuals versus host mass of $dm/d\log(M_*) = -0.042 \pm 0.013$ mag/dex for a sample of 195 SNe Ia at a median redshift of $z = 0.63$. When splitting the sample at $\log(M_*/M_\odot) = 10.0$, he found a magnitude difference of $\Delta m_{corr} = 0.08 \pm 0.02$. Lampeitl et al. (2010) found a linear trend of $dm/d\log(M_*) = -0.072 \pm 0.018$ mag/dex for a sample of 162 SNe Ia at a median redshift of $z = 0.16$. For the mean stellar masses of this sample in bins split at $\log(M_*/M_\odot) = 10.0$, this corresponds to a magnitude difference of $\Delta m_{corr} = 0.100 \pm 0.025$. Our value of the SNfactory linear trend with host mass is within 0.45σ and 1.66σ of those found by Sullivan et al. (2010) and Lampeitl et al. (2010), respectively, while our mass-split magnitude differences is within 0.25σ and 0.74σ of the same studies. Thus we have found good quantitative agreement with these results from two other untargeted SN Ia searches.

Now that we have shown the SNfactory stretch- and color-corrected Hubble residuals exhibit similar trends with host mass as those found by previous authors, we turn to the results of our flux-ratio corrected SN Ia Hubble residuals derived using the method of Bailey et al. (2009). For simplicity, we will compare these results only to those of Sullivan et al. (2010) and Lampeitl et al. (2010), as these studies span similar mass ranges and showed similar trends in Hubble residuals

corrected for stretch and color. The best fit linear trend for our flux-ratio Hubble residuals as a function of host mass is shallower than the trends measured by Sullivan et al. (2010) and Lampeitl et al. (2010) at 1.47σ and 2.54σ, respectively, while the mass-split magnitude difference is smaller by 1.37σ and 1.78σ. The disagreement of the flux ratio residuals linear trend with the SNfactory stretch- and color-based trend is 0.93σ, and the mass-split magnitude difference disagrees also at 0.93σ. Though the statistical significance of our decreased host bias is modest for SNfactory alone, our results are also significantly different from the stretch- and color-based trends found by previous authors. Thus we believe that our analysis of flux-ratio based Hubble residuals has shown a significant decrease in bias with respect to host galaxy mass. Indeed, if one were to posit that the brightnesses of SNe Ia differ in low-mass hosts and high-mass hosts by 0.10 magnitudes in a manner which cannot be recovered from SN Ia data alone, we are able to negate that hypothesis at 2.4σ. This implies that reduction of the host bias using SN Ia data alone is highly probable, a point we will return to shortly.

6.3.2 Origin of Observed Bias

The first major concern raised by the SN Ia brightness host bias is, what is the underlying physical cause of this observed bias? Is it a true correlation of SN Ia brightnesses with the properties of their progenitors? If so, is it age, metallicity, or some other physical parameter driving this effect? On the other hand, could this be a deficiency in the SN Ia models or standardization techniques?

Because galaxy stellar mass correlates with gas-phase metallicity (e.g. Tremonti et al. 2004) and specific star-formation rate (e.g. Salim et al. 2007), it was expected that the SN Ia Hubble residuals would correlate with these two properties as well. We showed here with SNfactory data that this is indeed the case, with roughly similar steps in magnitude between high- and low-metallicity hosted SNe Ia as that observed for SNe Ia split by host mass. Thus we have shown observationally that corrected SN Ia brightnesses correlate with the stellar masses, specific star formation rates, and gas-phase metallicities of their host galaxies.

Disentangling which of these galaxy physical properties is most strongly correlated is extremely difficult, leaving ambiguity as to whether these parameters are driving some residual SN Ia brightness correction. Indeed, the measured host galaxy metallicity for a SN Ia host may not necessarily reflect the metallicity of the progenitor itself (see Bravo & Badenes 2011, for a detailed discussion), a key point we will revisit in our discussion of how to correct SN Ia brightnesses below. If measurement of the *progenitor* metallicity and age were possible, it would provide a clearer answer to the strength of correlation between corrected SN Ia brightnesses and their progenitor properties.

An alternative explanation to the observed host bias is that, rather than being driven by some residual dependence on progenitor age or metallicity, perhaps the bias is an artifact of insufficient SN Ia stretch and color correction techniques. Consider the above investigation where we split our SNfactory sample by stretch and refit the light curve correction parameters α, β, and M_B, where the value of β differed significantly from low- to high-stretch SNe Ia. One potential interpretation is that the effect of SN Ia color on its brightness is different at different values of stretch. A failure to correct for this would leave low- and high-stretch SNe Ia, which are found more prevalently in high- and low-mass hosts respectively, to be insufficiently corrected in such a way that ends up correlating with host galaxy mass.

The mass-split fits can be interpreted in a similar way, where SNe Ia in high-mass hosts

are more likely to be affected by dust and thus have a different value of β than SNe Ia with low dust extinction. If intrinsic SN Ia color diversity drives the observed colors at low host mass (low extinction) and dust drives it at high mass, then the monolithic treatment of these two effects would result in biased corrected brightnesses. Because SN Ia light curve stretch and color show some correlation with host properties, it is difficult to discern whether the residual host bias is a product of a third intrinsic SN Ia parameter, or whether it reflects some deficiency in correcting for the first two parameters whose behavior is tied to the properties of the SN hosts. Thus we believe that a definitive interpretation of the host bias as being driven by an additional progenitor property is premature.

6.3.3 Correcting Bias in SN Ia Data

The second major concern provoked by the observed SN Ia brightness host bias is how to effectively correct for this effect in SN Ia cosmological data. Some authors (e.g. Lampeitl et al. 2010) have suggested including SN Ia host mass as a third brightness correction parameter such that corrected SN Ia brightnesses would be of the form:

$$d\mu = m_B - (M_B + \alpha \cdot S + \beta \cdot C + \gamma \cdot H) - \mu(z; \Omega_M, \Omega_\Lambda, H_0) \tag{6.1}$$

where $d\mu$ is the corrected Hubble residual, S and C are the usual stretch and color parameters with their respective correction coefficients α and β, and γ is the new correction coefficient for some host property H such as mass (or metallicity). Some authors have already performed SN Ia cosmology fits using a host-based brightness correction (Sullivan et al. 2011a) or a step-wise brightness correction for host mass where brightnesses of low-mass-hosted SNe Ia are adjusted by a constant amount (Suzuki et al. 2011). While these techniques may be viable as a short term means for correcting an observed bias in SN Ia data sets, we believe they are not the optimal means for correcting current (and future) SN Ia cosmological data. Instead, we advocate using SN Ia data itself to train new standardization techniques that are unbiased with respect to host properties. We describe both of these concepts below.

The Challenges of Host-Based Corrections

The first major problem with using SN Ia host galaxies for cosmology corrections is the observational requirements for obtaining host galaxy properties for all SN Ia cosmology data sets. Host galaxy masses derived from photometry are the easiest (and cheapest) form of host data to obtain. Typically photometric observations of host galaxies in numerous filter bands (ideally 5 optical bands, but as few as 2 bands would suffice), obtained long after the SN has faded, provide sufficient information to obtain a galaxy stellar mass. For high redshift surveys such as SNLS (Sullivan et al. 2010) which revisit the same small area of sky over a multi-year survey and take data in numerous filters, sufficient host imaging to obtain stellar masses is a natural data product arising from the usual survey operations. Similarly, the SDSS-SN survey (Lampeitl et al. 2010) revisited the same stripe of sky (SDSS Stripe 82) for multiple years, obtaining deep photometry over the whole survey area and at least a year after (or before) the SN explosion. For nearby surveys, such as SNfactory or the Palomar Transient Factory (Rau et al. 2009), that target a very large area of sky, uniform photometric data is very difficult. As described above (see Chapter 3), targeted photometric observations of varying depth were required to obtain the same mass precision

for all SNfactory SN Ia hosts. Additionally, a wealth of nearby SN Ia data is already on hand, but would require significant additional observations to provide the level of quality photometric host data needed to obtain host masses for brightness corrections. Thus the observational requirements of performing host-based SN Ia brightness corrections are challenging.

The second major problem with using host-based SN Ia brightness corrections is the extensive galaxy modeling requirements inherent in this method. Even for the simplest data, photometric host masses, assumptions must be made about (a) galaxy star-formation histories in order to obtain mass-to-light ratios, (b) the extinction law and physical distribution of dust within galaxies in order to correct observed galaxy brightnesses, and (c) stellar population models which must be invoked in order to convert the aforementioned SFHs into mass-to-light ratios. Further difficulty arises from the fact that stellar populations and galaxy SFHs evolve in redshift, such that the relationships between mass-to-light ratios and photometric colors employed for galaxies in the local universe will not be applicable at higher redshifts. The complexity of galaxy stellar population modeling inherent in assigning physical properties (i.e. stellar mass) to galaxy photometric data is such that a significantly large and new set of systematic errors must be accounted for in SN Ia cosmology. We believe that burdening SN Ia data sets with the systematics of galaxy modeling is not favorable.

The final, and most significant, problem with using host properties to correct SN Ia brightnesses is the fact that the properties of a SN Ia host are not the same as the properties of the SN Ia progenitor itself. Consider for example a SN Ia brightness correction that effectively corrects for host galaxy metallicity in order to account for an assumed progenitor metallicity effect. Suppose for argument's sake that the SN Ia brightness does indeed depend on the metallicity of its progenitor:

$$M_{B,\mathrm{true}} = M_{B,0} + \gamma \cdot Z_{SN} \tag{6.2}$$

where $M_{B,\mathrm{true}}$ is the true SN Ia brightness, $M_{B,0}$ is the standardized brightness to which we wish to correct the observed SN Ia brightness, Z_{SN} is the progenitor metallicity, and γ the scaling relation defining how the metallicity affects the true brightness. For simplicity we have removed reference to stretch and color under the simple assumption that we are correctly adjusting the observed SN Ia brightness for those parameters. Now suppose we model the observed SN Ia brightness based on the metallicity of its host as:

$$M_{B,\mathrm{model}} = M_{B,0} + \gamma \cdot Z_{host} \tag{6.3}$$

Then the Hubble residual we obtain will be the different between the true magnitude and the modeled value:

$$\begin{aligned} d\mu &= M_{B,\mathrm{model}} - M_{B,\mathrm{true}} && (6.4)\\ &= \gamma \cdot (Z_{host} - Z_{SN}) && (6.5) \end{aligned}$$

Thus our Hubble residuals will be mistakenly corrected by an amount proportional to the difference between the true SN metallicity and the average metallicity of its host. Since galaxies have a distribution of stellar metallicities and the SN was drawn randomly from this distribution, the difference $Z_{host} - Z_{SN}$ is a random variable which has no physical meaning, only a probabilistic one. Moreover, no means exists to recover this metallicity difference without measuring the SN metallicity itself, a feat not currently attainable. Thus a host-based SN Ia brightness correction obscures the true SN Ia brightness by a value which has no physical meaning and cannot be recovered observationally. This means that any future attempts to derive additional physically-motivated brightness correction parameters could be washed out by this random error.

Based on the mass trend observed above with SNfactory data coupled to the galaxy MZ relation, a galaxy with an internal metallicity dispersion of 0.5 dex (a typical range for elliptical metallicity gradients Spolaor et al. 2010) would introduce a random error on SN Ia brightnesses of about 0.03 mag. The range of observed galaxy metallicities has a much larger span than the typical internal metallicity dispersion of a single galaxy, so ultimately such a correction would introduce an error whose magnitude is smaller than the bias it is intended to correct. However, the random dispersion introduced into SN Ia brightnesses could possibly hinder further attempts to refine SN Ia standardization. This is our primary objection to using host data to correct SN Ia brightnesses.

The Case For Improved SN-Based Techniques

Now that we have outlined the reasons disfavoring use of host data to correct SN Ia brightnesses, we turn to a discussion of the potential improvement of SN Ia standardization methods using only SN data. SN Ia brightness corrections derived exclusively from SN Ia data have the advantages of being derived directly from the SN itself (rather than a proxy), and avoid being contaminated by the differences between the SN progenitor properties and the average properties of its host galaxy. An ideal standardization technique would be derived from SN photometric data, as this is the preferred method for observing SNe Ia in future high-redshift surveys (spectroscopy is expensive), and is the primary format of the expansive SN Ia data currently available.

It may be that a re-training of the methods for correcting SN Ia brightnesses from light curve data may be able to rectify this problem. We showed above that when the SN Ia data set is split by light curve width, the color-correction term β for the two subsamples was substantially different. This result was similar to that found when splitting the sample by host mass, which is expected because light curve width is known to correlate with host galaxy mass. Galaxy dust content is also expected to correlate with galaxy mass, such that significant amounts of dust (and thus more heavily extincted SNe Ia) can be found in higher mass galaxies. If intrinsic SN Ia color variations affect the SN Ia brightness in a way that is different from reddening by dust, then erroneous color-based brightness correction would be expected to correlate with dust content and thus by extension host galaxy mass. Alternatively, if the color behavior of SNe Ia is a function of stretch, this would produce a similar signal due to the host mass-stretch correlation. Similarly, if the reddening behavior of dust is a function of metallicity, then monolithic color corrections would not capture this effect and again produce a similar signal. All of these effects could potentially be disentangled from photometry (and thus corrected for), but sufficient data to do so have yet to be presented.

A full re-examination of SN Ia light curve correction techniques is beyond the scope of this work, but we can provide some support for the notion that a host-unbiased SN-based standardization technique is feasible by invoking the results from our flux-ratio-corrected Hubble residuals study above. The SN Ia Hubble residuals derived after correction for spectral flux ratios showed a decrease in host bias. While this alternate standardization method may not completely remove the bias, it does illustrate that SN-based techniques can be found which at least reduce the bias. We hope this is a proof of principle, and eagerly anticipate future standardization methods which can be tested for their impartiality with respect to SN Ia host properties.

Chapter 7

Conclusions

This thesis has presented observations of the host galaxies of SNe Ia from the Nearby Supernova Factory (SNfactory) along with analyses of the physical properties of those galaxies and their implications for the SNe Ia they hosted. In Chapter 4 we focused on the host galaxy of the probable super-Chandrasekhar-mass SN Ia SN 2007if, showing its host to be extremely low mass, the lowest observed SN Ia host metallicity to-date, and composed of a very young stellar population. Chapter 5 pursued three key investigations into the nature of SN Ia progenitors using the full sample of SNfactory host galaxies. First we demonstrated that SN Ia host galaxies show good agreement with the normal galaxy mass-metallicity relation. We then showed that the distribution of SN Ia host galaxy masses can be modeled using stellar mass and star-formation history distributions coupled to an SN Ia delay time distribution (DTD), thereby constraining the properties of the SN Ia DTD. Next we investigated the proposed low-metallicity inhibition of SNe Ia with the SNfactory host sample, and found that our sample contained no SN Ia hosts observed significantly below the proposed metallicity threshold, providing tentative evidence in support of this theory. Finally in Chapter 6 we compared the brightnesses of SNe Ia after application of several standardization methods to the properties of their host galaxies, and showed that the previously noted bias of stretch- and color-corrected SN Ia brightnesses with host mass was indeed present in the SNfactory sample, but definitely diminished when brightnesses were corrected with a spectroscopic correction method developed by SNfactory.

The foremost goals of this thesis have been twofold: to learn more about the nature of SN Ia progenitors through the study of their parent stellar populations, and thereby improve the potential for SN Ia luminosity standardization for cosmological applications. Our work has made contributions to both these endeavors, and below we remark on the progress made here as well as our preferred next steps in pursuing these research goals.

7.1 Host Galaxies of Super-Chandrasekhar-Mass SNe Ia

The discovery of exceptionally over-luminous SNe Ia whose progenitors likely exceed the Chandrasekhar mass has been one of the most interesting discoveries in SN Ia science in the past decade. Following the initial discovery of SN 2003fg (SNLS-03D3bb Howell et al. 2006), several other SNe have shown similar spectroscopic and photometric behavior. These SNe Ia challenge the fiducial progenitor model in which a Chandrasekhar mass white dwarf undergoes thermonuclear

runaway to produce a SN Ia.

We undertook the study of the host galaxies of these SNe, with a particular focus on the host galaxy (Childress et al. 2011) of SN 2007if (SNF20070825-001 Scalzo et al. 2010). This particular SN was the brightest known SN Ia at the time of its discovery, and we showed that its host has the lowest measured metallicity of any SN Ia host. Additionally, our inspection of the stellar absorption features in the host spectrum strongly indicated the host underwent a strong burst of star formation ≈ 100 Myr before the SN, possibly producing the SN progenitor in this starburst. We continued to examine the hosts of other probable super-Chandrasekhar SNe Ia (Taubenberger et al. 2011) and found that their host mass distribution was markedly lower in average mass than the host mass distribution from other surveys such as SNLS (Sullivan et al. 2010) and SDSS-SN (Lampeitl et al. 2010), implying a potential preference for low metallicity.

Our work has already been followed in the literature by several recent analyses. Khan et al. (2011) followed our analysis of super-Chandrasekhar SN Ia hosts from Taubenberger et al. (2011) and our analysis of the host of SN 2007if from Childress et al. (2011) by inspecting the local sites of the SN explosions for three key members of the super-Chandrasekhar subclass. They found that SN 2006gz was found in a region outside of $> 95\%$ of its host light, where the metallicity was more than 0.4 dex lower than at the core of its galaxy. Similarly, SN 2003fg and SN 2009dc, though found in interacting systems, were significantly far from the center of their possible hosts, implying low metallicity regions. Their conclusion was that the most definitive super-Chandrasekhar SNe Ia – SN 2003fg, SN 2006gz, SN 2007if, and SN 2009dc – were all found in low-metallicity environments, lending strong support for low metallicity being a requirement for the production of super-Chandrasekhar SNe Ia.

Hachisu et al. (2011) recently revisited possible SD progenitors of super-Chandrasekhar SNe Ia. They found that low metallicity was important in increasing the initial WD mass before the onset of accretion. With these higher mass WDs, they found that accretion in the SD scenario could lead to differential rotation supporting a significantly more massive WD than M_{Ch}. Indeed their mass estimates for super-Chandrasekhar SN Ia progenitors was very consistent with our estimate for SN 2007if in Scalzo et al. (2010). Additionally, they found that the SD companion needed to have a stellar mass ($M_* \sim 4M_\odot$) consistent with the main-sequence turn-off mass we estimated for the stellar population in the host of SN 2007if in Childress et al. (2011).

The study of super-Chandrasekhar SNe Ia and their possible progenitors is a highly popular and rapidly advancing field within the study of SNe Ia. Our work here has contributed to the study of the environments in which these SNe have been found, and will surely be advanced as more of these exceptional SNe are found.

7.2 Statistical Properties of SN Ia Host Galaxies

The nature of SN Ia progenitors remains a topic of great interest not only for the purpose of potentially improving their calibration for cosmology, but also for uncovering the stellar and binary evolution paths which lead to these exceptionally explosive events. The study of the parent stellar populations where SNe Ia are born is a useful tool for constraining SN Ia progenitor models. While the study of the host galaxy of an individual SN Ia can constrain the likely properties of its progenitor, the *statistical* study of the ensemble of SN Ia host galaxies provides clues to the *range* of SN Ia progenitor properties and the relative frequency of those properties.

SN Ia Host Galaxies and the MZ Relation

The agreement of SN Ia host galaxies with the normal galaxy mass-metallicity relation is a key assumption in the interpretation of SN Ia trends with host mass in terms of host metallicity. The agreement of SN Ia hosts with the MZ relation has been an implicit assumption in the observational tests of the Timmes et al. (2003) theory as presented by Howell et al. (2009) and Neill et al. (2009), as well as the numerous studies analyzing SN Ia Hubble residuals as a function of their host galaxy masses (Kelly et al. 2010; Sullivan et al. 2010; Lampeitl et al. 2010). This is an important aspect of SN Ia hosts to check, as deviation from the MZ relation could be caused by unusually intense star formation activity, as was discovered to be the case with LGRB hosts (Kocevski & West 2011; Mannucci et al. 2011).

Here for the first time we have inspected the agreement of SN Ia hosts with the MZ relation using a large sample of SN Ia host galaxies from SNfactory. The SNfactory sample proved to be ideal for this analysis because of the large range of host stellar masses for SNe Ia discovered with our search. Our impartial search technique is also advantageous in this endeavor because it avoids the selection biases that might arise from a search technique which targets specific galaxies. We showed that indeed SN Ia hosts show remarkably good agreement with the MZ relation over the mass range $8.5 \leq \log(M_*/M_\odot) \leq 11.0$, with mean offsets from the MZ relation of $\Delta Z = -0.003 \pm 0.012$. We also showed that the dispersion of SN Ia host metallicities about the MZ relation is very consistent (pull distribution RMS exactly equal to 1) with the observed dispersion of normal galaxies about the mean MZ relation.

Our analysis provides observational support for the previous inferences about host metallicity in trends observed with host mass. It also shows that the star formation activity of SN Ia hosts is likely to be very similar to that of a typical field galaxy sample, rather than being concentrated in regimes of extreme star formation. We thus conclude that future studies of SN Ia properties with respect to progenitor metallicity can be validly inspected by means of their host galaxy stellar masses.

SN Ia Host Galaxy Mass Distributions

The study of the SN Ia delay time distribution (DTD) is currently a very active field of research. Knowledge of the SN Ia DTD would be helpful not only in placing constraints on progenitor models, but also for calculating expected yields from future SN Ia surveys. To date most such studies have grown out of SN Ia rate calculations, where the total amount of stars observed in each age bin must be estimated from stellar population synthesis modeling of all galaxies in the search area of the SN survey. The calculations of these statistics from search data is very complex, especially in the determination of survey completeness and purity. Further systematics enter into the galaxy stellar population modeling, which is limited by the complexity of data available for the galaxies (i.e. spectroscopic data, or the number of photometric filter bands). While great progress is being made toward this end (see Maoz 2010, for a review), a simpler method that can be widely applied would be beneficial.

Here we presented a new method for constraining the SN Ia DTD using the distribution of SN Ia host galaxy masses. Building upon the deep base of knowledge regarding galaxy star formation histories and the distributions of stellar mass and star formation in the local universe, we can generate a prediction for the SN Ia host mass distribution for a given DTD. Using the observed SN Ia

host mass distribution from SNfactory we showed the power of this distribution in constraining DTD models. In the simplified "A+B" framework, we found the fraction of "prompt" SNe Ia to be approximately 80%, consistent with the value implied from rates studies (Scannapieco & Bildsten 2005). Adding complexity to the allowed DTD, we used galaxy SFHs measured from the SDSS survey to predict host mass distributions for a power law DTD and showed that the SNfactory host mass distribution favors a $s = -1.2$ power law index with a lower age cutoff of around $t_{prompt} = 20$ Myr. This power law index is fairly consistent with other observational studies (Totani et al. 2008; Maoz 2010; Barbary et al. 2010), and the lower age limit is consistent with the main sequence turn off time for the most massive likely white dwarf progenitors ($M \sim 10 M_{\odot}$).

Our analysis is contingent upon an accurate measurement of the true SN Ia host galaxy mass distribution, which is made possible for SNfactory due to our impartial SN search technique. SN Ia host galaxy stellar masses are available from numerous untargeted surveys (e.g. Sullivan et al. 2010; Lampeitl et al. 2010), and with some additional inspection of selection biases could likely be turned into additional measurements of the SN Ia host mass distribution at the redshift of these surveys. We emphasize here the power of using only the SN Ia host mass distribution to constrain the DTD, rather than resorting to galaxy star formation history modeling for all SN Ia hosts *and* other galaxies observed in a survey. Our method takes advantage of the fact that the average SFH of SN Ia hosts of a given stellar mass will be representative of the average SFH of all galaxies at that mass. This method will be further enhanced by the inclusion of host mass distributions from different redshifts where the local star formation histories will be different, enabling a unique variation of the input to the host mass distribution calculation.

Low-Metallicity Inhibition of SNe Ia

The study of preferred SN Ia environments can provide clues to SN Ia progenitors by revealing potential progenitor properties that favor (or disfavor) the production of SNe Ia. One theoretically proposed environmental preference was put forth by Kobayashi & Nomoto (2009), who predicted that SNe Ia could not occur at extremely low metallicities. For the first time, we attempted to confront this theory with observations by examining the low-metallicity SN Ia hosts from SNfactory. Using the best available data to calculate the expected gas phase metallicity threshold, we found that none of the observed SNfactory host galaxies show a metallicity below the fiducial predicted cutoff metallicity. Returning to our SN Ia host galaxy mass distribution modeling techniques, we showed this result to be in sharp contrast to the best fit prediction of $N \approx 6$ SNe Ia in galaxies of metallicity below the threshold. Given the observed effective sample size, this presented a P=1.6% likelihood of there being no cutoff, constituting provisional observational support of the proposed low metallicity SN Ia inhibition theory.

We note that some SNfactory hosts with extremely low masses have yet to be observed, but our calculations account for observational completeness and we have no reason to believe that we have mistakenly observed only those hosts which do not violate the KN09 threshold. Similarly, hosts for a number of SNe Ia could not be found despite very deep imaging and careful spectroscopic screening of nearby host candidates. While arguments citing probable host mass upper limits coupled to the galaxy mass-metallicity relation might favor an interpretation of these SNe Ia originating from progenitors with metallicities below the KN09 threshold, these arguments are undermined by the fact that such a large number of extremely low luminosity SN Ia hosts strongly disagrees with the observed distribution of stellar mass in galaxies. It was rather surprising that many of our faintest

candidate hosts turned out to be hostless SNe Ia, and that none of our normal low mass hosts showed metallicity below the KN09 value despite the expectation that some should.

Other nearby SN Ia surveys have found several other SNe Ia in low mass hosts, and could substantially augment the results we presented here. Our inspection of the KN09 low metallicity inhibition theory with SNfactory data is a representative example of the way in which theoretical predictions of SN Ia progenitor behavior can be tested with a statistical analysis of SN Ia host galaxy properties.

7.3 SN Ia Brightnesses and the Properties of Their Host Galaxies

One of the major motivations for studying SNe Ia is their utility in cosmological distance measurement. SNe Ia are the best standardizable candles for measuring the expansion rate of the universe by means of the Hubble diagram. However, the number of cosmological SNe Ia has become sufficiently large that systematic errors are becoming comparable in magnitude to statistical errors in SN Ia cosmology fits (Sullivan et al. 2011a). Understanding the progenitors of SNe Ia better is thought to be a fruitful means of improving their calibration for cosmology, and the study of SN Ia hosts plays an important role in this endeavor.

A critical secondary role of SN Ia host galaxies is to serve as a means of ensuring that our SN Ia standardization methods do not leave a residual bias of corrected SN Ia brightnesses with respect to the properties of their hosts. If corrected SN Ia brightnesses show a dependence on properties of their hosts which will evolve globally at higher redshifts, such as metallicity or stellar age, then this could indicate SN Ia cosmology will yield biased results at high redshifts. Such a bias was indeed uncovered in recent studies (Kelly et al. 2010; Sullivan et al. 2010; Lampeitl et al. 2010) of SN Ia Hubble residuals and the properties of their host galaxies. While these studies showed this bias to be present for stretch- and color-corrected Hubble residuals as a function of SN Ia host mass and specific star-formation rate, we showed here for the first time with SNfactory data that an analogous trend is present with respect to host galaxy gas-phase metallicity. Though this result was expected given our previous confirmation that SN Ia hosts follow the galaxy MZ relation, it provides important confirmation that corrected SN Ia brightnesses show a bias with respect to their host metallicity.

More importantly, we revisited this investigation using an alternate SN Ia brightness standardization technique Bailey et al. (2009) that employs spectral flux ratios. This provides an important check of whether the previously observed bias is a result of true SN Ia brightness dependence on host (and presumably progenitor) metallicity, or whether this might in fact be an artifact of inferior standardization techniques. While this host bias was still detected (although at low significance – roughly 1σ) using the Bailey et al. (2009) method, it was shown to be significantly decreased compared to the level of bias in stretch- and color-corrected Hubble residuals from SNfactory data, as well as the bias level found by and previous authors.

This result implies that the observed host bias may in fact be correctable through observations of SNe Ia alone. We argued that the use of host galaxy data to correct SN Ia brightnesses was not a favorable solution for several reasons. These include the difficulties in collecting host data, particularly for wide area nearby SN Ia searches, and employing consistent modeling of that galaxy data. Furthermore, if indeed there is some dependence of SN Ia brightness on progenitor metallicity (or some other property that scales with host mass and metallicity) then host-corrected

SN Ia brightnesses will be partially corrupted by the differences between the metallicities of their progenitors and the average metallicities or their hosts.

For the near future, correction of SN Ia cosmological data for this observed host bias is a viable means of ensuring cosmological parameters are not biased by the different progenitor populations along the redshift range of SN Ia observations. However, we would submit that our analysis employing a different standardization method illustrated that SN-based luminosity corrections that do not bias cosmological parameters could indeed exist. Host galaxy data is vital in providing a cross-check of such new standardization methods, as these data provide a means of confirming that SNe Ia are being born in different environments. It would likely be a worthwhile endeavor to revisit SN Ia light curve modeling in order to seek a new means of SN Ia calibration that results in host-unbiased SN Ia luminosities by means of SN Ia data alone.

7.4 Final Remarks

Type Ia supernovae are vital cosmological tools as well as interesting astrophysical objects in their own right. Their continuing utility as cosmological distance indicators is likely to be enhanced by a deeper understanding of their physical origin, so both cosmologists and stellar evolution experts seek insight into the nature of their progenitors. Most astronomers agree that SNe Ia likely come from the thermonuclear disruption of Chandrasekhar-mass white dwarfs. Unlike the luminous giant progenitors of many core collapse supernovae, SN Ia progenitor systems are likely to be so faint that their detection beyond the Local Group would be nearly impossible even with the best resolution space telescopes. Thus the mystery of SN Ia progenitors is unlikely to be resolved through direct detection. Instead we must turn to the study of SN Ia environments and host galaxies in order to uncover the nature of their stellar progenitors.

Though the study of SN Ia hosts can provide only an indirect probe of SN Ia progenitors, a wealth of information has already been gleaned from such studies. SN Ia environment studies have provided important constraints on theoretical SN Ia progenitor models, and SN Ia host science is well placed to aid in several key future areas of study.

SN Ia cosmology will continue to rely on host studies to ensure that our SN Ia standardization methods will not bias the measurement of cosmological parameters. The recent discovery that current SN Ia standardization methods leave a residual bias with respect to host properties is likely to inspire a close examination of those methods, and hosts will continue to play the critical role of testing corrected brightness trends with progenitor properties.

Another key effort we would like to see pursued with future host studies is the comparison of SN Ia environments for different subclasses of SNe Ia. Statistical properties of the environments where spectroscopically peculiar SNe Ia (e.g. 91T-like or 91bg-like) are found could shed light on the progenitor properties which drive their peculiarity. Similarly, studying the environments of SNe Ia grouped by light curve shape (e.g. SNe Ia binned by stretch) could provide key insight into the physical properties of their progenitors, and whether those progenitor properties vary along with the resultant behavior of the SNe themselves.

Finally, we believe SN Ia host galaxies will be critical to unraveling the most important issue facing SN Ia cosmology today: the disentanglement of intrinsic SN Ia color from extrinsic reddening by dust. External constraints on the amount of possible dust obscuring SNe Ia is critical to understanding the amount of color variability inherent in the full sample of SNe Ia. The study of

the dust content of SN Ia host galaxies is instrumental in constraining the amount of dust possibly obscuring SNe Ia, and the sample of dust-free SN Ia host galaxies will be particularly useful in this endeavor. A key source for such immaculate environments is the sample of low mass SN Ia hosts, whose probable low dust content (due to expected low metallicity) and low optical depth could provide key dust-free environments for studying the intrinsic colors of SNe Ia.

Host galaxies are likely to help answer these and other key questions in SN Ia science as the number of well observed SNe Ia continues to increase. The number of known SNe Ia is poised to make a tremendous leap forward in the coming years, with numerous nearby SN Ia search and followup campaigns currently underway (SNfactory, Palomar Transient Factory, Lick Observatory Supernova Search, SkyMapper Transient Survey, PanSTARRS-1, La Silla QUEST, ROTSE), several intermediate redshift campaigns completed (SNLS, SDSS-SN, ESSENCE) or ramping up (Dark Energy Survey), continued high-redshift campaigns employing the Hubble Space Telescope (SCP, CLASH, CANDELS), and future large telescopes (LSST, TMT) that will significantly increase the number of SNe Ia found. With these plentiful SNe Ia will surely come numerous opportunities to study their diverse environments and further our knowledge of the origin of these fascinating explosive events.

Bibliography

Abazajian, K. N., et al. 2009, ApJS, 182, 543

Aihara, H., et al. 2011, ApJS, 193, 29

Akerlof, C., et al. 2007, Central Bureau Electronic Telegrams, 1059, 2

Aldering, G., et al. 2002, in Society of Photo-Optical Instrumentation Engineers (SPIE) Conference Series, Vol. 4836, Society of Photo-Optical Instrumentation Engineers (SPIE) Conference Series, ed. J. A. Tyson & S. Wolff, 61–72

Aldering, G., et al. 2006, ApJ, 650, 510

Aller, L. H., ed. 1984, Astrophysics and Space Science Library, Vol. 112, Physics of thermal gaseous nebulae

Amanullah, R., et al. 2010, ApJ, 716, 712

Arnett, W. D. 1969, Ap&SS, 5, 180

—. 1971, ApJ, 169, 113

—. 1982, ApJ, 253, 785

Aubourg, É., Tojeiro, R., Jimenez, R., Heavens, A., Strauss, M. A., & Spergel, D. N. 2008, A&A, 492, 631

Bailey, S., Aragon, C., Romano, R., Thomas, R. C., Weaver, B. A., & Wong, D. 2007, ApJ, 665, 1246

Bailey, S., et al. 2009, A&A, 500, L17

Baldwin, J. A., Phillips, M. M., & Terlevich, R. 1981, PASP, 93, 5

Balogh, M. L., Morris, S. L., Yee, H. K. C., Carlberg, R. G., & Ellingson, E. 1999, ApJ, 527, 54

Baltay, C., et al. 2007, PASP, 119, 1278

Barbary, K., et al. 2010, ArXiv e-prints

Bell, E. F., & de Jong, R. S. 2001, ApJ, 550, 212

Bertin, E. 2006, in Astronomical Society of the Pacific Conference Series, Vol. 351, Astronomical Data Analysis Software and Systems XV, ed. C. Gabriel, C. Arviset, D. Ponz, & S. Enrique, 112–+

Bertin, E., & Arnouts, S. 1996, A&AS, 117, 393

Bertin, E., Mellier, Y., Radovich, M., Missonnier, G., Didelon, P., & Morin, B. 2002, in Astronomical Society of the Pacific Conference Series, Vol. 281, Astronomical Data Analysis Software and Systems XI, ed. D. A. Bohlender, D. Durand, & T. H. Handley, 228–+

Blais, E., & Nelson, L. 2011, in Bulletin of the American Astronomical Society, Vol. 43, American Astronomical Society Meeting Abstracts #217, 324.03–+

Blanton, M. R., et al. 2003, ApJ, 592, 819

Branch, D., & van den Bergh, S. 1993, AJ, 105, 2231

Bravo, E., & Badenes, C. 2011, MNRAS, 414, 1592

Brinchmann, J., Charlot, S., White, S. D. M., Tremonti, C., Kauffmann, G., Heckman, T., & Brinkmann, J. 2004, MNRAS, 351, 1151

Bruzual, G., & Charlot, S. 2003, MNRAS, 344, 1000

Cappellaro, E., Turatto, M., Tsvetkov, D. Y., Bartunov, O. S., Pollas, C., Evans, R., & Hamuy, M. 1997, A&A, 322, 431

Cardelli, J. A., Clayton, G. C., & Mathis, J. S. 1989, ApJ, 345, 245

Cardiel, N., Gorgas, J., Cenarro, J., & Gonzalez, J. J. 1998, A&AS, 127, 597

Chabrier, G. 2003, PASP, 115, 763

Charlot, S., & Longhetti, M. 2001, MNRAS, 323, 887

Childress, M., et al. 2011, ApJ, 733, 3

Chotard, N., et al. 2011, A&A, 529, L4+

Clemens, J. C., Crain, J. A., & Anderson, R. 2004, in Society of Photo-Optical Instrumentation Engineers (SPIE) Conference Series, Vol. 5492, Society of Photo-Optical Instrumentation Engineers (SPIE) Conference Series, ed. A. F. M. Moorwood & M. Iye, 331–340

Conroy, C., Gunn, J. E., & White, M. 2009, ApJ, 699, 486

Cooper, M. C., Newman, J. A., Madgwick, D. S., Gerke, B. F., Yan, R., & Davis, M. 2005, ApJ, 634, 833

Croxall, K. V., van Zee, L., Lee, H., Skillman, E. D., Lee, J. C., Côté, S., Kennicutt, R. C., & Miller, B. W. 2009, ApJ, 705, 723

Davies, R. L., et al. 1997, in Society of Photo-Optical Instrumentation Engineers (SPIE) Conference Series, Vol. 2871, Society of Photo-Optical Instrumentation Engineers (SPIE) Conference Series, ed. A. L. Ardeberg, 1099–1106

de Vaucouleurs, G. 1948, Annales d'Astrophysique, 11, 247

Delahaye, F., Pinsonneault, M. H., Pinsonneault, L., & Zeippen, C. J. 2010, ArXiv e-prints

Donahue, M., Aldering, G., & Stocke, J. T. 1995, ApJ, 450, L45+

Drake, A. J., et al. 2008, Central Bureau Electronic Telegrams, 1589, 1

—. 2009, ApJ, 696, 870

Filippenko, A. V. 1989, PASP, 101, 588

—. 1997, ARA&A, 35, 309

Fink, M., Röpke, F. K., Hillebrandt, W., Seitenzahl, I. R., Sim, S. A., & Kromer, M. 2010, A&A, 514, A53+

Fioc, M., & Rocca-Volmerange, B. 1997, A&A, 326, 950

Foley, R. J., et al. 2009, AJ, 138, 376

Förster, F., & Schawinski, K. 2008, MNRAS, 388, L74

Fruchter, A. S., et al. 2006, Nature, 441, 463

Gallazzi, A., & Bell, E. F. 2009, ApJS, 185, 253

Gallazzi, A., Charlot, S., Brinchmann, J., White, S. D. M., & Tremonti, C. A. 2005, MNRAS, 362, 41

Garn, T., & Best, P. N. 2010, MNRAS, 409, 421

Graves, G. J., & Schiavon, R. P. 2008, ApJS, 177, 446

Greggio, L. 2005, A&A, 441, 1055

Gunn, J. E., & Stryker, L. L. 1983, ApJS, 52, 121

Guy, J., Astier, P., Nobili, S., Regnault, N., & Pain, R. 2005, A&A, 443, 781

Guy, J., et al. 2007, A&A, 466, 11

—. 2010, A&A, 523, A7+

Hachisu, I., Kato, M., & Nomoto, K. 2008, ApJ, 679, 1390

Hachisu, I., Kato, M., Saio, H., & Nomoto, K. 2011, ArXiv e-prints

Hamuy, M., Phillips, M. M., Suntzeff, N. B., Schommer, R. A., Maza, J., & Aviles, R. 1996, AJ, 112, 2391

Hamuy, M., Trager, S. C., Pinto, P. A., Phillips, M. M., Schommer, R. A., Ivanov, V., & Suntzeff, N. B. 2000, AJ, 120, 1479

Hamuy, M., et al. 2003, Nature, 424, 651

Han, Z., & Podsiadlowski, P. 2004, MNRAS, 350, 1301

Hanuschik, R. W. 2003, A&A, 407, 1157

Hayden, B. T., et al. 2010, ApJ, 722, 1691

Hicken, M., Garnavich, P. M., Prieto, J. L., Blondin, S., DePoy, D. L., Kirshner, R. P., & Parrent, J. 2007, ApJ, 669, L17

Hicken, M., Wood-Vasey, W. M., Blondin, S., Challis, P., Jha, S., Kelly, P. L., Rest, A., & Kirshner, R. P. 2009, ApJ, 700, 1097

Hillebrandt, W., & Niemeyer, J. C. 2000, ARA&A, 38, 191

Hinshaw, G., et al. 2009, ApJS, 180, 225

Hoeflich, P., Wheeler, J. C., & Thielemann, F. K. 1998, ApJ, 495, 617

Höflich, P. A., & et al. 1997, in NATO ASIC Proc. 486: Thermonuclear Supernovae, ed. P. Ruiz-Lapuente, R. Canal, & J. Isern, 659–+

Howell, D. A., et al. 2006, Nature, 443, 308

—. 2009, ApJ, 691, 661

Iben, Jr., I., & Tutukov, A. V. 1984, ApJS, 54, 335

Ivanova, L. N., Imshennik, V. S., & Chechetkin, V. M. 1974, Ap&SS, 31, 497

Izotov, Y. I., & Thuan, T. X. 2007, ApJ, 665, 1115

James, P. A., & Anderson, J. P. 2006, A&A, 453, 57

Jha, S. 2002, PhD thesis, HARVARD UNIVERSITY

Jha, S., Riess, A. G., & Kirshner, R. P. 2007, ApJ, 659, 122

Kasen, D. 2010, ApJ, 708, 1025

Kasen, D., Röpke, F. K., & Woosley, S. E. 2009, Nature, 460, 869

Kauffmann, G., et al. 2003, MNRAS, 341, 33

Kelly, P. L., Hicken, M., Burke, D. L., Mandel, K. S., & Kirshner, R. P. 2010, ApJ, 715, 743

Kelly, P. L., Kirshner, R. P., & Pahre, M. 2008, ApJ, 687, 1201

Kennicutt, Jr., R. C. 1998, ARA&A, 36, 189

Kennicutt, Jr., R. C., Bresolin, F., & Garnett, D. R. 2003, ApJ, 591, 801

Kessler, R., et al. 2009, ApJS, 185, 32

Kewley, L. J., & Dopita, M. A. 2002, ApJS, 142, 35

Kewley, L. J., & Ellison, S. L. 2008, ApJ, 681, 1183

Kewley, L. J., Groves, B., Kauffmann, G., & Heckman, T. 2006, MNRAS, 372, 961

Khan, R., Stanek, K. Z., Stoll, R., & Prieto, J. L. 2011, ArXiv e-prints

Khokhlov, A. M. 1991, A&A, 245, 114

Kim, A., Goobar, A., & Perlmutter, S. 1996, PASP, 108, 190

Kobayashi, C., & Nomoto, K. 2009, ApJ, 707, 1466

Kobayashi, C., Tsujimoto, T., Nomoto, K., Hachisu, I., & Kato, M. 1998, ApJ, 503, L155+

Kobulnicky, H. A., Kennicutt, Jr., R. C., & Pizagno, J. L. 1999, ApJ, 514, 544

Kobulnicky, H. A., & Kewley, L. J. 2004, ApJ, 617, 240

Kocevski, D., & West, A. A. 2011, ApJ, 735, L8+

Kromer, M., Sim, S. A., Fink, M., Röpke, F. K., Seitenzahl, I. R., & Hillebrandt, W. 2010, ApJ, 719, 1067

Lampeitl, H., et al. 2010, ApJ, 722, 566

Lantz, B., et al. 2004, in Society of Photo-Optical Instrumentation Engineers (SPIE) Conference Series, Vol. 5249, Society of Photo-Optical Instrumentation Engineers (SPIE) Conference Series, ed. L. Mazuray, P. J. Rogers, & R. Wartmann, 146–155

Le Borgne, D., & Rocca-Volmerange, B. 2002, A&A, 386, 446

Leaman, J., Li, W., Chornock, R., & Filippenko, A. V. 2011, MNRAS, 412, 1419

Lee, H., Skillman, E. D., Cannon, J. M., Jackson, D. C., Gehrz, R. D., Polomski, E. F., & Woodward, C. E. 2006, ApJ, 647, 970

Lee, J. C., et al. 2009, ApJ, 706, 599

Leibundgut, B. 2000, A&A Rev., 10, 179

Lentz, E. J., Baron, E., Branch, D., Hauschildt, P. H., & Nugent, P. E. 2000, ApJ, 530, 966

Lequeux, J., Peimbert, M., Rayo, J. F., Serrano, A., & Torres-Peimbert, S. 1979, A&A, 80, 155

Levesque, E. M., Kewley, L. J., Berger, E., & Jabran Zahid, H. 2010, AJ, 140, 1557

Li, W., Chornock, R., Leaman, J., Filippenko, A. V., Poznanski, D., Wang, X., Ganeshalingam, M., & Mannucci, F. 2011, MNRAS, 412, 1473

Liu, W., Chen, W., Wang, B., & Han, Z. W. 2010, A&A, 523, A3+

Livio, M. 2000, in Type Ia Supernovae, Theory and Cosmology, ed. J. C. Niemeyer & J. W. Truran, 33–+

Livio, M. 2001, in Supernovae and Gamma-Ray Bursts: the Greatest Explosions since the Big Bang, ed. M. Livio, N. Panagia, & K. Sahu, 334–355

Mannucci, F., Cresci, G., Maiolino, R., Marconi, A., & Gnerucci, A. 2010, MNRAS, 408, 2115

Mannucci, F., Della Valle, M., & Panagia, N. 2006, MNRAS, 370, 773

Mannucci, F., Della Valle, M., Panagia, N., Cappellaro, E., Cresci, G., Maiolino, R., Petrosian, A., & Turatto, M. 2005, A&A, 433, 807

Mannucci, F., Salvaterra, R., & Campisi, M. A. 2011, MNRAS, 414, 1263

Maoz, D. 2010, in American Institute of Physics Conference Series, Vol. 1314, American Institute of Physics Conference Series, ed. V. Kologera & M. van der Sluys, 223–232

Maoz, D., Mannucci, F., Li, W., Filippenko, A. V., Valle, M. D., & Panagia, N. 2011, MNRAS, 412, 1508

McGaugh, S. S. 1991, ApJ, 380, 140

McWilliam, A. 1997, ARA&A, 35, 503

Mennekens, N., Vanbeveren, D., De Greve, J. P., & De Donder, E. 2010, A&A, 515, A89+

Miller, J. S., & Stone, R. P. S. 1993, Lick Obs. Tech. Rep. 66 (Santa Cruz: Lick Obs.)

Mink, D. 2006, in Astronomical Society of the Pacific Conference Series, Vol. 351, Astronomical Data Analysis Software and Systems XV, ed. C. Gabriel, C. Arviset, D. Ponz, & S. Enrique, 204–+

Modjaz, M., et al. 2008, AJ, 135, 1136

Monet, D., ed. 1996, USNO A - 1.0 a catalog of astrometric standards

Nava, A., Casebeer, D., Henry, R. B. C., & Jevremovic, D. 2006, ApJ, 645, 1076

Neill, J. D., et al. 2009, ApJ, 707, 1449

Nomoto, K. 1980, Space Sci. Rev., 27, 563

—. 1982, ApJ, 253, 798

Nomoto, K., Iwamoto, K., Yamaoka, H., & Hashimoto, M. 1995, in Astronomical Society of the Pacific Conference Series, Vol. 72, Millisecond Pulsars. A Decade of Surprise, ed. A. S. Fruchter, M. Tavani, & D. C. Backer, 164–+

Nomoto, K., & Kondo, Y. 1991, ApJ, 367, L19

Nugent, P. 2007, The Astronomer's Telegram, 1213, 1

Nugent, P., Baron, E., Branch, D., Fisher, A., & Hauschildt, P. H. 1997, ApJ, 485, 812

Nugent, P., Kim, A., & Perlmutter, S. 2002, PASP, 114, 803

Oke, J. B., et al. 1995, PASP, 107, 375

Osterbrock, D. E., & Ferland, G. J. 2006, Astrophysics of gaseous nebulae and active galactic nuclei, ed. Osterbrock, D. E. & Ferland, G. J.

Peeples, M. S., Pogge, R. W., & Stanek, K. Z. 2008, ApJ, 685, 904

Perlmutter, S., et al. 1997, ApJ, 483, 565

—. 1999, ApJ, 517, 565

Pettini, M., & Pagel, B. E. J. 2004, MNRAS, 348, L59

Phillips, A. C., Miller, J., Cowley, D., & Wallace, V. 2006, in Society of Photo-Optical Instrumentation Engineers (SPIE) Conference Series, Vol. 6269, Society of Photo-Optical Instrumentation Engineers (SPIE) Conference Series

Phillips, M. M. 1993, ApJ, 413, L105

Piro, A. L. 2008, ApJ, 679, 616

Prieto, J. L., Stanek, K. Z., & Beacom, J. F. 2008, ApJ, 673, 999

Prieto, J. L., et al. 2007, ArXiv e-prints

Quimby, R., Castro, F., Maund, J., Shetrone, M., & Riley, V. 2006, Central Bureau Electronic Telegrams, 413, 1

Raskin, C., Scannapieco, E., Rhoads, J., & Della Valle, M. 2008, ApJ, 689, 358

Raskin, C., Scannapieco, E., Rockefeller, G., Fryer, C., Diehl, S., & Timmes, F. X. 2010, ApJ, 724, 111

Rau, A., et al. 2009, PASP, 121, 1334

Riess, A. G., Press, W. H., & Kirshner, R. P. 1996, ApJ, 473, 88

Riess, A. G., et al. 1998, AJ, 116, 1009

—. 2007, ApJ, 659, 98

—. 2011, ApJ, 730, 119

Ruiter, A. J., Belczynski, K., & Fryer, C. 2009, ApJ, 699, 2026

Ruiz-Lapuente, P., Burkert, A., & Canal, R. 1995, ApJ, 447, L69+

Salim, S., et al. 2007, ApJS, 173, 267

Salpeter, E. E. 1955, ApJ, 121, 161

Sánchez Almeida, J., Aguerri, J. A. L., Muñoz-Tuñón, C., & Vazdekis, A. 2009, ApJ, 698, 1497

Sánchez Almeida, J., Muñoz-Tuñón, C., Amorín, R., Aguerri, J. A., Sánchez-Janssen, R., & Tenorio-Tagle, G. 2008, ApJ, 685, 194

Scalzo, R. A., et al. 2010, ApJ, 713, 1073

Scannapieco, E., & Bildsten, L. 2005, ApJ, 629, L85

Schechter, P. 1976, ApJ, 203, 297

Schlegel, D. J., Finkbeiner, D. P., & Davis, M. 1998, ApJ, 500, 525

Searle, L., & Sargent, W. L. W. 1972, ApJ, 173, 25

Silverman, J. M., Ganeshalingam, M., Li, W., Filippenko, A. V., Miller, A. A., & Poznanski, D. 2011, MNRAS, 410, 585

Skrutskie, M. F., et al. 2006, AJ, 131, 1163

Smith, J. A., et al. 2002, AJ, 123, 2121

Spolaor, M., Kobayashi, C., Forbes, D. A., Couch, W. J., & Hau, G. K. T. 2010, MNRAS, 408, 272

Stoughton, C., et al. 2002, AJ, 123, 485

Strolger, L., et al. 2002, AJ, 124, 2905

—. 2004, ApJ, 613, 200

—. 2005, ApJ, 635, 1370

Sullivan, M., et al. 2006, ApJ, 648, 868

—. 2010, MNRAS, 406, 782

—. 2011a, ArXiv e-prints

—. 2011b, ApJ, 732, 118

Suntzeff, N. B. 2000, in American Institute of Physics Conference Series, Vol. 522, American Institute of Physics Conference Series, ed. S. S. Holt & W. W. Zhang, 65–74

Suzuki, N., et al. 2011, ArXiv e-prints

Tanaka, M., et al. 2010, ApJ, 714, 1209

Taubenberger, S., et al. 2011, ArXiv e-prints

Thomas, R. C., et al. 2007, ApJ, 654, L53

Timmes, F. X., Brown, E. F., & Truran, J. W. 2003, ApJ, 590, L83

Tojeiro, R., Heavens, A. F., Jimenez, R., & Panter, B. 2007, MNRAS, 381, 1252

Tojeiro, R., Wilkins, S., Heavens, A. F., Panter, B., & Jimenez, R. 2009, ApJS, 185, 1

Tolstoy, E., Hill, V., & Tosi, M. 2009, ARA&A, 47, 371

Tonry, J., & Davis, M. 1979, AJ, 84, 1511

Totani, T., Morokuma, T., Oda, T., Doi, M., & Yasuda, N. 2008, PASJ, 60, 1327

Tremonti, C. A., et al. 2004, ApJ, 613, 898

Tripp, R. 1998, A&A, 331, 815

Tucker, B. E. 2011, Ap&SS, 40

Umeda, H., Nomoto, K., Kobayashi, C., Hachisu, I., & Kato, M. 1999a, ApJ, 522, L43

Umeda, H., Nomoto, K., Yamaoka, H., & Wanajo, S. 1999b, ApJ, 513, 861

van den Bergh, S. 1991, Phys. Rep., 204, 385

van Dokkum, P. G. 2001, PASP, 113, 1420

van Zee, L., & Haynes, M. P. 2006, ApJ, 636, 214

Vazdekis, A., Sánchez-Blázquez, P., Falcón-Barroso, J., Cenarro, A. J., Beasley, M. A., Cardiel, N., Gorgas, J., & Peletier, R. F. 2010, MNRAS, 404, 1639

Weaver, T. A., & Woosley, S. E. 1980, in American Institute of Physics Conference Series, Vol. 63, Supernovae Spectra, ed. R. Meyerott & H. G. Gillespie, 15–32

Whelan, J., & Iben, Jr., I. 1973, ApJ, 186, 1007

Wood-Vasey, W. M., Aldering, G., Nugent, P., Helin, E. F., Pravdo, S., Hicks, M., & Lawrence, K. 2002, IAU Circ., 7842, 1

Wood-Vasey, W. M., Wang, L., & Aldering, G. 2004, ApJ, 616, 339

Wood-Vasey, W. M., et al. 2007, ApJ, 666, 694

Woosley, S. E., Axelrod, T. S., & Weaver, T. A. 1984, in Stellar Nucleosynthesis. Proceedings of the 3rd. Workshop of the Advanced School of Astronomy of the Ettore Majorana Centre for Scientific Culture, Erice, Italy, May 11-21, 1983. Editors, Cesare Chiosi, Alvio Renzini; Publisher, D. Reidel Publishing Company, Dordrecht, The Netherlands, Boston, MA, Sold and distributed in the U.S.A. and Canada by Kluwer Academic Publishers, 1984. LC # QB450 .S74 1984. ISBN # 90-277-1729-X. P.263, 1984, ed. C. Chiosi & A. Renzini, 263–+

Woosley, S. E., & Weaver, T. A. 1994, ApJ, 423, 371

Worthey, G., Faber, S. M., Gonzalez, J. J., & Burstein, D. 1994, ApJS, 94, 687

Worthey, G., & Ottaviani, D. L. 1997, ApJS, 111, 377

Wright, E. L. 2006, PASP, 118, 1711

Yamanaka, M., et al. 2009, ApJ, 707, L118

York, D. G., et al. 2000, AJ, 120, 1579

Yuan, F., et al. 2010, ApJ, 715, 1338

Yungelson, L., & Livio, M. 1998, ApJ, 497, 168

Yungelson, L. R., & Livio, M. 2000, ApJ, 528, 108

Zahid, H. J., Kewley, L. J., & Bresolin, F. 2011, ApJ, 730, 137

Zaritsky, D., Kennicutt, Jr., R. C., & Huchra, J. P. 1994, ApJ, 420, 87

Zhao, Y., Gu, Q., & Gao, Y. 2011, AJ, 141, 68

Zwicky, F. 1942, ApJ, 96, 28